SISSA - SCUOLA
INTERNAZIONALE
SUPERIORE
DI STUDI AVANZATI
TRIESTE
Strada Costiera 11

ISAS - INTERNATIONAL SCHOOL FOR ADVANCED STUDIES

ATTESTATO DI RICERCA

"DOCTOR PHILOSOPHIAE"

FREEZING OF IONIC LIQUIDS IN CORRELATION TO HOT-SOLID STRUCTURE

CANDIDATO:

Bruno D'Aguanno

RELATORE:

Prof. M.P. TOSI

Anno Accademico 1983/84

TRIESTE

FREEZING OF IONIC LIQUINDS IN CORRELATION TO HOT-SOLID STRUCTURE

Thesis submitted for the degree of "Doctor Philosophiae" at the International School for Advanced Studies, Trieste, Italy

Candidato: Bruno D'Aguanno

Relatore: Prof. M.P. Tosi

Classe di Fisica

Settore: Stati Condensati della Materia

Anno Accademico: 1983/84

AKNOWLEDGMENTS

I would like to express my gratitude to Professor M.P. Tosi for his encouragement and assistance throughout this research, as well as for his help in the preparation of this manuscript.

I thank Dr. M. Rovere for his very helpful suggestions about the details of the calculations. I also wish to express my appreciation for helpful discussions with Dr. G. Senatore. I am grateful to Professor L.G. Conti from University of Rome, for his continuous encouragement and technical advice.

CONTENTS

INTRODUCTION

The present work is concerned with two particular problems in the theory of ionic systems: (i) a comparative study of the freezing of molten alkali halides into a normal solid phase and of molten alkaline-earth halides into a superionic phase and (ii) a discussion of the high temperature defective structure of some ionic solids.

A theory of the first order liquid/solid (or solid/liquid) phase transition should start from the evaluation of the free energies of the solid and liquid phase. There is no need to comment on the difficulties of such a program (1). Much effort has consequently been devoted to predict the conditions under which a solid will melt or a fluid will freeze (2). Various authors have in this context looked for an instability in either the liquid or the solid phase. Instabilities of the solid phase associated, for instance, with the spontaneous multiplication of defects (3,4,5), or instabilities of the liquid against the appearance of long-range order are, of course, inconsistent with the phenomena of superheating and supercooling.

Empirical melting/freezing rules have also benn developed for each individual phase (e.g. the Lindemann rule (6) for the solid

and the Hansen-Verlet rule (7) for the liquid). These empirical 'laws' summarise the 'universality' of the information gained from laboratory (8,9) and computer (10,11,12) experiments. For our purpose the information can be condensed in the following statements. (i) The transition is largely independent of the details of the interparticle potentials; the essential role is played only by the repulsive part of the potential while the attractive part introduces minor corrections (13,14). (ii) The volume change on melting as well as the melting temperature show large variations but definite trends (15). (iii) The height of the first peak of the static structure factor of the fluid phase near freezing is remarkably constant within each class of materials (i.e. noble gases, metals, alkali halides). (iv) The entropy variation on freezing and the mean square displacement in the solid phase at the melting point also show 'universalities'. A theory of freezing should be able to present an explaination of these phenomena starting from first principles.

A modern approach to crystallisation is based on the density functional theory of non-uniform systems. Haymet and Oxtoby (16) have reformulated on this ground the Ramakrishnan and Yussouff theory of freezing (17). In this theory the response of the density to a fictitious external potential is studied, and a set of non-linear integral equations for the volume change and for the 'order

parameters' of the transition is obtained, the liquid structure coming in through the direct correlation functions. Applications have been made only for simple systems like Ar, Na and hard spheres.

In the present work, after a summary of all these relevant aspects (Chapter I and II), we study the freezing of alkali halides (NaCl and RbCl) and of alkaline-earth halides ($BaCl_2$ and $SrCl_2$) which freeze into a superionic phase (Chapter III). For this aim the March and Tosi scheme (18,19,20) has been used.

The strong charge ordering in NaCl and RbCl and the free energy gain associated with the large volume on freezing are the main qualitative factors which govern the freezing of these materials, good agreements with experimental data being found in the actual calculations. In the case of freezing into a superionic phase, the major features are the strong ordering of the divalent component and the difference in the partial molar volumes of anion and cation. The results indicate that the disordered chlorine ions behave in the hot solid to some extent as a liquid in an external potential created by the cation lattice. At present a theoretical description, on a microscopic scale, of the superionic materials when the temperature is progressively lowered is still lacking.

The principal observed characteristics of superionic

materials with the fluorite structure are: (i) a peak in the specific heat at a temperature below the melting point and (ii) an increase of the electrical conductivity to values of the same order of ionic melts. The transition is due to disordering of anion sublattice (21). The superionic transition temperature has been successfully correlated to the Frenkel energy using the Debye-Hückel theory to account for the Coulomb interaction between defects (4).

The final part of the present work (Chapter IV) is concerned with the behaviour of AgBr in the high temperature region below melting. AgBr, which is also a Frenkel conductor at low temperatures like fluorite-type crystals, does not become superionic before melting. In order to make comparison between AgBr and superionic conductors, the relevant defect parameters of the former are determined in detail. For this calculation N.M.R. (22,23), diffusion (24,25) and ionic conductivity (26) data are extensively used. Both Frenkel and Schottky defects appear to be present in this material at high temperatures. Using a Debye-Hückel model modified for saturation of screening at high defect concentrations, it has been suggested that this behaviour 'frustates' a superionic transition before melting (27), though high ionic conductivity is induced in the hot solid.

CHAPTER I

A BRIEF SURVEY OF THE EXPERIMENTAL AND THEORETICAL SITUATION OF FREEZING

CHAPTER I

A brief survey of the experimental and theoretical situation of freezing

The freezing/melting phenomenon is one of the most important fundamental processes in nature and we can observe it in virtually every substance. The coexistence between the two condensed states of matter, the liquid state and the solid state, is the particular characteristic of this phenomenon. A great deal of experimental data and empiric generalisations concerning freezing/melting have been collected (8,9,10). But in spite of this, the progress made in equilibrium statistical mechanics, that in principle should be able to describe all the characteristics of a phase diagram, has been very slow. A 'complete' description of the phenomenon is only now beginning to be available, thanks mainly to models sufficiently suited to the liquid state (12).

The aim of this introductory Chapter is to present some basic information on the freezing phenomenon both from the experimental and the theoretical point of view. Section 1 deals with some important relations that characterise the thermodynamics of transitions in simple model systems. The proof of the existence of phase transitions for

these simple model systems is given in Section 2, in which the principal and most recent results of numerical or computer experiments are collected.

Section 3 describes connections between data obtained for real systems and those obtained for model systems. The conclusion of this Section is that it is possible to establish that thermodynamic relations of Section 1 are still valid for the real systems in the limit of high temperatures and densities. In this way the role of the interatomic forces in the phase transition is made clear.

Section 4 examines the empirical laws of freezing/melting (Lindemann's rule, Ross's rule, Hansen-Verlet's rule). They account for the 'universality' of the properties listed in the previous Sections and they allow for the localisation of the transition. These considerations are extended in Section 5 to ionic materials, these being of main concern in the present work.

Section 6 offers a brief examination of the 'first principle' theories of freezing up to the recent Ramakrishnan and Yussouff theory (17), whose application to ionic materials will be described later in Chapter III.

I.1 Thermodynamics of simple model systems

A simple idealisation of interparticle force laws is given by the inverse power potential

$$\varphi(r) = \varepsilon\left(\frac{\sigma}{r}\right)^n$$

in which ε and σ are constants with the dimensions of energy and length and r is the distance between particles. The hardness or rigidity of the particles is measured by the exponent n: to $n = \infty$ corresponds, in 3-D, the hard spere system, to n = 1 corresponds the one-component classical plasma (O.C.P.). The potentials for five values of n are shown in Fig. (I.1-1).

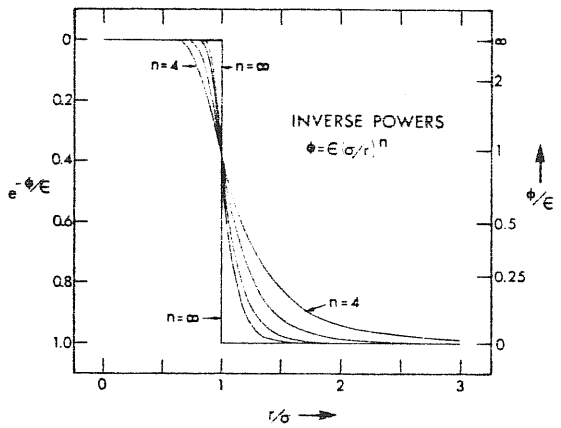

Fig. I.1-1: Interparticle potential energy functions for the five inverse power potentials, n = 4, 6, 9, 12 and ∞ . From ref. (28)

The thermodynamic properties of inverse power potential

systems are particularly simple. This follows from Klein's theorem (29,30) which says that for a system whose potential energy is a homogeneous function of order n of the particle coordinates, the non-ideal part of the partition function depends only on the variable $x = \rho\left(\frac{\varepsilon}{K_B T}\right)^{3/n}$, with $\rho \equiv \frac{N}{V}\sigma^3$, rather than on V and T separately. The canonical partition function, $Z(T,V,N)$, using the reduced distance $\vec{s} \equiv \vec{r}\left(\frac{N}{V}\right)^{1/3}$ is given by

$$Z(T,V,N) = \frac{V^N}{N!\,\lambda^{3N}} \int \cdots \int \exp\left(-\rho^{\frac{n}{3}} \frac{\varepsilon}{K_B T} \sum_{ij} s_{ij}^{-n}\right) d\vec{s}_1 \cdots d\vec{s}_N \qquad \text{(I.1-1)}$$

with $\lambda = \left(h^2/(2\pi m K_B T)\right)^{1/2}$.

It is easy to show that all the thermodynamic properties obtainable by differentiation of the partition function depend only on the variable x (11). So a single isotherm, with x varying from 0 to ∞ , will be needed to describe the whole state equation of the system. From eq. (I.1-1) we get a state equation such as

$$z = 1 + \Phi\left(\rho\left(\frac{\varepsilon}{K_B T}\right)^{3/n}\right) \qquad \text{(I.1-2)}$$

where $z = \frac{PV}{N K_B T}$ is the compressibility factor. The onset and the end of the melting phase transition will be indicated by two universal values of x

$$x_s = \rho_s \left(\frac{\varepsilon}{k_B T}\right)^{3/n} \quad , \quad x_l = \rho_l \left(\frac{\varepsilon}{k_B T}\right)^{3/n} \qquad \text{(I.1-3)}$$

in which ρ_s and ρ_l are the solid and liquid phase density. From eq.s (I.1-2) and (I.1-3) we get the equation of the melting curve and the volume and entropy discontinuities

$$\frac{P\sigma^3}{\varepsilon} = \left(\frac{k_B T}{\varepsilon}\right)^{\frac{n+3}{n}} z_i x_i \qquad \text{(I.1-4)}$$

$$\frac{\Delta V}{V} = \text{const.} \qquad \text{(I.1-5)}$$

$$\frac{\Delta S}{R} = \text{const.} \qquad \text{(I.1-6)}$$

In the case of the hard spheres, relations (I.1-5) and (I.1-6) remain unchanged, while the relations (I.1-3) and (I.1-4) become

$$x_s = \rho_s \quad , \quad x_l = \rho_l \qquad \text{(I.1-7)}$$

$$P = \text{const.} \times T \qquad \text{(I.1-8)}$$

In the case of the O.C.P. (system of point-like charged particles in a uniform compensating background), the canonical partition function is

$$Z(T,V,N) = \frac{V^N}{N!\,\lambda^{3N}} \int \cdots \int \exp\left(-\Gamma\, \eta(\vec{s}_1, \ldots, \vec{s}_N)\right) d\vec{s}_1 \ldots d\vec{s}_N \qquad \text{(I.1-9)}$$

in which $\eta(\vec{s}_1, \ldots, \vec{s}_N)$ is a function that characterises the spatial arrangement of the ions, and

$$\Gamma = \frac{Z^2 e^2}{r_\alpha K_B T} \qquad \text{(I.1-10)}$$

is a function that expresses the ratio between Coulomb energy and thermal energy with r_α radius of the sphere containing one ion. The thermodynamics of the transition of the O.C.P. will be determined by the Γ parameter. For the density at the phase coexistence we have

$$\rho_{s,l} \propto (K_B T)^3 \qquad \text{(I.10-11)}$$

For this system we do not have volume change at the transition.

I.2 Computer experiments on freezing/melting

The preceeding thermodynamic relations have been proved for all the systems drawn in Fig. (I.1-1) by means of computer experiments (28). In addition, numerical studies of phase transition have been made for a system of particles interacting by a Lennard-Jones potential (7,31-34) and for the O.C.P. (35-38). These studies determine the melting curve from the properties of the homogeneous phases. Indeed, the fraction of particles in the interface between the two phases, of the order $N^{2/3}$, is not negligible for the systems that can be studied with the computer. The free energy of these particles is higher than the free energy of the bulk, and the computer results, for the two phases in equilibrium, would then strongly depend on the number of particles.

The thermodynamic criterion for the coexistence of the two phases is that the Gibbs free energy of the two phases is the same at the equal pressure and temperature. From computer experiments the free energies of the two phases cannot be directly calculated. In order to determine them one starts from a reference state in which the free energy is exactly known (e.g. ideal gas) and one calculates the difference between the free energy of the liquid (or solid) phase and that of the reference state. An efficient method has been developed

by Hoover and Ree (39). In their scheme the reference state is still the ideal gas and the solid is artificially stabilised down to low densities by dividing the whole volume into Wigner-Seitz cells, and imposing a 'single occupation' constrain on the particles. The thermodynamic state equation thus determined in shown in Fig. (I.2-1) for the potentials with n = 4, 12, ∞ . Fig. (I.2-2) shows the phase boundaries for the same systems. As expected from relation (I.1-7)

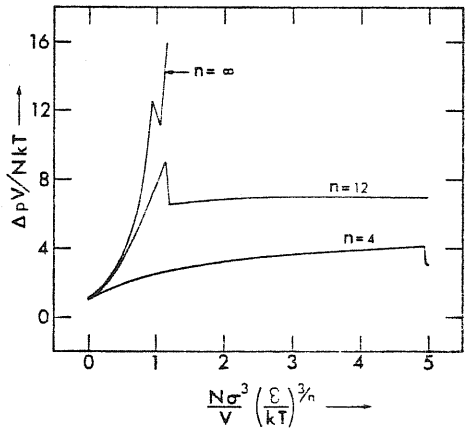

Fig. I.2-1: Thermodynamic equations of state for three inverse power potentials from computer experiments. $\Delta \frac{pV}{N k_B T}$ is the increase in the compressibility factor over that of a perfect static lattice at the same density and temperature. The discontinuities in the slopes of the three curves correspond to the melting and freezing transition. From ref. (11).

the melting and freezing densities for the hard spheres (n = ∞) are temperature independent.

Fig. (I.2-3) shows the phase diagram for the Lennard-Jones

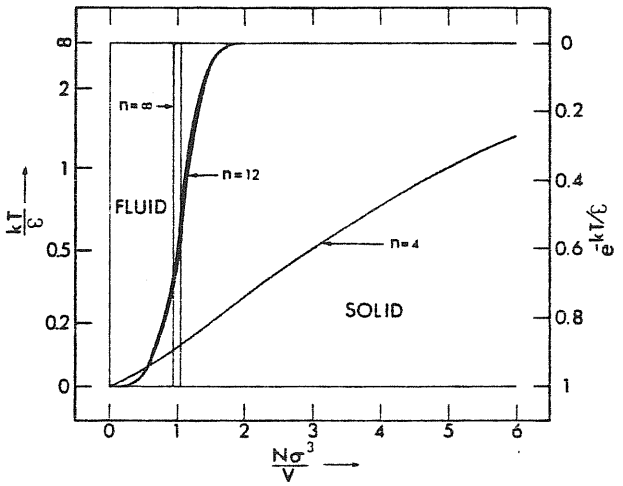

Fig. I.2-2: Boundaries of the two phases, fluid and solid, for inverse power potentials. The narrow strips (clear for n = ∞ and black for n = 12) correspond to the two phase region where fluid and solid can coexist. This region is very narrow for the case n = 4. From ref. (11).

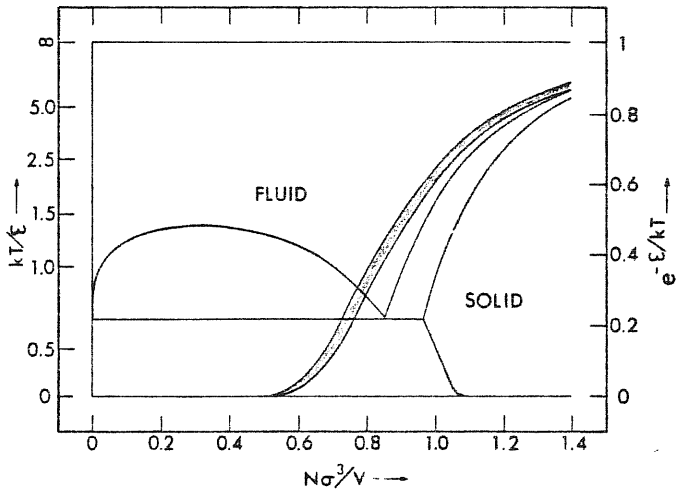

Fig. I.2-3: The Lennard-Jones phase diagram. Superimposed on this diagram is the soft-sphere phase diagram resulting when only repulsive forces are used. The fluid-solid two-phase region for the soft-sphere potential is lightly shaded. From ref. (11).

system ($\varphi(r) = Ar^{-12} - Br^{-6}$). A region, corresponding to the gaseous phase, is generated because of the introduction of the attractive part in the potential. The data characterising the thermodynamics of freezing for a certain number of model systems are shown in Table (I.2-1) both for the 3 - D and 2 - D cases.

3 - D	$\rho_s\left(\frac{\varepsilon}{k_BT_m}\right)^{3/n}$	$\rho_l\left(\frac{\varepsilon}{k_BT_m}\right)^{3/n}$	$\frac{\Delta F}{NK_BT}$	$\frac{\Delta U}{NK_BT}$	$\frac{\Delta S}{R}$	$\frac{\Delta V}{V_s}$	$\frac{PV_0}{NK_BT}\left(\frac{\varepsilon}{k_BT}\right)^{3/n}$
n = ∞	0.736	0.667	-1.16	0.00	1.16	0.103	8.3
n = 12	0.844	0.813	-0.72	0.18	0.90	0.038	16
n = 9	0.971	0.943	-0.63	0.21	0.84	0.030	22
n = 6	1.56	1.54	-0.50	0.25	0.75	0.013	61
n = 4	3.94	3.92	-0.45	0.35	0.80	0.005	426
2 - D							
n = ∞	0.798	0.761					8.08
O.C.P.							
3 - D	$\Gamma_m = (Ze)^2(4\pi\rho/3)^{1/3}/k_BT$		= 155±10			$\Delta\rho/\rho \approx 3\times10^{-4}$	
2 - D	$\Gamma_m = (Ze)^2(\pi\rho)^{1/2}/k_BT$		= 125±15			$\Delta\rho/\rho \leq 4\times10^{-4}$	

Table I.2-1: Thermodynamic properties of the crystal-liquid phase transition of a number of inverse power potential systems.

I.3 Real systems

The thermodynamic relations on freezing in the model systems discussed above and the results of the computer experiments can be connected to the liquid/solid phase transition in real systems.

The volume change, $\Delta V/V_s$, and the entropy change, $\frac{\Delta S}{N k_B}$, for a certain number of elements are shown in Table (I.3-1) together with the respective melting temperatures to give an idea of the order of magnitude. The elements are grouped according to their crystalline structure at high temperature.

It is interesting to follow the behaviour of $\Delta V/V_s$ and $\Delta S/Nk_B$ along the melting curve. In Fig.s (I.3-1), (I.3-2), (I.3-3) the curves $\Delta V/V_s$ and $\Delta S/Nk_B$ against T for argon and sodium, and against P for NaCl, are traced. We see that $\Delta V/V_s$ and $\Delta S/Nk_B$, after a rapid decrease at low temperatures, become practically constant. For the asymptotical values of $\Delta V/V_s$ and $\frac{\Delta S}{N k_B}$ Figures (I.3-4) and (I.3-5) give additional information. The conclusions are that

$$\left.\begin{aligned} \frac{\Delta V}{V_s} &\longrightarrow \text{const.} \\ \frac{\Delta S}{N k_B} &\longrightarrow \text{const.} \end{aligned}\right\} \quad T \to \infty$$

B.C.C.	T_m (°K)	$\Delta V/V_s$	$\Delta S/k_B$
Li	454	0.0165	0.795
Na	371	0.025	0.84
K	337	0.0255	0.835
Rb	312	0.025	0.845
Cs	302	0.026	0.835
Ca	1111	-----	0.93
Sr	1041	-----	1.1
Ba	987	-----	0.93
La	1193	-----	0.62
Cr	2148	-----	0.815
Mo	2883	-----	1.35
W	3683	-----	1.16
Mn	1518	0.017	1.16
Fe	1809	0.035	0.92
Tl	576	0.022	0.86
F.C.C.			
Ag	1234	0.038	1.10
Al	933	0.060	1.4
Au	1336	0.051	1.13
Co	1768	0.035	1.10
Cu	1356	0.0415	1.16
Ni	1726	0.054	1.22
Pb	600	0.035	0.96
Pd	1825	0.059	1.13
Pt	2042	0.066	1.16
H.C.P.			
Cd	321	0.040	1.25
Mg	650	0.041	1.17
Zn	419	0.042	1.27

Table I.3-1: Melting temperatures, volume changes and entropy changes for a number of elements.

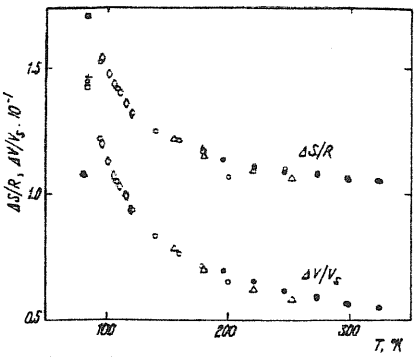

Fig. I.3-1: Temperature dependence of the relative volume discontinuity $\Delta V/V_s$ and entropy discontinuity $\Delta S/R$ in the melting of argon. From ref. (8).

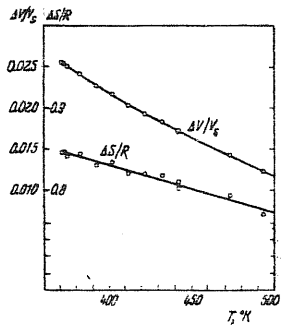

Fig. I.3-2: Temperature dependence of the relative volume discontinuity $\Delta V/V_s$ and entropy discontinuity $\Delta S/R$ in the melting of sodium. From ref. (8).

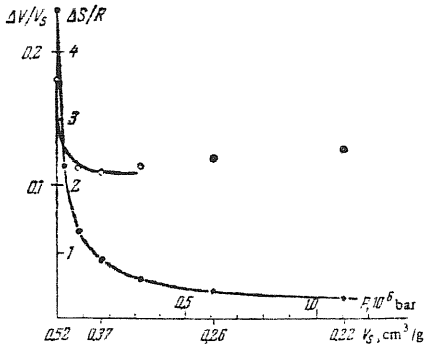

Fig. I.3-3: Pressure dependence of relative volume discontinuity and entropy discontinuity during melting of NaCl. From ref. (9).

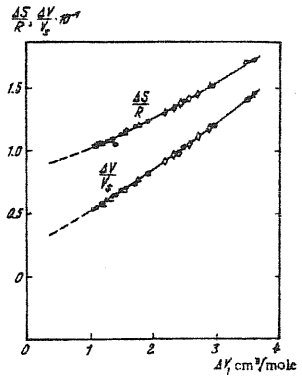

Fig. I.3-4: Relative volume discontinuity $\Delta V/V_s$ and entropy discontinuity $\Delta S/R$ in the melting of argon, as functions of the volume discontinuity ΔV ($\Delta V \to 0$ corresponds to $P \to \infty$). From ref. (8).

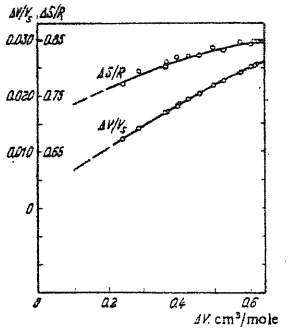

Fig. I.3-5: Entropy of melting $\Delta S/R$ and relative volume discontinuity $\Delta V/V_S$ as functions of the volume discontinuity ΔV in the melting of sodium ($\Delta V \to 0$ corresponds to $P \to \infty$). From ref. (8).

For argon the extrapolated values of $\Delta S/NK_B$ and $\Delta V/V_S$ are

$$\left.\begin{aligned} \frac{\Delta S}{NK_B} &\longrightarrow \sim 0.9 \\ \frac{\Delta V}{V_S} &\longrightarrow \sim 0.03 \end{aligned}\right\} \quad T \to \infty$$

which are practically the same values obtained from the computer simulation of the freezing of particles interacting with the law $\varphi(r) = \varepsilon(\sigma/r)^{12}$ (see Table (I.2-1)). For sodium the extrapolated value of $\Delta S/Nk_B$ is ≈ 0.7 while the limiting value of $\Delta V/V_S$ is not well defined; in this case we cannot make comparison with the computer simulation results of Table (I.2-1). This asymptotic value of the melting entropy, $\frac{\Delta S}{Nk_B} \cong \ln 2$ when $\Delta V/V_S \to 0$, has been also found for a range of metals (see Fig. (I.3-6)).

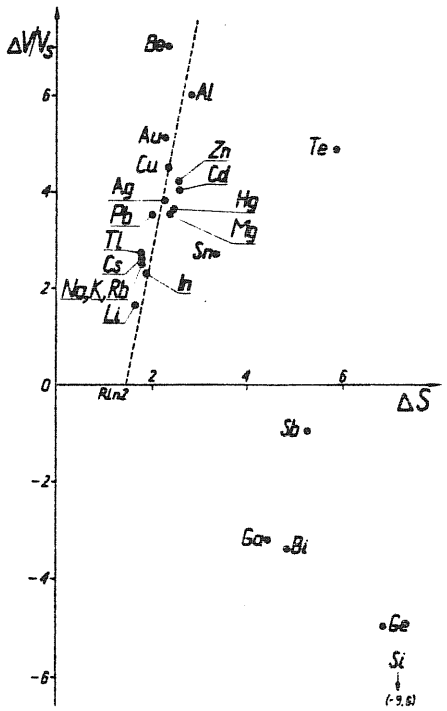

Fig. I.3-6: Relationship between entropy of melting ΔS and relative change in volume on melting $\Delta V/V_S$. Data from ref. (40).

I.4 Empirical laws of freezing/melting

In eq. (I.1-3) it is confirmed that freezing and melting happens at characteristic values of x. So, every x dependent structural characteristic can be used as a transition indicator. One of these indicators is the Lindemann law (41), stating that along the melting curve the ratio between the root-mean-square displacement of a particle from its lattice site and the first-neighbour distance, $f = \langle (\Delta r)^2/d^2 \rangle^{1/2}$, is constant. Table (I.4-1) shows the values of f for a certain number of model systems and for some B.C.C. and F.C.C.

B.C.C. elements	Li	Na	K	Rb	Cs	
f	0.116	0.111	0.112	0.115	0.111	
F.C.C. elements	Al	Cu	Ag	Au	Pb	Ni
f	0.072	0.069	9.071	0.073	0.065	0.077
Model systems	n= ∞	n= 12	n= 9	n= 6	n= 4	n= 1
f	0.13	0.15	0.16	0.17	0.18	0.17
Hard disks system		f = 0.17				
Lennard-Jones system		f = 0.15				

Table I.4-1: Values of the Lindemann parameter f for some B.C.C. and F.C.C. materials and for model systems.

metals. In the model systems f shows only a weak dependence on the 'hardness' parameter n; in the case of the metals Lindemann's law applies to each structure separately.

Another criterion on melting has been proposed by Ross (42). Ross's law states that the excess part of the free energy, F_{ex}, is constant along the melting curve. That is

$$\frac{F_{ex}}{Nk_BT} = \frac{F}{Nk_BT} - Ln\left(\frac{N}{V}\right) + 1 - \frac{V_o}{Nk_BT} = \text{const.} \qquad \text{(I.4-1)}$$

where F is the total free energy of the solid and V_o is the potential energy of the solid if all the particles are fixed in their lattice sites. Eq. (I.4-1) is exact for the inverse power potentials. Ross's law, that determines a value of $F_{ex} \approx 6\,Nk_BT$, shows less variation compared to Lindemann's law, as can be seen from Fig. (I.4-1). For

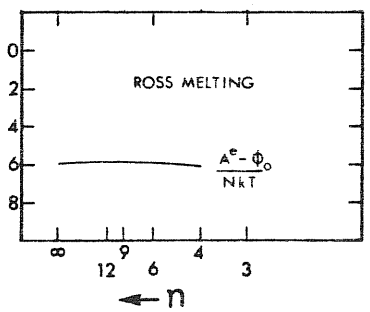

Fig. I.4-1: Ross's melting rule as function of softness, s = 3/n. The figure indicates a proportionality constant $6Nk_BT$. Form ref. (28).

hard disks, $F_{ex} = 3.9\ Nk_BT$ (39); for a 2 - D Lennard-Jones system, $F_{ex} = 3.7\ Nk_BT$ (43).

A freezing criterion based on liquid phase structural properties, has been formulated by Hansen and Verlet (7). This criterion states that along the freezing curve the height of the main peak of the static structure factor, S(k), is constant. Near freezing the height of the main peak, in the hard sphere case, is $S_{peak} = 2.85$ (44). From the work of Hansen and Shiff (44) we observe that for the inverse power potential systems with n = 12, 9, 6, 4, 1, S_{peak} lies between 3.05 (n = 12) and 2.57 (n = 1). In the Lennard-Jones system a value $S_{peak} = 2.85$ allows one to predict the correct shape of the freezing curve over a large pressure interval (7). Table (I.4-2) shows the values of S(k) at the first peak and near freezing for a certain number of metals. In the Table are also presented the values of c(k), the direct correlation function, which is related to S(k) through $S(k) = 1 / (1-c(k))$.

B.C.C.	S(k)	c(k)
Li	2.64	0.62
Na	2.80	0.64
K	2.73	0.63
Rb	2.8	0.64
Cs	2.5	0.6
Ca	2.61	0.62
Sr	2.65	0.62
Ba	2.6	0.61
La	2.66	0.62
Zr	2.37	0.58
Cr	2.46	0.59
Mn	2.5	0.6
Fe	2.41	0.58
F.C.C.		
Ag	2.48	0.6
Al	2.53	0.61
Au	2.49	0.6
Co	2.44	0.59
Cu	2.59	0.61
Ni	2.42	0.59
Pb	2.78	0.64
Pd	2.64	0.62
Pt	2.69	0.63
H.C.P.		
Cd	2.5	0.6
Mg	2.54	0.61
Zn	2.85	0.65

Table I.4-2: Experimental values of the static structure factor S(k) at the first peak and near freezing. c(k) is linked to S(k) through the relation $S(k)=(1-c(k))^{-1}$.

I.5 Solid - liquid transition in ionic systems

In classical ionic materials both thermodynamic and transport data on the hot solid phase show a variety of behaviours that can be described, broadly speaking, as premelting phenomena. The best known example is the appearance of a high-electric-conductivity ('superionic') state in some of these materials before melting occurs.

Table (I.5-1) reports data on the fractional volume change $\Delta V/V_s$ and on the entropy change ΔS on melting for the alkali halides, the alkaline-earth halides and the silver halides. The volume change in the alkali halides, as shown by Biggin and Enderby (45), can be related to the coordination numbers in the liquid and in the solid through the semi-empirical relation (46)

$$n_l = n_s \frac{v_s}{v_l} \left(\frac{a_l}{a_s}\right)^3 \qquad \text{(I.5-1)}$$

where n_l and n_s are the coordination numbers in the liquid and in the solid, v_l and v_s are the corresponding molar volumes, a_l is the position of the first peak in the radial distribution function for unlike ions $g_{+-}(r)$ (see next Chapter), and a_s is the nearest neighbour distance in the solid. Table (I.5-2) summarises the known

Alkali halides	$\Delta V/V_s$ (%)	ΔS (cal.°K^{-1}mole^{-1})
LiF	29.4	5.77
LiCl	26.2	5.39
LiBr	24.3	5.13
LiI	----	4.72
NaF	27.4	6.2
NaCl	25.0	6.23
NaBr	22.4	6.12
NaI	18.6	6.04
KF	17.2	5.97
KCl	17.3	6.08
KBr	16.6	6.06
KI	15.9	6.02
RbF	----	5.76
RbCl	14.3	5.70
RbBr	13.5	5.77
RbI	----	5.73
CsF	----	5.32
CsCl	10.0	5.27
CsBr	26.8	6.20
CsI	28.5	6.27
Alkaline-earth halides		
$CaCl_2$	0.9	6.49
$CaBr_2$	----	6.85
CaI_2	----	9.5
$SrCl_2$	4.2	3.39
$SrBr_2$	----	2.70
SrI_2	----	5.80
$BaCl_2$	3.5	3.17
$BaBr_2$	----	6.75
BaI_2	----	6.44
Silver halides		
AgCl	8.9	4.34
AgBr	8.2	3.28
AgI	----	2.7

Table I.5-1: Melting parameters of the alkali halides, alkaline-earth halides and silver halides. Data from ref. (2).

coordinations for both alkali chloride and alkaline-earth chloride compounds at standard temperature and pressure for the solid phase and near freezing for the liquid phase. As one example, the large increase in molar volume on melting for NaCl (25 % see Table) reflects the decrease from a value of 6 for the coordination number in the solid at standard temperature and pressure, n_s, to a value of 4 for the 'close contact' coordination number in the liquid, n_l.

salt	n_{+-} solid at S.T.P.	n_{+-} melt
NaCl	6	4
KCl	6	4.1
RbCl	6	3.8
$CaCl_2$	8	5.8
$SrCl_2$	8	6.5
$BaCl_2$	4	7.5

Table I.5-2: Coordination numbers for alkali chlorides and alkaline-earth chlorides.

The alkaline-earth halides show instead very low values of the volume change. Several of these salts show, in the high temperature solid phase, ionic conductivities of the same order of

magnitude as those of simple ionic melts: they are superionic materials. Three kinds of behaviour have been found as the temperature of the crystal is progressively raised toward melting (47): (i) salts such as $MgCl_2$, $CaCl_2$, $CaBr_2$ and $BaBr_2$ show a smooth increase of ionic conductivity, with a jump by several orders of magnitude on melting; (ii) salts such as $BaCl_2$ or $SrBr_2$ show a structural phase transition below T_m accompained by a large increase in ionic conductivity; (iii) salts such as CaF_2, SrF_2, BaF_2 and $SrCl_2$ show a continuous increase in conductivity and a slight jump on melting. Both type-(ii) and type-(iii) materials of the alkaline-earth halide family have fluorite structure in the high-conductivity state.

The total entropy change, ΔS, found at melting for alkali halides is roughly constant, with a value of about 6 cal/°K. A proposed interpretation of this value is that about 2.2 cal/°K arise from a random distribution of 'defects' in the liquid, and about 3.8 cal/°K from changes in vibrational entropy (48). Table (I.5-3) shows data of entropy change in the solid-solid and melting transition for some class-(ii) superionic materials, while Table (I.5-4) shows data of melting entropy for some class-(iii) materials. For class-(ii) superionic conductors we see that, as in the melting of alkali halides, the sum of the solid-solid transition entropy and the melting entropy is of 10 to 12 $J°K^{-1}$ per mole of ions. But

Salt	Solid transition T_t (°K)	ΔS_t (J °K^{-1} mole^{-1})	Melting T_m (°K)	ΔS_m (J °K^{-1} mole^{-1})
AgI	419	14.5	830	11.3
Ag_2S	452	9.3	1115	12.6
Ag_2Se	406	10.0	---	---
CuBr	664	9.0	761	12.6
Cu_2S	376	9.9	---	---
	708	1.8	1402	---
Cu_2Se	395	17.3	---	---
CuI	642	11.1	878	---
$SrBr_2$	918	13.3	930	11.3
$BaCl_2$	1193	14.4	1233	13.3
LuF_3	1230	20.4	1457	20.8

Table I.5-3: Entropy changes in the solid-solid and melting transition for some class-ii materials. Data from ref. (15).

Salt	T_m (°K)	ΔS_m (J °K^{-1} mole^{-1})
$SrCl_2$	1146	14.2
PbF_2	1095	16.4
CaF_2	1691	17.5
UO_2	3115	24.4
K_2S	1221	13.8
AgBr	703	13.6
LaF_3	1766	28.4

Table I.5-4: Entropy of fusion of some class-iii materials. From ref. (15).

the melting entropy for both class-(ii) and class-(iii) superionic conductors is anomalously low.

The entropy change, ΔS_m, has been described successfully as the sum of a volume dependent term and a fundamental entropy term, as follows (49)

$$\Delta S_m = \alpha B_T \Delta V_m + \sigma R \ln 2 \qquad \text{(I.5-2)}$$

in which α is the coefficient of thermal expansion, B_T is the isothermal bulk modulus, ΔV_m the molar volume change on melting and σ the stoichiometry of the system. For a monatomic system like Ar or Na $\sigma = 1$; for a binary system like NaCl $\sigma = 2$; and for a ternary system like $BaCl_2$ $\sigma = 3$. The possibility of the use of eq. (I.5-2) lies in the relative constancy of the αB_T product (50). The equation (I.5-2) is plotted in Fig. (I.5-1) against $\alpha B_T \Delta V_m$ for a range of materials and the three solid lines are $\sigma = 1$, 2 and 3. As expected, monatomic Ar and Na lie close to the line $\sigma = 1$ and the alkali halides close to the line $\sigma = 2$. The fast-ion conductors $SrCl_2$ and CaF_2, on the other hand, lie close to the line $\sigma = 1$. This is consistent with the premelting transition as shown in Figures (I.5-2) and (I.5-3). The transition is signalled by the peak in the heat capacity from which one fixes the superionic

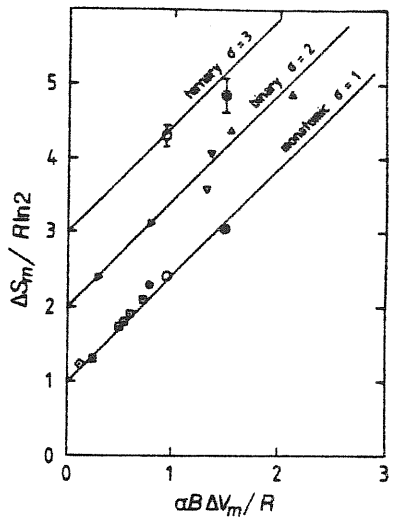

Fig. I.5-1: Entropy change on melting as a function of $\alpha B_T \Delta V_m$. The symbols are: $SrCl_2$: o ; CaF_2: ● ; Ar: □ ; Na: ◇ ; inverse-12 soft sphere: ■ ; NaCl: ▲ ; KCl: △ ; NaI: ▼ ; KBr: ▽ ; KI: ▶ ; AgBr: ▷ and $BaCl_2$: ◐ . Data from Ref. (51).

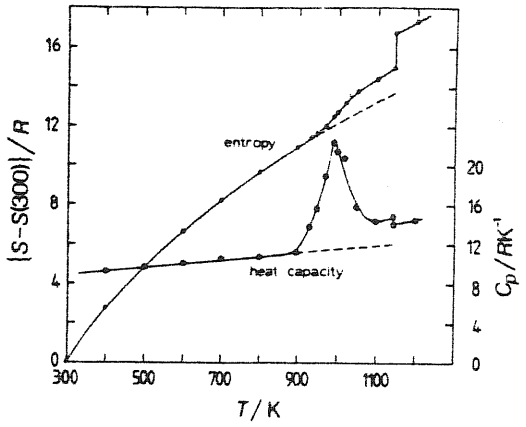

Fig I.5-2: Heat capacity and entropy for $SrCl_2$. From ref. (51).

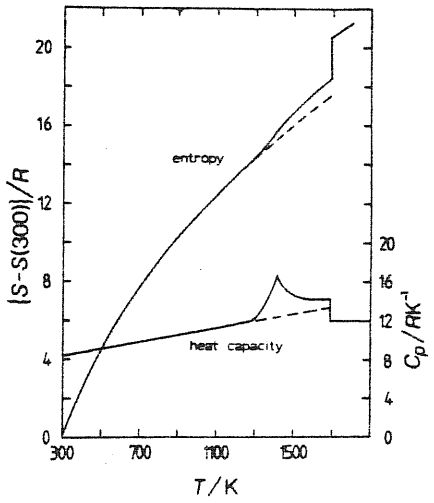

Fig. I.5-3: Heat capacity and entropy for CaF_2. From ref. (51).

transition temperature. In a somewhat simplistic view, at this transition the anion sublattice 'melts', and σ at the melting becomes the stoichiometry of the cation sublattice. Also plotted for $SrCl_2$ and CaF_2 is the sum of the entropies of the fast-ion and melting transitions and it lies close to the σ = 3 line. When ΔV = 0 the entropy change ΔS_m will be determined by the term $\sigma R \ln 2$ (see eq. (I.5-2) and Fig. (I.3-6)). This fundamental term has been interpreted as arising from the localisation of the σN pairs of propagating transverse waves (52). A last comment can be made on AgBr, whose ionic conductivity increases smoothly but rapidly

until melting occurs. Its entropy change is well described with $\sigma = 2$ (see Fig. (I.5-1)). Its behaviour is, in a certain sense, intermediate between alkali halides and superionic conductors (but we shall speak extensively on this system in the last Chapter).

Empirical melting rules have been stated also for ionic systems. In order to correlate melting temperatures with the interionic pair potentials in the alkali halides, a corresponding-states equation of state has been developed (15). This equation of state takes the form

$$P = \frac{e^2}{\lambda^4} f\left(\frac{v}{\lambda^3}, \frac{\lambda k_B T}{e^2}\right) \qquad \text{(I.5-3)}$$

where p is the pressure, f is a 'universal' function of the variables in parenthesis and λ is a scaling length (which may be taken as the near-neighbour distance). One obtain a good correlation between melting temperatures for alkali halides by expressing T_m simply as

$$T_m \cong (3 \times 10^{-5}/\lambda)\ ^\circ K\ . \qquad \text{(I.5-4)}$$

The data are shown in Table (I.5-5). This rule is not followed by lithium salts for which the neglect of short-range repulsions between anions in the pair potential is less justified (15).

Salt	T_m (°K)	λT_m (10^{-5} cm °K)
LiF	1121	2.25
LiCl	887	2.27
LiBr	823	2.27
LiI	718	2.21
NaF	1265	2.92
NaCl	1074	3.02
NaBr	1023	3.04
NaI	933	3.01
KF	1129	3.02
KCl	1045	3.28
KBr	1013	3.34
KI	958	3.39
RbF	1048	2.96
RbCl	988	3.26
RbBr	953	3.27
RbI	913	3.34
CsF	955	2.88
CsCl	918	3.18
CsBr	909	3.29
CsI	894	3.42

Table I.5-5: Scaling melting temperature λT_m . From ref. (15).

The systematic variation of λT_m with the anion radius suggests another melting rule based on the ratio of the ionic radii (53). The rule is formulated in terms of a lattice instability due to the overlap between the large ions (anions), and a linear relation between the ionic radii ratio and the square root of the melting

temperature T_m has been found, as well illustrated in Fig. (I.5-4).

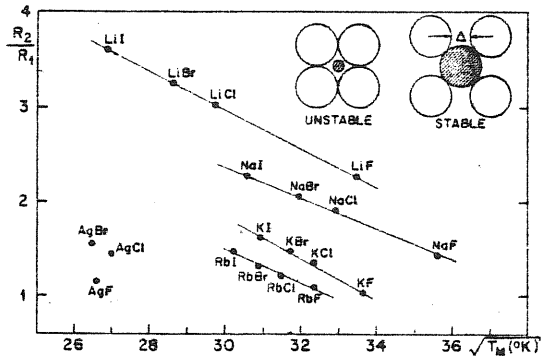

Fig. I.5-4: Ratio of the ionic radii versus the square root of the melting temperature in the alkali halides. R_2 is the ratio of the large ion and R_1 the radius of the smaller. $\Delta = \sqrt{2}\,R_1 - (2-\sqrt{2})\,R_2$. Data from ref. (53).

We may also look for melting 'uniformities' in the Lindemann theory of vibrational instability of crystal lattices. The theory leads to a 'Lindemann melting parameter'

$$L_m = \Theta_D V^{1/3} (M/T_m)^{1/2} \qquad \text{(I.5-5)}$$

based on accesible experimental parameters. Θ_D is the Debye

temperature, V the molar volume and M the atomic mass. Table (I.5-6) reports the values of L_m for a range of salts.

Salt	L_m	T_m (°K)
NaCl	210	1074
KCl	195	1045
AgCl	239	728
KI	180	958
RbI	189	913
RbBr	206	953
AgBr	229	701
LiF	200	1121
CaF_2	211	1633

Table I.5-6: Values of the Lindemann parameter, L_m, for a range of salts. From ref. (2).

A criterion for freezing of molten alkali halides has been proposed by March and Tosi (54) using the peak height of the charge-charge liquid structure factor, S_{QQ}. In a two component liquid, three partial structure factors are necessary for a structural description, i.e. $S_{NN}(k)$, $S_{NQ}(k)$ and $S_{QQ}(k)$ (see next Chapter). The number-number structure factor S_{NN} has a gas-like structure, the cross-correlation S_{NQ} is little structured while the charge-

charge structure factor S_{QQ} shows a very prominent principal peak (see Fig. (I.5-5)) reflecting the residual short-range ordering in the ionic liquid. The values of S_{QQ}^{max} at temperatures near freezing

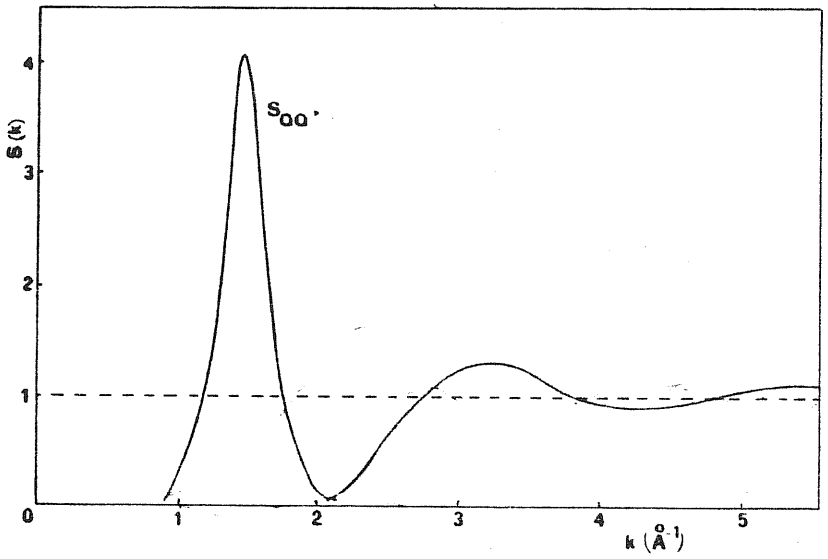

Fig. I.5-5: Charge-charge structure factor for molten RbCl from neutron diffraction data on partial structure factors.

point are listed from neutron diffraction data in Table (I.5-7). Also listed is the percentage deviation of the temperature of measurement from the melting temperature. Extrapolation to the melting temperature leads to a value of $S_{QQ}^{max} \approx 4 \div 5$ at freezing.

	NaCl	KCl	RbCl	CsCl
S_{QQ}^{max}	3.6	4.4	4.1	3.1
$(T-T_m)/T_m$	0.070	0.023	0.035	0.059
$e^2/(a k_B T_m) = \Gamma$	71	65	66	65

Tab. I.5-7: Height of main peak in S_{QQ} in molten alkali chlorides and Γ parameter. From ref. (15).

The last row of the Table shows the remarkably constant values of the plasma parameter Γ previously defined in eq. (I.1-10). If in the definition we replace r_α by the sum of ionic radii, $R_+ + R_-$, we reach, apart from a scaling factor, the Reiss et al. (55) criterion which states that the melting temperature of alkali halides is directly correlated with $e^2 / (R_+ + R_-)$.

I.6 Survey of theories of freezing

All the theories of freezing developed until now and which try to explain the experimental results shown in Sections 4 and 5 in terms of a 'first principles' theory, can be put into two groups: (i) distribution function theories and (ii) density functional theories.

The theories in the first group have been developed starting from the work of Kirkwood and Monroe (56) of 1941. Kirkwood and Monroe observe that, for a certain type of closure, the Kirkwood hierarchical equations for the one-particle distribution function are non-linear (and therefore they allow for more than one solution for a given set of constraints). They examine whether changes in the analytic structure of the one-particle distribution function are to be associated with the beginning of a phase transition. The results obtained are not satisfactory and the amount of input thermodynamic data is considerable.

Developments in this direction have been facilitated by the fact that the distribution functions satisfy various systems of integro-differential or non-linear integral equations. Tyablikov (57) has studied the Bogoliubov hierarchy; Vlasov (58) his own equation; Raveché-Stuart (59) and Raveché-Kayser (60) the Yvon-Born-Green

hierarchy; Weeks et al. (61) and Jancovici (62) a modified version of the Kirkwood-Monroe theory. None of these authors have applied the theory to real systems and when applied to model systems, like hard spheres in 1, 2 and 3 dimensions, the results are often contradictory. The explanation for these failures is to be found in a series of reasons: (i) the linearisation of the equations is obtained by treating the liquid/solid transition as a 'soft bifurcation' problem while the first order character of the transition requires the use of a 'hard bifurcation' treatement; (ii) the closure of hierarchical equations leads them to give great importance to the first peak of the pair correlation function while the phase transition is linked to the oscillations which follow the first peak; (iii) in hierarchical equations the interparticle potential explicitly appears, while the experimental data of Sections 4 and 5 show a non-critical dependence of the transition phenomenon from the potential details.

Problems (ii) and (iii) are easily resolved in the framework of the density functional theories. This modern approach to the transition was begun by Lovett (63) and Lovett and Buff (64). They try to determine the bifurcation point by investigating the stability of the liquid compared with the crystalline state on the basis of a relation between the one-particle distribution function and the direct correlation function. The solutions found are

characteristic of a second order transition. The discontinuous character of the solid/liquid transition is restored by Ryzhov and Tareeva (65) and Bagchi and Rice (66). The results are not quantitative and the connections between the mechanical instability of the liquid, the bifurcation point and the transition point are not yet clear. Quantitative agreement with the experimental results for hard spheres, argon and sodium has been obtained by Ramakrishnan and Yussouff(17). They add to the theory the balance and minimum conditions of the grand-canonical thermodynamic potential at the two phase equilibrium. Haymet and Oxtoby (16) have reformulated the Ramakrishnan and Yussouff theory in the scheme of the 'density functional' theory of non-uniform systems (67). March and Tosi (18) have developed a scheme for the application of the theory to more complex systems like alkali halides and alkaline-earth halides. These developments will be presented below in detail.

CHAPTER II

EQUILIBRIUM STATISTICAL MECHANICS OF THE LIQUID-SOLID PHASE TRANSITION

CHAPTER II

Equilibrium statistical mechanics of the liquid-solid phase transition

In this Chapter we present the freezing theory following the Haymet and Oxotoby method (16). A great deal of the material shown here is absolutely necessary for the applications that will be made in the next Chapters.

Sections 1 and 2 of this Chapter are dedicated to the formal theory of statistical mechanics of non-uniform fluids. Two key quantities $\mathcal{F}[\rho]$ and $\Omega_v[\rho]$ (the Helmholtz free energy and the grand canonical potential), which are functionals of the one-particle density $\rho(\vec{r})$, are introduced and the variational principle for the grand potential is derived. The functional derivatives of $\mathcal{F}[\rho]$ with respect to $\rho(\vec{r})$ give rise to the direct correlation functions, while the functional derivatives of $\Omega[\rho]$ with respect to a fixed external potential give the n-particle distribution functions.

In Section 3 we derive the general equations of freezing. They are obtained by considering the solid as a perturbation about the uniform liquid. Ramakrishnan and Yussouff (17) have shown that such a simple idea correctly correlates structural features of the liquid with the order parameters of the hot solid in equilibrium

with the liquid. The approximations regarding the replacement of the generalised direct correlation functions $c(\vec{r}_1,\vec{r}_2)$ and $c^{(3)}(\vec{r}_1,\vec{r}_2,\vec{r}_3)$ with the corresponding $c(|\vec{r}_1-\vec{r}_2|)$ and $c^{(3)}(|\vec{r}_1-\vec{r}_2|, |\vec{r}_1-\vec{r}_3|)$ defined in the infinite fluid phase, are introduced. In this Section we also illustrate the microscopic physical interpretation of the freezing process that the equations suggest. We will reach this objective by looking at the connection between an external perturbation, the response of the fluid and the energy balance of the process (15).

Section 4 is dedicated to a simple application of the theory to the freezing of metallic systems into b.c.c., f.c.c. and h.c.p. lattices. The main approximation here concerns the 'incompressibility limit', i.e. volume change $\eta \rightarrow 0$.

Section 5 deals with the freezing of the hard sphere system (68). Here we have listed all the approximations that we must perform for the practical solution of the equations.

Section 6 is dedicated to the 'subtle' problem of the determination of the entropy change per particle at freezing, $\frac{\Delta S}{N k_B}$. Here we have presented the results obtained for the entropy change in the case of the hard sphere system.

II.1 Thermodynamic potentials

Let us consider a classical system of N identical particles in a volume V. Let the total Hamiltonian of the system be composed of (i) a term due to the free motion of the particles, (ii) a term corresponding to the interactions of the particles with each other and (iii) a term describing the action of an arbitrary external potential depending only on the coordinates of the particles. We can write it as

$$H_N = T + U + V \qquad \text{(II.1-1)}$$

where

$$T = \sum_{j=1}^{N} \vec{p}_j^{\,2}/2m \quad ,$$

$$U \equiv U_N(\{\vec{r}_j\}) \quad ,$$

$$V = \sum_{j=1}^{N} V_{ext.}(\vec{r}_j) \quad ,$$

m is the mass of the particles and U_N is the potential energy. U_N includes any containing walls present in the system and no pairwise additivity is assumed for it. The system, with a prescribed chemical potential μ , is in thermal equilibrium in a bath at temperature T.

For the thermodynamic description of the system we will

use a grand canonical ensemble because the equilibrium phase conditions, that is P, T and μ constant, are in it easy accesible. The equilibrium probability density, f_{eq}, is defined as

$$f_{eq} = \mathcal{Z}_G^{-1} \exp[-\beta(H_N - \mu N)] \quad . \tag{II.1-2}$$

The grand canonical partition function is given by

$$\mathcal{Z}_G(V,T,\mu) = Tr_{Cl}\{\exp[-\beta(H_N - \mu N)]\} \tag{II.1-3}$$

where Tr_{Cl} denotes the usual classical trace operation, that is

$$Tr_{Cl} = \sum_{N=0}^{\infty} \frac{1}{N!} \prod_{j=1}^{N} \int d\vec{r}_j \int \frac{d\vec{p}_j}{h^3} \ldots \quad . \tag{II.1-4}$$

The macroscopic value of a generic operator $\hat{A}$ is defined by taking the configurational average

$$\langle \hat{A} \rangle = Tr_{Cl}\, f_{eq} \cdot \hat{A} \tag{II.1-5}$$

and for the equilibrium density, $\rho_{eq}(\vec{r})$, we have

$$\rho_{eq}(\vec{r}) = \langle \hat{\rho}(\vec{r}) \rangle \tag{II.1-6}$$

where

$$\hat{\rho}(\vec{r}) = \sum_{j=1}^{N} \delta(\vec{r} - \vec{r}_j) \qquad \text{(II.1-7)}$$

is the number density operator.

The connection between the thermodynamic properties and the grand canonical ensemble is obtained starting from the relation between the grand canonical potential, Ω , and the grand partition function, Z_G ,

$$\beta^{-1} \ln Z_G = -\Omega = PV \qquad \text{(II.1-8)}$$

Other useful thermodynamic functions are the 'intrinsic' Helmholtz free energy, $\mathcal{F}$, and the Helmholtz total free energy, F ,

$$\mathcal{F} = \Omega - \int d\vec{r}\, \rho_{eq}(\vec{r})\, V_{ext}(\vec{r}) + \mu \int d\vec{r}\, \rho_{eq}(\vec{r}) \qquad \text{(II.1-9)}$$

$$F = \mathcal{F} + \int d\vec{r}\, \rho_{eq}(\vec{r})\, V_{ext}(\vec{r}) \qquad \text{(II.1-10)}$$

The role of these two thermodynamic functions will be clarified in the following paragraph concerning the density functional theory.

II.2 The density functional formalism

According to Mermin (69), we introduce the functional of the probability density f

$$\Omega[f] = Tr_{cl}\, f(H_N - \mu N + \beta^{-1} \ln f) \qquad \text{(II.2-1)}$$

which, in the case of the equilibrium probability density f_o, coincides with the grand canonical potential

$$\Omega[f_o] \equiv \Omega(V,T,\mu) \quad . \qquad \text{(II.2-2)}$$

From the Gibbs-Bogoliubov inequality (12) for two arbitrary distribution functions f and g,

$$Tr_{cl}(f \ln f) \geqslant Tr_{cl}(f \ln g) \quad , \qquad \text{(II.2-3)}$$

we immediately obtain the following relation

$$\Omega[f] > \Omega[f_o] \qquad \text{(II.2-4)}$$

where we have used the relations (II.1-2), (II.2-1) and (II.2-2).

Using the same arguments of Hohenberg-Kohn-Mermin (70) it is possible to show that, for a given interaction potential U and chemical potential μ, $V_{ext}(\vec{r})$ is a functional of $\rho_o(\vec{r})$: it means that $V_{ext}(\vec{r})$ is inequivocally determined if the density $\rho_o(\vec{r})$ is known in all $\vec{r}$ points of the system. Omitting the exact proof we can see (from relation (II.1-2)), that f_o is a function of $V_{ext}(\vec{r})$ and therefore the more important result that f_o is a functional of $\rho_o(\vec{r})$.

Let us introduce, now, the two key quantities of the theory, that is the functionals

$$\mathcal{F}[\rho] = Tr_{cl}\, f_o (T + U + \beta^{-1} \ln f_o) \qquad \text{(II.2-5)}$$

and

$$\Omega_v[\rho] = \int d\vec{r}\, \rho(\vec{r}) V_{ext}(\vec{r}) + \mathcal{F}[\rho] - \mu \int d\vec{r}\, \rho(\vec{r}) \,. \qquad \text{(II.2-6)}$$

Let us derive the variational principle for the grand canonical ensemble. The functional $\Omega_v[\rho]$ will coincide with the grand canonical potential when the density ρ is equal to the equilibrium density ρ_o. For a generic density ρ' and probability density f' we obtain

$$\Omega[f'] = \mathcal{F}[f'] + \int d\vec{r}\, \rho'(\vec{r}) V_{ext}(\vec{r}) - \mu \int d\vec{r}\, \rho'(\vec{r})$$

$$= \Omega_v[\rho'] \qquad \text{(II.2-7)}$$

and from the relation $\Omega[f'] > \Omega[f_o]$ it follows that

$$\Omega_v[\rho'] > \Omega_v[\rho_o] . \qquad \text{(II.2-8)}$$

We can conclude that $\Omega_v[\rho]$ reaches its minimum value when $\rho(\vec{r}) = \rho_o(\vec{r})$. These results can be expressed through the relations

$$\left.\frac{\delta \Omega_v[\rho]}{\delta \rho(\vec{r})}\right|_{\rho_o} = 0 \qquad \text{(II.2-9)}$$

$$\Omega_v[\rho_o] = \Omega . \qquad \text{(II.2-10)}$$

Remembering the general definitions of functional derivative,

$$\delta G = \int_{y_1}^{y_2} dy\, A(y, [\psi(y)])\, \delta\psi(y) \qquad \text{(II.2-11)}$$

namely

$$\frac{\delta G}{\delta \psi(y)} = A(y, [\psi(y)]) , \qquad \text{(II.2-12)}$$

we can calculate the functional derivative of the equation (II.2-9) using for $\Omega_v[\rho]$ the expression (II.2-6). We obtain in this way the fundamental equation of the theory of non-homogeneous fluids

$$V_{ext}(\vec{r}) + \mu_{in}[\rho_o; \vec{r}] = \mu \qquad \text{(II.2-13)}$$

with

$$\mu_{in} = \frac{\delta \mathcal{F}[\rho]}{\delta \rho(\vec{r})} . \qquad \text{(II.2-14)}$$

In fact, if we give some meaning to $\mathcal{F}[\rho]$, the relation (II.2-13) is an explicit equation for the equilibrium density.

Let us apply the relation (II.2-13) to the system of Section 1, that is to a system of interacting particles. The effect of interactions may be put in evidence by decomposing $\mathcal{F}[\rho]$ in an ideal part, $\mathcal{F}_{id}[\rho]$, and a part corresponding to the interactions, $\Phi[\rho]$,

$$\mathcal{F}[\rho] = \mathcal{F}_{id}[\rho] - \Phi[\rho] \quad . \tag{II.2-15}$$

The ideal contribution is easily determined from the non-interacting system (U = 0). We have for it

$$\mathcal{F}_{id}[\rho] = \beta^{-1} \int d\vec{r} \, [\ln(\rho_o(\vec{r})\Lambda) - 1] \rho_o(\vec{r}) \tag{II.2-16}$$

and

$$\rho_o(\vec{r}) = z \exp[-\beta V_{ext}(\vec{r})] \tag{II.2-17}$$

where $\Lambda = (h^2/(2\pi m k_B T))^{3/2}$ and $z = \Lambda^{-1} \exp(\beta\mu)$ is the fugacity. The relation (II.2-14) then becomes

$$\beta\mu_{in} = \ln(\Lambda\rho(\vec{r})) - c[\rho;\vec{r}] \tag{II.2-18}$$

where

$$c[\rho;\vec{r}] = \frac{\delta\Phi[\rho]}{\delta\rho(\vec{r})} \tag{II.2-19}$$

is the contribution due to the interactions. The equation (II.2-13)

can be explicitly solved and for the equilibrium density we obtain

$$\rho_o(\vec{r}) = z \exp\left\{-\beta V_{ext}(\vec{r}) + c\,[\rho_o;\vec{r}]\right\} \quad . \qquad \text{(II.2-20)}$$

This equation tells us that the effect of the interactions may be dealt with through the one-body effective potential $c\,[\rho_o;\vec{r}]$.

If we calculate the successive functional derivatives of the equation (II.2-19) we generate a hierarchy of correlation functions

$$c[\rho;\vec{r}_1,\vec{r}_2] = \frac{\delta c[\rho;\vec{r}_1]}{\delta\rho(\vec{r}_2)} = \frac{\delta^2 \Phi[\rho]}{\delta\rho(\vec{r}_1)\,\delta\rho(\vec{r}_2)}$$

$$c^{(3)}[\rho;\vec{r}_1,\vec{r}_2,\vec{r}_3] = \frac{\delta^2 c[\rho;\vec{r}_1]}{\delta\rho(\vec{r}_3)\,\delta\rho(\vec{r}_2)} \quad \text{etc.} \quad . \qquad \text{(II.2-21)}$$

The meaning of these functions is further clarified by introducing another hierarchy of functions. We define a local potential

$$u(\vec{r}) \equiv \mu - V_{ext}(\vec{r}) \qquad \text{(II.2-22)}$$

and we transform the equation (II.2-6) as

$$\Omega_v[\rho] = -\int d\vec{r}\,\rho(\vec{r})\,u(\vec{r}) + \mathcal{F}[\rho] \quad . \qquad \text{(II.2-23)}$$

If we take the functional derivative with respect to $u(\vec{r})$ we obtain

$$\frac{\delta \Omega_v [\rho]}{\delta u(\vec{r})} = -\rho_o(\vec{r}) \quad , \tag{II.2-24}$$

and that is, by successive iterations, another series of hierarchic functions. Explicitly

$$G(\vec{r}_1,\vec{r}_2) \equiv \beta^{-1} \frac{\delta \rho_o(\vec{r}_1)}{\delta u(\vec{r}_2)}$$

$$= \rho^{(2)}(\vec{r}_1,\vec{r}_2) + \rho_o(\vec{r}_1)\delta(\vec{r}_1-\vec{r}_2) - \rho_o(\vec{r}_1)\rho_o(\vec{r}_2) \tag{II.2-25}$$

where $\rho^{(2)}(\vec{r}_1,\vec{r}_2)$ is the usual pair distribution function (71). By using the eq. (II.2-20) we can write the first of equations (II.2-21) in the form

$$\beta \frac{\delta u(\vec{r}_1)}{\delta \rho_o(\vec{r}_2)} = \frac{\delta(\vec{r}_1-\vec{r}_2)}{\delta \rho_o(\vec{r}_1)} - c[\rho_o;\vec{r}_1,\vec{r}_2] \equiv K(\vec{r}_1,\vec{r}_2) \, . \tag{II.2-26}$$

One can see that $K(\vec{r}_1,\vec{r}_2)$ is the inverse of $G(\vec{r}_1,\vec{r}_2)$

$$\int d\vec{r}_1 \, G(\vec{r}_1,\vec{r}) \, K(\vec{r}_1,\vec{r}') = \delta(\vec{r}-\vec{r}') \, . \tag{II.2-27}$$

With these definitions we can see that eq. (II.2-27) is nothing but the Ornstein-Zernike equation, providing that $c[\rho_o;\vec{r}_1,\vec{r}_2] \equiv c(|\vec{r}_1-\vec{r}_2|)$. We can conclude by saying that the function $c[\rho_o;\vec{r}_1,\vec{r}_2]$ is the direct correlation function of Ornstein-Zernike, generalised to the case of

a non-uniform fluid.

The last step of the theory consists in expanding the difference in the grand canonical potential, $\Delta\Omega \equiv \Omega[\rho] - \Omega_l$ between the non-homogeneous and homogeneous fluid, in terms of the corresponding difference in density, $\Delta\rho(\vec{r}) \equiv \rho(\vec{r}) - \rho_l$, for sufficiently small differences. The effective potential $c[\rho;\vec{r}]$, as defined in eq. (II.2-19), can be functionally expanded around its value c_1 corresponding to the uniform fluid

$$c(\vec{r}) = c_l + \int d\vec{r}_2\, c(\vec{r}_1,\vec{r}_2)\,\Delta\rho(\vec{r}_2) + \frac{1}{2}\int d\vec{r}_2\, d\vec{r}_3\, c^{(3)}(\vec{r}_1,\vec{r}_2,\vec{r}_3)$$

$$\times\, \Delta\rho(\vec{r}_2)\,\Delta\rho(\vec{r}_3) + \ldots \qquad \text{(II.2-28)}$$

where $c(\vec{r}_1,\vec{r}_2)$ and $c^{(3)}(\vec{r}_1,\vec{r}_2,\vec{r}_3)$ are the quantities defined in eq. (II.2-21) (we have omitted the functional dependencies on $\rho(\vec{r})$). In the same manner one can expand the contribution of the interactions to the free energy Φ,

$$\Phi = \Phi_l + \int d\vec{r}_1\, c_l\,\Delta\rho(\vec{r}_1) + \frac{1}{2}\int d\vec{r}_1\, d\vec{r}_2\, c(\vec{r}_1,\vec{r}_2)\,\Delta\rho(\vec{r}_1)\,\Delta\rho(\vec{r}_2) + \ldots \qquad \text{(II.2-29)}$$

The difference $\Delta\Omega$ we were looking for can be easily determined by writing again the eq. (II.2-23) as

$$\Omega = \mathcal{F} - \mathcal{F}_{id} + \mathcal{F}_{id} - \int d\vec{r}\, \rho(\vec{r})\, u(\vec{r})$$

$$= -\Phi + \beta^{-1} \int d\vec{r}\, \rho(\vec{r}) \left[c(\vec{r}) - 1 \right] \qquad \text{(II.2-30)}$$

and substituing in it equations (II.2-28) and (II.2-29)

$$\beta \Delta\Omega = \beta (\Omega - \Omega_L) = -\int d\vec{r}_1\, \Delta\rho(\vec{r}_1) + \frac{1}{2} \int d\vec{r}_1 d\vec{r}_2\, c(\vec{r}_1, r_2)\, \Delta\rho(\vec{r}_2) \left[\rho(\vec{r}_1) + \rho_L \right]$$

$$+ \frac{1}{6} \int d\vec{r}_1 d\vec{r}_2 d\vec{r}_3\, c^{(3)}(\vec{r}_1, \vec{r}_2, \vec{r}_3) \left[2\rho(\vec{r}_1) + \rho_L \right] \Delta\rho(\vec{r}_2)\, \Delta\rho(\vec{r}_3) + \ldots \qquad \text{(II.2-31)}$$

II.3 Freezing in a crystalline phase

The volume change at freezing, as we can see from Tables (I.3-1) and (I.5-1) of Chapter I, only in a few cases exceeds 15 %. Then, assuming that the transition can be treated as only weakly of the first order we apply the density functional theory of Section 2 at the uniform fluid - perfect crystal transition.

In a theory of freezing one start from the fluid phase side. We describe the uniform fluid phase by a uniform density ρ_l and we inquire for the existence of coexisting crystalline solutions of prescribed lattice symmetry at the equilibrium between the two phases. We simplify the problem inquiring for freezing of the fluid into a prescribed crystal lattice leaving the question of the relative thermodynamic stability of the different crystalline lattices to later studies.

Let us expand the solid phase density in its Fourier components,

$$\rho_s(\vec{r}) = \rho_l(1+\eta) + \rho_l \sum_n \mu_n e^{i\vec{k}_n\cdot\vec{r}} \qquad \text{(II.3-1)}$$

where $\eta = \frac{\rho_s - \rho_l}{\rho_l}$ is the fractional density change and the Fourier coefficients, μ_n, are the 'order parameters' of the theory ($\mu_n = 0$

in the liquid phase, $\mu_n \neq 0$ in the solid phase). The translational and rotational crystalline symmetry of $\rho_s(\vec{r})$ is guaranteed by eq. (II.3-1) if respectively $\vec{k}_n$ is a reciprocal lattice vector of the given direct crystalline lattice and if all the μ_n, corresponding to a given 'star' of reciprocal lattice vectors, are identical. Taking the infinite volume limit and relaxing to external field V = 0, for the non-uniform equilibrium density we get the equation

$$\rho_s = \Lambda^{-1} e^{\beta\mu_s} e^{c(\vec{r})} . \qquad \text{(II.3-2)}$$

If we use for $c(\vec{r})$ the expansion (II.2-28) truncated at the second order, the equation (II.3-2) becomes

$$\rho_s(\vec{r}) = \rho_L e^{\beta\Delta\mu} e^{\left\{\int d\vec{r}_1 c(\vec{r},\vec{r}_1)[\rho(\vec{r}_1)-\rho_L] + \int d\vec{r}_1 d\vec{r}_2 c^{(3)}(\vec{r},\vec{r}_1,\vec{r}_2)[\rho(\vec{r}_1)-\rho_L][\rho(\vec{r}_2)-\rho_L]\right\}} \qquad \text{(II.3-3)}$$

where $\rho_L = \Lambda^{-1} e^{\beta\mu_L + c_L}$ and $\Delta\mu$ is the difference of chemical potentials between the two phases (vanishing at coexistence).

For the determination of coefficients $c(\vec{r},\vec{r}_1)$ and $c^{(3)}(\vec{r},\vec{r}_1,\vec{r}_2)$ we refer to the uniform liquid. It follows that

$$c(\vec{r},\vec{r}_1) = c(|\vec{r}-\vec{r}_1|) . \qquad \text{(II.3-4)}$$

Inserting the eq. (II.3-1) in eq. (II.3-3) we obtain

$$\ln \frac{\rho_s(\vec{r})}{\rho_l} = \beta\Delta\mu + c_0\eta + \frac{1}{2} c^{(3)}_{0,0}\eta^2 + \frac{1}{2}\sum_n c^{(3)}_{n,-n}\mu_n^2 + \sum_n (c_n + c^{(3)}_{n,0}\eta)\mu_n e^{i\vec{k}_n\cdot\vec{r}}$$

$$+ \frac{1}{2}\sum_{n,m} c^{(3)}_{n,m}\mu_n\mu_m e^{i(\vec{k}_n+\vec{k}_m)\cdot\vec{r}} \qquad \text{(II.3-5)}$$

where c_n and $c^{(3)}_{n,m}$ are the Fourier transforms of the Ornstein-Zernike direct correlation function, c(r), and of the triplet direct correlation function, $c^{(3)}(\vec{r}_1,\vec{r}_2,\vec{r}_3)$,

$$c_n \equiv \rho\int d\vec{r}\, c(r)\, e^{i\vec{k}_n\cdot\vec{r}} \qquad \text{(II.3-6)}$$

$$c_{n,m} \equiv \rho^2\int d\vec{r}_{12}\, d\vec{r}_{13}\, c^{(3)}(\vec{r}_1,\vec{r}_2,\vec{r}_3)\, e^{[i\vec{k}_n\cdot\vec{r}_{12} + i\vec{k}_m\cdot\vec{r}_{13}]}. \qquad \text{(II.3-7)}$$

The integration on $\vec{r}$ of the exponential form of the eq. (II.3-5) leads, for the components at $\vec{k}_n = 0$ and at $\vec{k}_n \neq 0$, to the set of equations

$$1+\eta = \frac{e^{x_0+\beta\Delta\mu}}{V}\int d\vec{r}\, e^{\left\{\sum_n x_n e^{i\vec{k}_n\cdot\vec{r}} + \sum_{n,m} x_{n,m} e^{i(\vec{k}_n+\vec{k}_m)\cdot\vec{r}}\right\}}, \qquad \text{(II.3-8)}$$

$$\mu_i = \frac{e^{x_0+\beta\Delta\mu}}{V}\int d\vec{r}\, e^{i\vec{k}_i\cdot\vec{r}}\, e^{\left\{\sum_n x_n e^{i\vec{k}_n\cdot\vec{r}} + \sum_{n,m} x_{n,m} e^{i(\vec{k}_n+\vec{k}_m)\cdot\vec{r}}\right\}}, \qquad \text{(II.3-9)}$$

where for conciseness we have put

$$x_0 = c_0\eta + \frac{1}{2}c^{(3)}_{0,0}\eta^2 + \frac{1}{2}\sum_n c^{(3)}_{n,-n}\mu_n^2 ,$$

$$x_n = (c_n + c^{(3)}_{n,0}\eta)\mu_n ,$$

$$x_{n,m} = \frac{1}{2}c^{(3)}_{n,m}\mu_n\mu_m .$$

The equations (II.3-8) and (II.3-9) can be solved for a set a values $\{c_n\}$ and $\{c_{n,m}\}$. The conditions $\eta = 0$ and $\mu_i = 0$, corresponding to the liquid phase, are always a solution while a solution with $\eta \neq 0$, $\mu_i \neq 0$ and periodic $\rho(\vec{r})$ can occur for an opportune choice of $\{c_n\}$ and $\{c_{n,m}\}$.

The two phases will be in equilibrium if the difference between the thermodynamic potential, Ω_s , of the solid and that, Ω_l , of the liquid is zero. The thermodynamic potential variation in the liquid-solid transformation, $\Delta\Omega$, is obtained by substituing in the eq. (II.2-31) the Fourier expansion (II.3-1) and using the equations (II.3-6) and (II.3-7)

$$\beta\frac{\Delta\Omega}{N_l} = (c_0-1)\eta + \frac{1}{2}(c_0+c^{(3)}_{0,0})\eta^2 + \frac{1}{3}c^{(3)}_{0,0}\eta^3 + \frac{1}{2}\sum_n[c_n+(2\eta+1)c^{(3)}_{n,0}]\mu_n^2$$

$$+ \frac{1}{3}\sum_{n,m} c^{(3)}_{n,m}\mu_n\mu_m\mu_p \quad . \qquad \text{(II.3-10)}$$

The last sum will appear only if the condition $\vec{k}_p = \vec{k}_n + \vec{k}_m$ is satisfied. The equations (II.3-8), (II.3-9) and (II.3-10) are the basic equations that is necessary to solve in any application of the

freezing theory. The first order character of the liquid/solid phase transition is preserved by the non-linearity of the equations.

Some insight into the physical interpretation of the freezing process can be gained if we are able to connect quantities like $c(\vec{r})$ and $c(\vec{r}_1,\vec{r}_2)$, that appear in the freezing equations, to more immediate physical concepts.

It is well known that the static response function $\chi(k)$ of a classical fluid to a weak external perturbation, which couples with the density fluctuations, is correlated with the static structure factor, S(k), through the equation

$$\chi(k) = -\frac{\rho}{k_B T} S(k) \quad . \qquad \text{(II.3-11)}$$

And, if we remember the Ornstein-Zernike relation, we can also connect the response function to the Fourier transform of the direct correlation function, c(k), using the relation

$$S(k) = \frac{1}{1 - c(k)} \quad . \qquad \text{(II.3-12)}$$

S(k) is simply proportional to the static response and it can be interpreted as a 'generalised softness' of the fluid in

response to a weak density perturbation with wave number $\vec{k}$. This interpretation of S(k) is a direct extension of the well known relation

$$\lim_{\vec{k}\to 0} S(k) = \rho k_B T K_T \qquad \text{(II.3-13)}$$

where K_T, the isothermal compressibility of the fluid, denotes the degree of 'softness' of the system in response to a uniform compression. The equation (II.3-11) is the generalisation of eq. (II.3-13) to an arbitrary wave vector.

In Fig. (II.3-1) is shown the structure factor, S(k), for a monatomic fluid in two different thermodynamic states, (i) real gas and (ii) liquid near freezing. Qualitatively one can state that it is much more difficult to compress the liquid in the thermodynamic limit (rel. (II.3-13)), and that it is instead much softer and can be easily modulated in the density through perturbations with wave number in the region of the peaks (rel. (II.3-11)).

Let us return now to the equations of freezing (II.3-8), (II.3-9) and (II.3-10). The eq. (II.3-10) is composed of the sum of terms depending on η and terms depending on μ_n. Then the solution $\Delta\Omega = 0$, which corresponds to the equilibrium of the two phases, exists if the change in free energy due to the change in the average

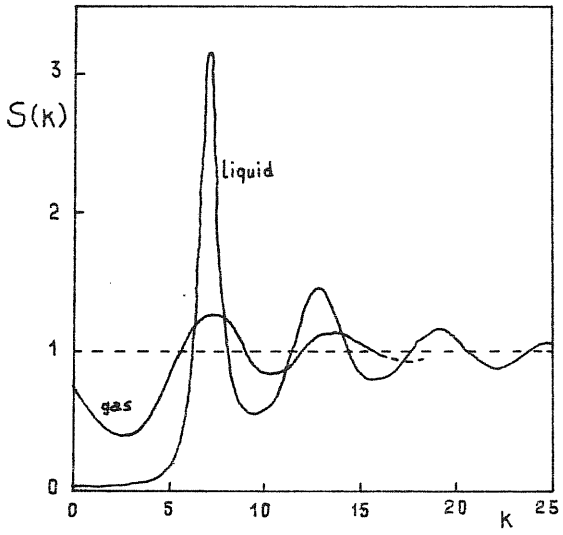

Fig. II.3-1: Structure factor, S(k), for two thermodynamic states: real gas and liquid near freezing.

density is compensated by the change in free energy due the modulation in density. More particularly, free energy is gained in the first case while it is expended in the second case. The most efficient way of 'switching on' the transition is therefore to modulate the system with a perturbation with wave number in the region of the peaks.

The development and first applications of this theory have been given by Ramakrishnan and Yussouff (17). They analyse the freezing of the hard sphere system and of argon in the f.c.c. lattice,

the freezing of molten sodium in the b.c.c. lattice and the freezing of the hard disk system in a two-dimensional h.c.p. structure.

The input information required are only the crystal structure and the fluid compressibility (related to c_o). In Table (II.3-1) the crystallographic data for the s.c., f.c.c. and b.c.c. lattices are collected. The first 12 stars of reciprocal lattice vectors of the s.c. structure are classified according to the increasing value of $|\vec{k}|^2 = h^2 + k^2 + l^2$.

The output obtained are values of the direct correlation functions c_j, of the volume change on freezing η, of the entropy change ΔS and of the Debye-Waller factor at freezing.

In Table (II.3-2) are reported the freezing parameters for argon (f.c.c.) determinad by Ramakrishnan and Yussouff. The results in the first row have been obtained using only the first star of the reciprocal lattice vectors, of the type (1,1,1). In the second row, the results obtained introducing a second star of reciprocal lattice vectors of the type (3,1,1) are shown. The third row reports the results obtained introducing the three-body direct correlation function $c_{oo}^{(3)}$ in the equation for the grand potential change. The same considerations hold for the freezing parameters of sodium (b.c.c.) listed in Table (II.3-3). The numbers are all in good agreement with those available experimentally.

$(\vec{k}_n)^2=n$	$\vec{k}_n$	s_n	B.c.c.	F.c.c.	exp $i(\vec{k}_n \cdot \vec{r})$
0	(0,0,0)	1	yes	yes	1
1	(1,0,0)	6	no	no	2(cos x + cos y + cos z)
2	(1,1,0)	12	yes	no	4(cos x cos y + cos x cos z + cos y cos z)
3	(1,1,1)	8	no	yes	8(cos x cos y cos z)
4	(2,0,0)	6	yes	yes	2(cos2x + cos2y + cos2z)
5	(2,1,0)	24	no	no	4(cos x cos2y + cos2x cos y + cos x cos2z + cos2x cos z + cos y cos2z + cos2y cos z)
6	(2,1,1)	24	yes	no	8(cos x cos y cos2z + cos x cos2y cos z + cos2x cos y cos z)
7	---	0	---	---	----------
8	(2,2,0)	12	yes	yes	4(cos2x cos2y + cos2x cos2z + cos2y cos2z)
9	(2,2,1)	24	no	no	8(cos2x cos2y cos z + cos2x cos y cos2z + cos x cos2y cos2z)
	(3,0,0)	6	no	no	2(cos3x + cos3y + cos3z)
10	(3,1,0)	24	yes	no	4(cos x cos3y + cos3x cos y + cos x cos3z + cos3x cos z + cos y cos3z + cos3y cos z)
11	(3,1,1)	24	no	yes	8(cos3x cos y cos z + cos x cos3y cos z + cos x cos y cos3z)
12	(2,2,2)	8	yes	yes	8(cos2x cos2y cos2z)

Table II.3-1: The successive stars of the s.c. structure listed according to increasing wave-vector length $|\vec{k}_n| = k_n$ up to $k_n = (12)^{1/2}$. s_n is the number of r.l.v. in the star n.

	c_j	c_n	η	μ_j	μ_n
Theory I (one order parameter)	0.95	0.00	0.074	0.059	0.20
Theory II (two order parameters)	0.65	0.23	0.270	0.90	0.75
Theory III (two order parameters with $c_{oo}^{(3)}$=-110.0)	0.65	0.23	0.166	0.91	0.74
Experiment	0.65	0.23	0.148	----	----

Table II.3-2: Freezing parameters for argon (f.c.c.). From ref.(17).

	c_j	c_n	η	μ_j	μ_n
Theory I (one order parameter)	0.69	0.00	0.048	0.70	0.31
Theory II (two order parameters)	0.63	0.07	0.052	0.71	0.71
Theory III (two order parameters, $c_{oo}^{(3)}$=-75.0, $c_{j'j''}^{(3)}$=-0.103)	0.67	0.13	0.029	0.63	0.34
Experiment	0.66	0.12	0.026	----	----

Table II.3-3: Freezing parameters for sodium (b.c.c.). From ref. (17).

II.4 A simple application to freezing of metallic systems

The volume change associated with the liquid/solid transition of metallic systems rarely exceeds a value of 6 % for metals that freeze in b.c.c., f.c.c. and h.c.p. lattices (see Table (I.3-1)). This suggests to consider the fluid phase as 'virtually' incompressible. So the freezing equations can be simplified using the incompressibility limit approximation , i.e. volume change $\eta \to 0$, $-c_o \to \infty$ but $c_o\eta$ finite. Using this approximation we have applied the Ramakrishnan-Yussouff theory to the freezing of metallic systems.

For molten metals that freeze in the b.c.c. lattice we have used only the smallest set of reciprocal lattice vectors ignoring all other order parameter modes. The smallest set $\{\vec{G}_1\}$ are reciprocal vectors of the type (1,1,0) and correspond to the principal peak in the structure factor S(k) (see Fig. (II.4-1)).

The structure factor of a f.c.c. metal (Al) is shown in Fig. (II.4-2). The dominant order parameter comes from the density fluctuation mode with a wave vector k corresponding to the position of the first peak. Placing the first star of reciprocal lattice vectors (vectors of the type (1,1,1)) under the first peak we see that also the second star of reciprocal lattice vectors (vectors of

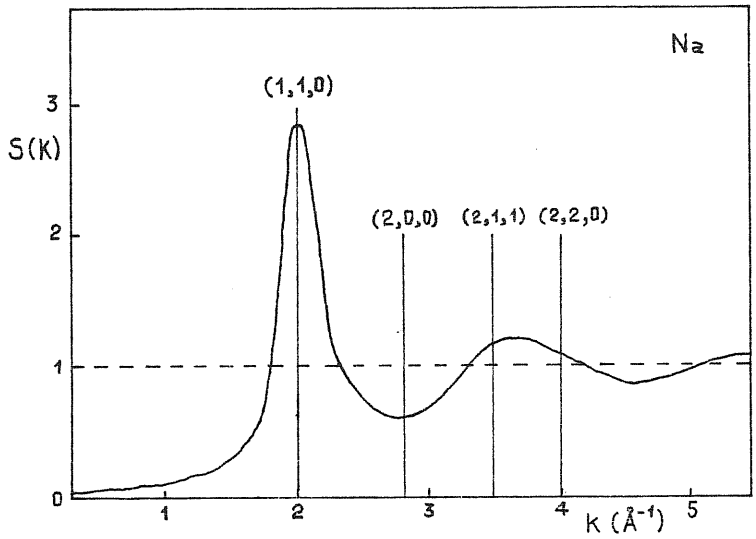

Fig. II.4-1: Structure factor of molten Na near freezing. The vertical lines are the relative star positions of r.l.v. for the b.c.c. lattice.

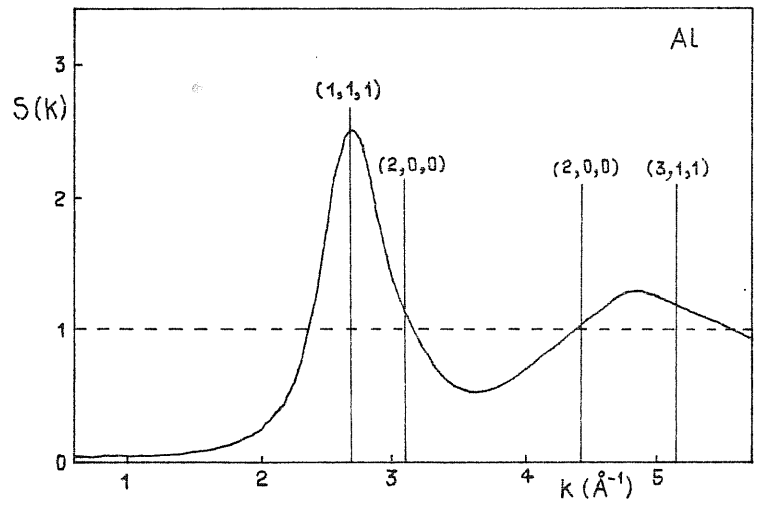

Fig. II.4-2: Structure factor of molten Al near freezing. The vertical lines are the relative star positions of r.l.v. for the f.c.c. lattice.

the type (2,0,0)), is situated in the region of the first principal peak of S(k). For the f.c.c. metals we have done two distinct calculations. In the first one only the first star of r.l.v. has been considered while in the second one we have added the second star $\{2,0,0\}$ to the first star $\{1,1,1\}$. In the second case the freezing equations are practically equal to the first case, the only difference being the number of reciprocal lattive vectors taken into account.

For metals that freeze in the h.c.p. lattice quite similar considerations to the b.c.c. case hold. The structure factor S(k) of zinc is illustrated in Fig. (II.4-3). Under the first peak we have placed the second star of r.l.v. because the vectors of the first star have a too small length. Also in this case two distinct calculations have been performed. In the first calculation we have used the set named 2 (see Fig. (II.4-3)), while in the second calculation we have used both sets 2 and 1. Nevertheless, the equations necessary to describe the freezing into a h.c.p. lattice are different from those of the f.c.c. and b.c.c. cases. The basic difference resides in the fact that in the h.c.p. lattice there are two atoms per unit cell. The adapted set of freezing equations for the h.c.p. systems have been developed by Yussouff (72) introducing a 'density structure factor' f in order to take account for the density variations within the unit cell.

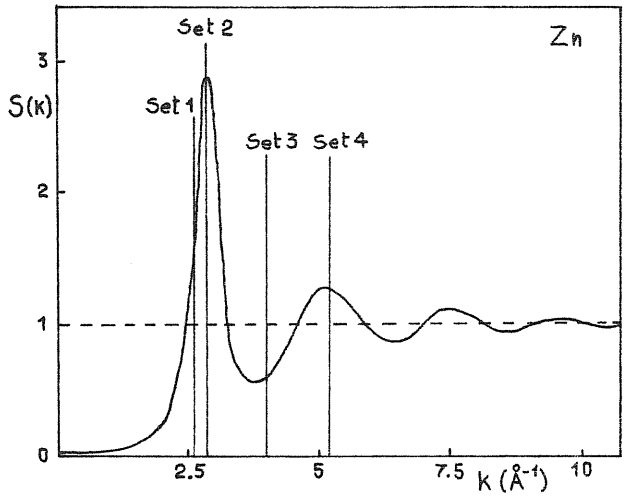

Fig. II.4-3: Structure factor of molten Zn near freezing. The vertical lines are the relative star positions of r.l.v. for the h.c.p. lattice. Set 1: (100), (010), (1-10), (-100), (0-10), (-110). Set 2: (101), (-101), (0-11), (-10-1), (011), (10-1), (01-1), (0-1-1), (1-11), (-111), (-11-1), (1-1-1). Set 3: (102), (-102), (012), (0-12), (-10-2), (10-2), (0-1-2), (01-2), (1-12), (-112), (-11-2), (1-1-2). Set 4: (112), (-1-12), (11-2), (-1-12), (2-12), (-212), (1-22), (-122), (-21-2), (2-1-2), (-12-2), (1-2-2).

The results of all calculations are shown in Table (II.4-1) in which the experimental ranges are derived considering all the metals listed in Table (I.3-1). Qualitative agreement with the experimental values is obtained despite the roughness of the model.

		c_1	$-\eta c_o$
B.C.C. metals	Theory	0.7	1.71
	Exp. range	0.58 - 0.64	0.82 - 1.51
F.C.C. metals	Theory I (1 star of r.l.v.)	0.98	0.8
	Theory II (2 stars of r.l.v.)	0.56	0.8
	Exp. range	0.59 - 0.64	1.2 - 3.5
H.C.P. metals	Theory I (1 star of r.l.v.)	0.94	1.35
	Theory II (2 stars of r.l.v.)	0.63	1.35
	Exp. range	0.6 - 0.65	1.7 - 3.1

Table II.4-1: Freezing parameters for B.C.C., F.C.C. and H.C.P. metals in the'incompressibility limit' approximation. Experimental ranges refere to the metals listed in Table (I.3-1).

II.5 Application of the theory of freezing to the hard sphere system

The freezing of the hard sphere liquid is one of the most direct applications of the theory. Using analytical structural information about the liquid of hard spheres and no computer simulation results, Haymet (68) has been able to predict the liquid and solid densities at which the freezing into a face cubic centred lattice occours. We shortly present the Haymet results.

The theory of freezing as it has previously presented needs, for the purpose of calculation, same well-defined approximations. The first approximation concernes the expansion (II.3-1). The sum that appears is, in principle, over an infinite number of vectors but in practice it must be truncated after a finite number of terms. The second approximation is connected with the expansion of $c(\vec{r})$ around the value C_1 corresponding to the uniform liquid (eq. (II.2-28)). This expansion is truncated after the second order terms $c^{(3)}(\vec{r}_1,\vec{r}_2,\vec{r}_3)$. The third approximation consists in putting equal to zero the coefficients $c^{(3)}_{nm}$ for $\vec{k}_n$ and $\vec{k}_m$ different from zero that appear in the equations (II.3-8), (II.3-9) and (II.3-10). The last approximation concerns the choice of a theory of the liquid structure from which to obtain the coefficients c_n and $c^{(3)}_{no}$. The analytic

solution of Thiele (73) and Wertheim (74) of the integral equation of Percus - Yevick (75), has been chosen. In this scheme we have

$$c_n = -4\pi\rho\sigma^3(k\sigma)^{-1}\left[\lambda_1 I_1(k_n) + 6y\lambda_2 I_2(k_n) + \frac{1}{2}y\lambda_1 I_4(k_n)\right], \quad \text{(II.5-1)}$$

$$c_{n,0} = -c_n + \rho\frac{\partial}{\partial\rho}c_n \quad \text{(II.5-2)}$$

where

$$I_j(k_n) = \int_0^1 dx\; x^j \sin(k_n\sigma x) \;,$$

$$\lambda_1 = (1+2y)^2/(1-y)^4 \quad \text{and} \quad \lambda_2 = -(1+y/2)/(1-y)^4$$

with $y = \frac{\pi}{6}\rho\sigma^3$ packing fraction. The equations of the freezing (II.3-8), (II.3-9) and (II.3-10), with the use of structural data of the liquid (equations (II.5-1) and (II.5-2)) can be numerically solved.

Table (II.5-1) and Fig. (II.5-1) show the freezing results of the hard sphere into the f.c.c. lattice. As clearly shown by the Table, 15 shells of R.L.V. have been used to obtain convergence. From Fig. (II.5-2) one can see the relative position of the 15 shells once the first one has been fixed at the first peak position of the structure factor S(k). In Table (II.5-2) the values of the liquid and solid densities and of the volume change are compared with those of the

$\lvert\vec{k}_n\rvert^2$	s_n	k_n	μ_n	x_n	A_n
0			0.060	-5.096	
3	8	(111)	0.998	0.719	0.895
4	6	(200)	0.891	-0.027	0.436
8	12	(220)	0.918	-0.151	-1.483
11	24	(311)	0.875	0.244	0.898
12	8	(222)	0.863	0.080	0.425
16	6	(400)	0.805	-0.252	-1.138
19	24	(331)	0.773	0.005	-0.188
20	24	(420)	0.760	0.079	0.164
24	24	(422)	0.717	0.079	0.383
27	8	(333)	0.686	-0.061	-0.237
27	24	(511)	0.680	-0.060	-0.237
32	12	(440)	0.636	-0.068	-0.407
35	48	(531)	0.608	0.017	0.017
36	24	(442)	0.601	0.039	0.146
36	6	(600)	0.593	0.039	0.146

Table II.5-1: Freezing parameters for hard spheres at the density 0.976 from the Percus-Yevick structure factor. x_n is defined as $x_0 = c_0\eta + \frac{1}{2}c_{00}^{(3)}\eta^2 + \frac{1}{2}\sum_n c_{n0}^{(3)}\mu_n$; $x_n = (c_n + c_{n0}^{(3)}\eta)\mu_n$. A_n is defined as $c_n + (2\eta+1)c_{n0}^{(3)}$. Data from ref. (68).

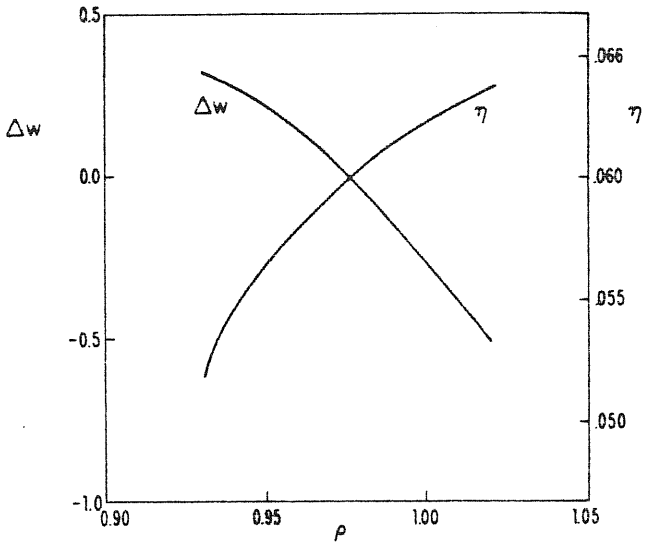

Fig. II.5-1: The thermodynamic potential Δw and the fractional density change on freezing η for the hard sphere freezing. From ref. (68).

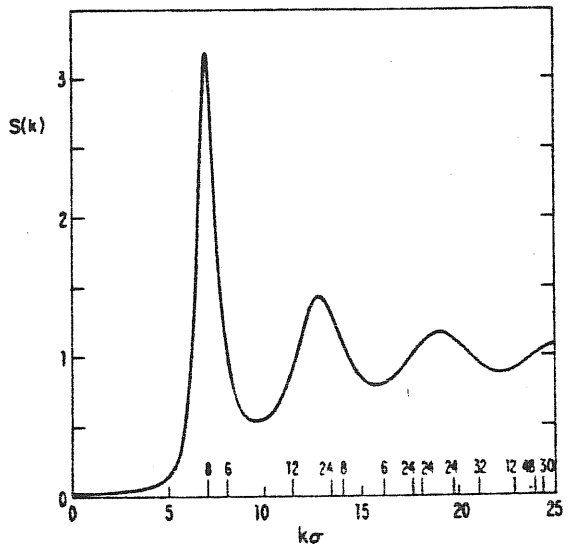

Fig. II.5-2: The liquid structure factor, S(k), for hard spheres at a density close to freezing ρ = 0.95 and the relative magnitudes of the r.l.v. of the f.c.c. crystal. From ref. (68).

	Theory	Monte Carlo simulations
ϱ_s	1.035	1.036 - 1.041
ϱ_l	0.976	0.939 - 0.948
η	0.06	0.09 - 0.11

Table II.5-2: Numerical and computer predictions for freezing of hard spheres into an f.c.c. lattice. The values are in units of σ^3, where σ is the hard sphere diameter.

Monte Carlo simulation of Hoover and Ree (39). The predictions of the theory are in good agreement with them.

The freezing of the hard sphere system has been reinvestigated by us using a self-consistent procedure for the choice of the lattice constant and consequently for the input liquid structural data. No solution of the set of freezing equations was found. Afterwards, we have enquired for the freezing of hard spheres into a b.c.c. and a h.c.p. lattice. Also, in the b.c.c. case no solution has been found. The main reason for this failure is the strongly negative value of the direct correlation function $c_{\vec{G}_2}$ ($\vec{G}_2$ denoting the (2,0,0) star). Nevertheless, we cannot exclude the freezing of hard spheres into a b.c.c. phase because of omission of terms like the three body correlation function $c^{(3)}_{\vec{G}_1,\vec{G}_2}$ in the freezing equations. That this would be the case has been demonstrated by Rovere and Tosi (76) for the freezing of a classical plasma on a neutralizing background into a b.c.c. lattice. They found that a quantitative role is played by couplings between some of the order parameters of the transition, the more important one being that between the order parameters $\mu_{\vec{G}_1}$ and $\mu_{\vec{G}_2}$, i.e. $c^{(3)}_{\vec{G}_2,\vec{G}_1}$.

At the time of writing, we have only preliminary results for the freezing of hard spheres into the h.c.p. lattice.

II.6 Entropy change on freezing

The change of the thermodynamic quantities on melting/freezing is experimentally determined by measuring the (P-T)-coordinates of the melting curve and one of the quantities appearing in Clausius-Clapeyron equations $\frac{dP}{dT} = \frac{\Delta H}{T\Delta V}$, i.e. either the heat of melting ΔH or the volume change ΔV at melting. From calorimetric measurements, the enthalpy of melting per mole (or per particle) can be obtained. These experimental values of the entropy change must be compared with those coming from the theory of freezing.

From the theory, which is developed in the grand canonical ensemble, we obtain the change of the grand potential "per unit volume", $\Delta\Omega/V$. The corresponding entropy change per unit volume, defined as $\frac{\Delta S}{V} = (S_s - S_l)/V$, is given by

$$\frac{\Delta S}{V} = -\left.\frac{\partial(\Omega_s/V)}{\partial T}\right|_{V,\mu} + \left.\frac{\partial(\Omega_l/V)}{\partial T}\right|_{V,\mu} = -\left.\frac{\partial(\Delta\Omega/V)}{\partial T}\right|_{V,\mu} \qquad \text{(II.6-1)}$$

However, caution is needed in using the theoretical expression of the grand potential change $\Delta\Omega$ (eq. (II.3-10)) in this calculation, since the theory is approaching the coexistence point from the liquid side only. If no caution is taken on this point, one finds a result for ΔS which (obviously incorrectly) depends on the atomic mass.

To overcome this difficulty we have sought to determine the entropy change on freezing by starting from the chemical potential change $\Delta\mu$. More precisely, we have solved the set of equations

$$\frac{1}{3}c_{0,0}^{(3)}\eta^3+\frac{1}{2}(c_0+c_{0,0}^{(3)})\eta^2+(c_0-1)\eta+\frac{1}{2}\sum_n\left[c_n+(2\eta+1)c_{n,0}^{(3)}\right]\mu_n^2=0 \qquad \text{(II.6-3)}$$

$$\mu_i=(1+\eta)\frac{\int d\vec{r}\, e^{i\vec{k}_i\cdot\vec{r}}\, e^{\left\{\sum_n x_n e^{i\vec{k}_n\cdot\vec{r}}+\sum_{n,m}x_{n,m}e^{i(\vec{k}_n+\vec{k}_m)\cdot\vec{r}}\right\}}}{\int d\vec{r}\, e^{\left\{\sum_n x_n e^{i\vec{k}_n\cdot\vec{r}}+\sum_{n,m}x_{n,m}e^{i(\vec{k}_n+\vec{k}_m)\cdot\vec{r}}\right\}}}\,, \qquad \text{(II.6-4)}$$

the condition on the equality of the chemical potentials of the two phases at equilibrium being expressed by

$$\beta\Delta\mu=\ln(1+\eta)-x_0-\ln\left\{\frac{1}{V}\int d\vec{r}\, e^{\left\{\sum_n x_n e^{i\vec{k}_n\cdot\vec{r}}+\sum_{n,m}x_{n,m}e^{i(\vec{k}_n+\vec{k}_m)\cdot\vec{r}}\right\}}\right\}=0 \qquad \text{(II.6-5)}$$

By solving the new freezing equations (II.6-3), (II.6-4) and (II.6-5) we get a function $\Delta\mu=\Delta\mu(\rho_l)$ which vanishes at the transition.

We now present the application of the above freezing equations to the entropy change determination of the hard sphere system.

From thermodynamics we have for the entropy change per particle

$$\Delta s=s_s-s_l=\left.\frac{\partial\mu_l}{\partial T}\right|_p-\left.\frac{\partial\mu_s}{\partial T}\right|_p=\left.\frac{\partial\Delta\mu}{\partial T}\right|_p \qquad \text{(II.6-6)}$$

and using the P-Y equation of state for hard spheres,

$$\frac{P}{\rho k_B T} = \frac{1 + y + y^2}{(1-y)^3} \qquad \text{(II.6-7)}$$

we get

$$\frac{\Delta s}{k_B} = \rho_l \frac{1 - y^3}{(1+2y)^2} \frac{\partial(\beta\Delta\mu)}{\partial\rho} \qquad \text{(II.6-8)}$$

in which all the quantities can be extracted from the theory.

By means of $\Delta\mu$ one can also, in a certain sense, verify the thermodynamic self-consistency of the theory. In fact, starting from the thermodynamic relation $v = \left.\frac{\partial\mu}{\partial P}\right|_T$ we get, for hard spheres, the equality

$$\frac{1}{1+\eta} = -\rho_l \frac{(1-y)^4}{(1+2y)^2} \frac{\partial(\beta\Delta\mu)}{\partial\rho} \qquad \text{(II.6-9)}$$

which must be verified at the two-phase equilibrium once we have solved the equations (II.6-3), (II.6-4) and (II.6-5). Using 21 stars of reciprocal lattice vectors, we have obtained for the entropy change $\Delta s = -0.62\ k_B$ (to be compared with $\Delta s_{exp} = -1.16\ k_B$ from Table (I.2-1)). The values of the two sides of the equality (II.6-9) differ for about 24 %. The reason for which this "thermodynamic consistency" fails is not yet well understood because of the complexity of the approsimations involved.

CHAPTER III

FREEZING OF IONIC LIQUIDS

CAHPTER III

Freezing of ionic liquids

In this Chapter we present a theory for the process of freezing of ionic liquids (19,19,77). For this aim one will have to refer to much of the content of Section 5 of Chapter I and of Section 3 of Chapter II, i.e. the introductory survey on the experimental data of the liquid-solid transition in ionic systems, and the general description of the freezing in a crystalline phase.

Section 1 of this Chapter deals with main features of ionic systems near freezing. The structural properties, as derived from neutron scattering experiments, of the alkali chlorides NaCl, KCl and RbCl and of 2 : 1 chlorides $CaCl_2$, $SrCl_2$, $BaCl_2$ and $ZnCl_2$ are compared and contrasted. In this Section we also put in evidence the transition of $SrCl_2$ and $BaCl_2$ into a superionic phase with fluorite-type structure.

In Sections 2 and 3 we examine more specifically the freezing mechanisms of molten alkali halides typified by NaCl and RbCl on one hand, and of molten fluorite-type materials $SrCl_2$ and $BaCl_2$ on the other hand. A rather different mechanism is found for these two classes of materials since: (i) the volume change across

the transition for alkali chlorides is large ($\sim$ 20 %) and the fluid phase is characterised by a strong charge ordering; (ii) the volume change for 2 : 1 chlorides is small ($\sim$ 3 %), they freeze into a superionic phase and the liquid is characterised by a strong ordering of the divalent cation component. The results we have obtained are presented and discussed in these Sections.

In Section 4 we give a comparative discussion of freezing for the two previous classes of compounds, based on the numerical results and on the freezing mechanism described in Sections 2 and 3.

III.1 Partial structure factors and pair correlation functions

In view of the application of the theory of freezing to the alkali halides and to the superionic conductors it is essential to know the liquid structure. In fact, one will finds that the freezing process is strictly related to the behaviour near freezing of the partial structure factors $S_{\alpha\beta}(k)$ or of the Bhatia-Thornton (78) structure factors $S_{NN}(k)$, $S_{NQ}(k)$, $S_{QQ}(k)$. First of all we review the way in which all the structural informations can be extracted from the X-ray and neutron diffraction experiments.

(a) X-ray and neutron diffraction

The natural way to introduce the liquid structure factor, $S(k)$, is to look at the scattered intensity $I(\theta)$ measured in an X-ray diffraction experiment. If we introduce the variable $k = (4\pi/\lambda)\sin\theta$, in which λ is the wavelength of the incident radiation and θ is half the scattering angle, then $S(k)$ is defined (for monatomic fluids), by

$$S(k) = I(\theta)/(N f^2(k)) \qquad \text{(III.1-1)}$$

where N is the number of atoms in the liquid sample and f(k) is the atomic scattering amplitude. The liquid structure factor is related to the pair distribution function g(r) through

$$S(k) = 1 + 4\pi n \int_0^\infty [g(r) - 1] \frac{\sin(kr)}{kr} r^2 dr \qquad \text{(III.1-2)}$$

where n is now the number density of particles in the sample. g(r) is defined so that $dn_r = 4\pi n g(r) r^2 dr$ gives the number of paticles occupying a spherical shell of radii r and r + dr. Alternatively

$$g(r) = 1 + \frac{1}{2\pi^2 n} \int [S(k) - 1] \frac{\sin(kr)}{r} k\, dk \ , \qquad \text{(III.1-3)}$$

which allow us to derive g(r) rather directly from the measured S(k).

For a two-component liquid, such as NaCl, there are three partial pair distribution functions $g_{++}(r)$, $g_{--}(r)$ and $g_{+-}(r)$ and correspondingly three partial structure factors $S_{++}(k)$, $S_{--}(k)$ and $S_{+-}(k)$. The partial pair distribution funtion $g_{\alpha\beta}(r)$ is defined by placing an α-type ion at the origin and asking for the number of β-type ions that occupy a spherical shell of radii r and r + dr. That number is given by

$$dn_r = 4\pi n_\beta g_{\alpha\beta}(r) r^2 dr \qquad \text{(III.1-4)}$$

where $n_\beta = N_\beta / V$ is the number density of ions of species β (for alkali halides, $n_+ = n_- = 1/2\ n$ with n the total number density of ions). The partial structure factors are defined by

$$S_{\alpha\beta}(k) = \delta_{\alpha\beta} + 4\pi(n_\alpha n_\beta)^{1/2} \int_0^\infty [g_{\alpha\beta}(r) - 1] \frac{\sin(kr)}{kr} r^2 dr \quad . \quad \text{(III.1-5)}$$

The scattered intensity per unit volume is given by

$$I(k) = n_+ f_+^2(k) S_{++}(k) + n_- f_-^2(k) S_{--}(k) + 2(n_+ n_-)^{\frac{1}{2}} f_+(k) f_-(k) S_{+-}(k) \quad \text{(III.1-6)}$$

where $f_\alpha(k)$ is the scattering amplitude of the ions of species α. The experimental results are often presented in the form of functions $a_{\alpha\beta}(k)$ defined by

$$a_{\alpha\beta}(k) = 1 + \frac{n}{(n_\alpha n_\beta)^{1/2}} (S_{\alpha\beta}(k) - \delta_{\alpha\beta}) \quad \text{(III.1-7)}$$

in terms of which the scattered intensity is given by

$$I(k) = \sum_\alpha n_\alpha f_\alpha^2(k) + \sum_{\alpha,\beta} \left(\frac{n_\alpha n_\beta}{n}\right) f_\alpha(k) f_\beta(k) [a_{\alpha\beta}(k) - 1] \quad . \quad \text{(III.1-8)}$$

The same expressions (III.1-6) and (III.1-8) hold for neutron diffraction, with $f_\alpha(k)$'s replaced by the neutron scattering

length f_α . f_α is now independent from k but dependent on the isotopic state.

The experimental scattered intensity I(k) is a weighted average of all the partial structure factors but if I(k) can be changed by isotopic substitution, enough data can be obtained in order to extract the partial structure factors. More precisely, for a binary fluid (such as molten NaCl) the "isotopic substitution" technique requires measurements from three samples of the same chemical material prepared with different isotopic concentrations of the components. The different isotopic concentrations change the value of each f_α that can be made very different in three samples, while the partial structure factors remain the same in the three samples.

This method was applied extensively to the study of molten alkali halides (79 - 82) and of molten alkaline-earth halides (83 - 85). The experimental results are sensitive to errors in the neutron scattering amplitudes. One good way to test the reliability of these experimental results is to compare the measured X-ray pattern with the one obtained from neutron data. Such a test is shown in Fig. (III.1-1) for molten NaCl (81). In order to obtain a good agreement an adjustement of the scattering amplitude of ^{37}Cl is necessary.

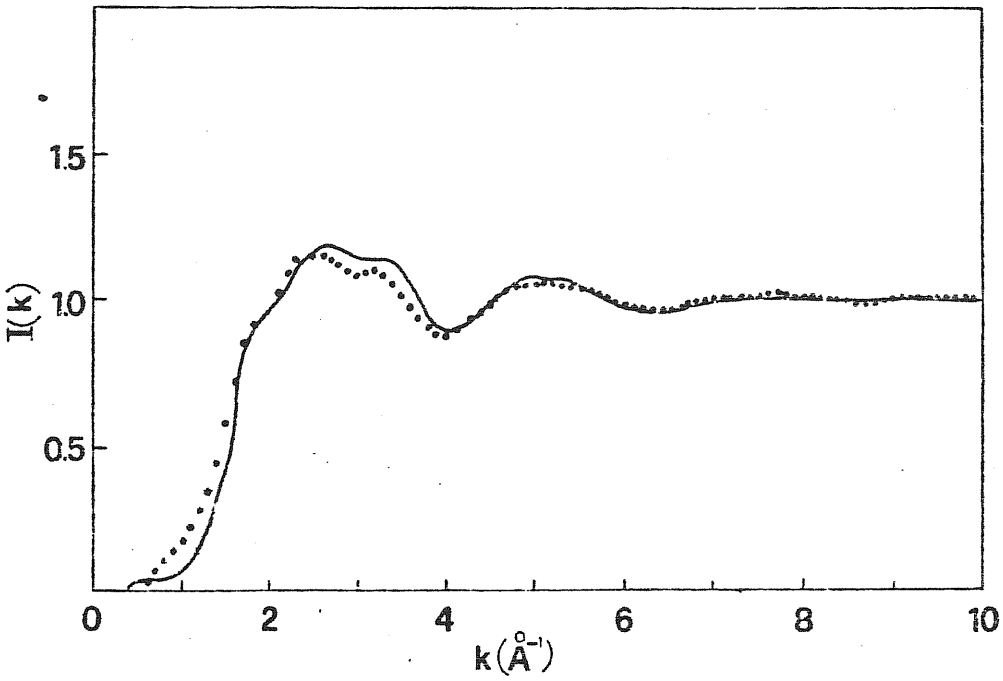

Fig. III.1-1: The normalized coherent x - ray scattering intensity i (k) of molten NaCl. Full curve, derived from neutron partial structure factors; dotted curve, from x - ray diffraction experiments. From ref. (81).

(b) Structure of molten salts

Let us first consider the results of a neutron experiment on the molten NaCl at 875 °C, carried out by Biggin and Enderby (81). The partial structure factors and the pair distribution functions are shown in Figures (III.1-2) and (III.1-3). From these data some general properties of $S_{\alpha\beta}(k)$ and $g_{\alpha\beta}(r)$ for 1 : 1 ionic melts

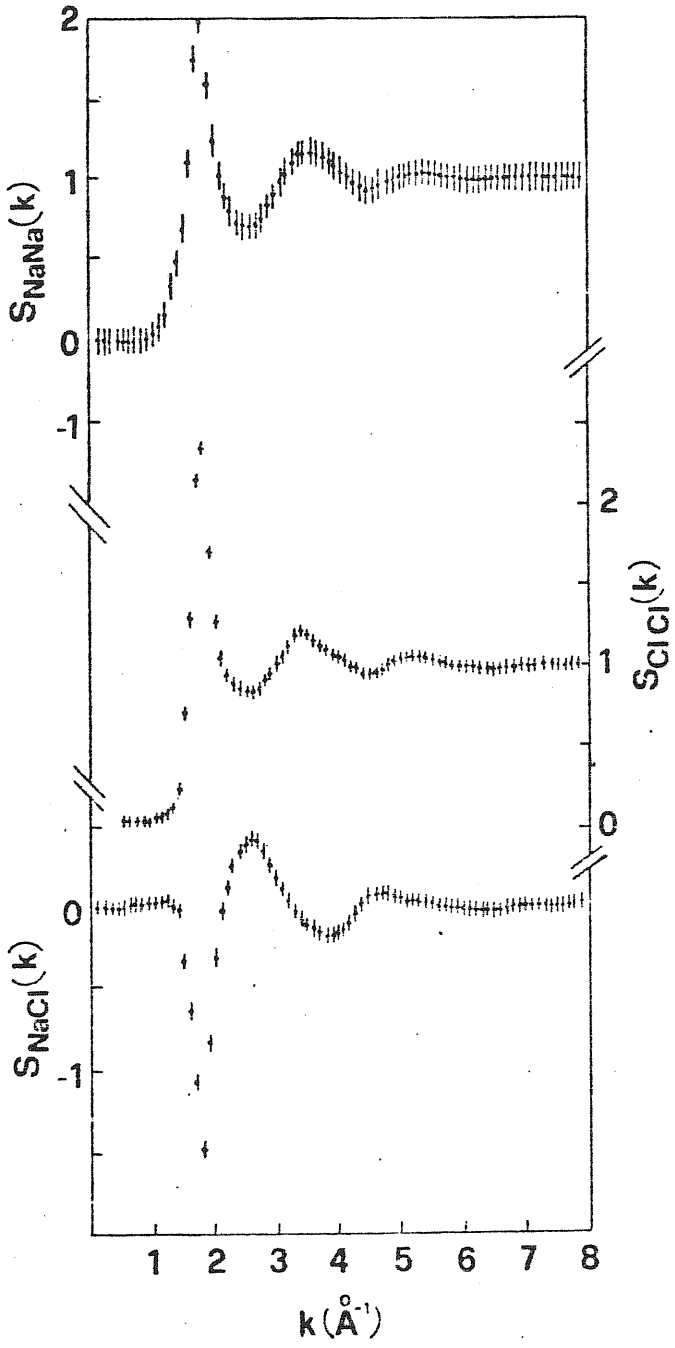

Fig.III.1-2: Partial structure factors for molten NaCl at 875 °C. From ref. (81).

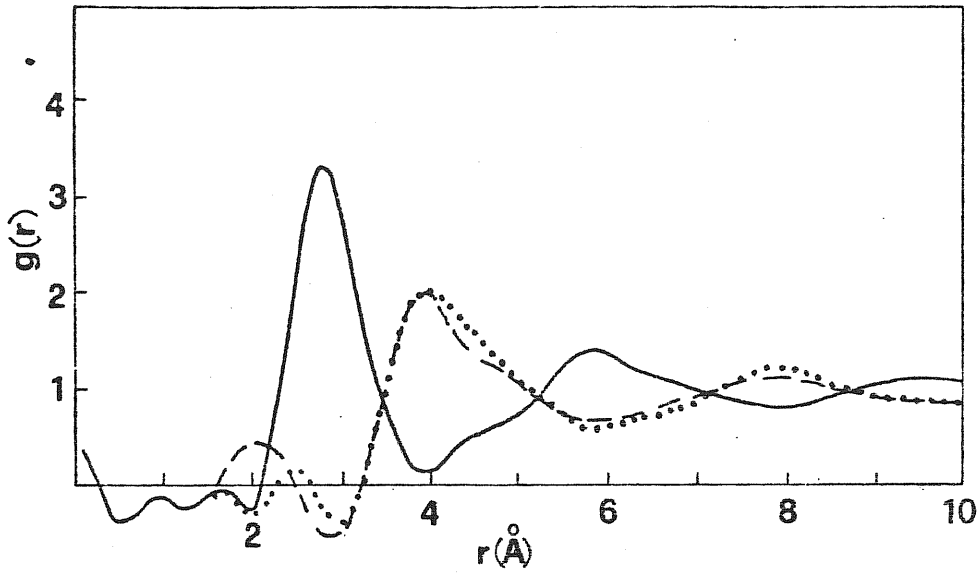

Fig. III.1-3: Pair distribution functions for molten NaCl at 875 °C. Full curve, g_{NaCl}; broken curve, g_{ClCl}; dotted curve, g_{NaNa}. From ref. (81).

can be identified. They include:

(i) a peak in $S_{++}(k)$ and $S_{--}(k)$ at the same wave number ($k \sim 2$ Å^{-1}), where a corresponding dip is presented in $S_{+-}(k)$. The Fourier transforms of $S_{\alpha\beta}(k)$ consequentely show an alternation of the distribution of the charge as shown by Fig. (III.1-3). One sees a well defined first-neighbour shell of anions (cations) around a cation (anion). The presence of a second shell of like ions is also evident.

(ii) The first peak of $S_{--}(k)$ is rather weak.

(iii) $g_{++}(r)$ and $g_{--}(r)$ are very similar (even though the ionic size of Na^+ and Cl^- ions is quite different.

(iv) $g_{++}(r)$, $g_{+-}(r)$ and $g_{--}(r)$ are in phase and for $r \geqslant 4$ Å the cancellation of charge is complete.

(v) a small penetration of the like species into the first coordination shell.

Property (i) reflects the relative ordering of the two ionic species induced by the Coulomb interaction, while property (ii) indicates that the order is rapidly destroied beyond the first coordination shell.

Some of the features previously stated can be better appreciated by introducing the Bhatia-Thornton (78) structure factors. For 1 : 1 ionic melts they are defined by

$$S_{QQ}(K) = \frac{1}{2}\left[S_{++}(k) + S_{--}(k) - 2\, S_{+-}(k)\right] , \qquad \text{(III.1-9)}$$

$$S_{QN}(K) = \frac{1}{2}\left[S_{++}(k) - S_{--}(k)\right] , \qquad \text{(III.1-10)}$$

$$S_{NN}(k) = \frac{1}{2}\left[S_{++}(k) + S_{--}(k) + 2\, S_{+-}(k)\right] . \qquad \text{(III.1-11)}$$

$S_{QQ}(k)$, $S_{NN}(k)$ and $S_{NQ}(k)$ are respectively linked to the fluctuation in number density $n(\vec{r}) = n_+(\vec{r}) + n_-(\vec{r})$ and to the fluctuation in "concentration" $q(\vec{r}) = n_+(\vec{r}) - n_-(\vec{r})$ through the relations

$$S_{QQ}(k) = \frac{1}{2n} \langle q(\vec{k})\, q(-\vec{k}) \rangle , \qquad \text{(III.1-12)}$$

$$S_{NN}(k) = \frac{1}{2n} \langle n(\vec{k})\, n(-\vec{k}) \rangle , \qquad \text{(III.1-13)}$$

$$S_{NQ}(k) = \frac{1}{4n} \langle n(\vec{k})\, q(-\vec{k}) + n(-\vec{k})\, q(\vec{k}) \rangle \qquad \text{(III.1-14)}$$

Fig. (II.1-4) illustrates these three functions for molten NaCl from the data of Fig. (III.1-2). The previous properties are easily recognized from Fig. (III.1-4):

(a) property (i) is reflected in the strong main peak of $S_{QQ}(k)$ at the same wave number k showing a good short-range order in the charge density.

(b) Property (ii) is reflected in the small coupling between charge-charge and density-density fluctuations, that is in the small value of $S_{NQ}(k)$.

(c) Property (iii) is reflected in the behaviour of $S_{NN}(k)$ which shows a poor ordering in the number density.

Now let us proceed to an analysis of some specific properties of a range of molten salts and more precisely of the alkali chlorides NaCl, KCl and RbCl and of the divalent-ion chlorides $SrCl_2$, $BaCl_2$, $CaCl_2$ and $ZnCl_2$.

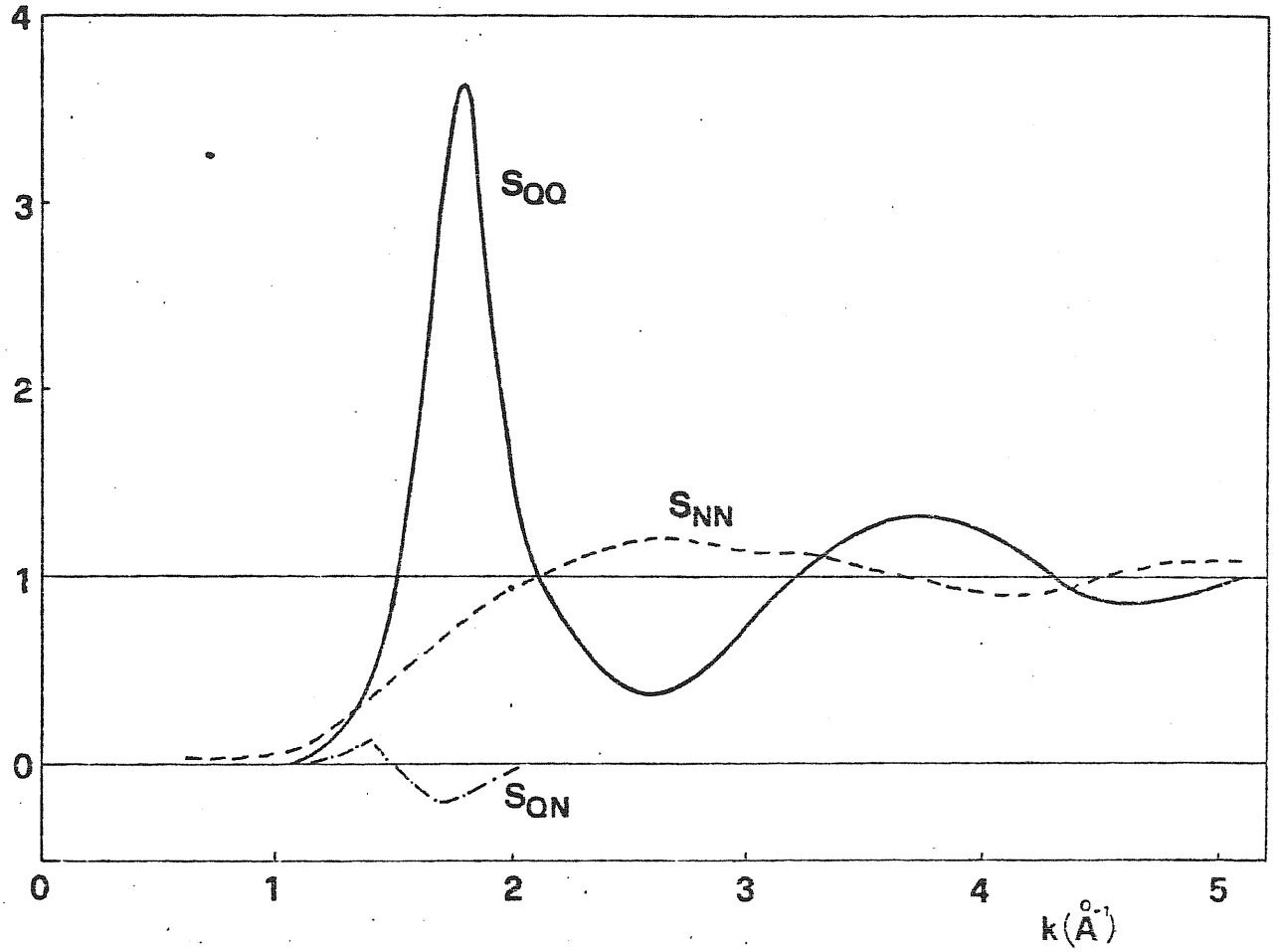

Fig. III.1-4: Charge-number structure factors for molten NaCl at 875 °C from the data of Fig. (III.1-2). From ref. (86).

(b. 1) NaCl, KCl and RbCl

Table (III.1-1) collects a set of structural data for molten NaCl, KCl and RbCl. In the first three columns are reported the wave numbers k_1 and k_3, that correspond to the position of the

	k_1 ($Å^{-1}$)	k_2 ($Å^{-1}$)	k_3 ($Å^{-1}$)	r_{+-} (Å)	r_{++} (Å)	r_{--} (Å)	n_c	n_n
NaCl(875°C)	1.8	2.6	3.5	2.78	3.96	3.91	3.9	5.2
KCl (800°C)	1.6	2.3	3.0	3.06	4.84	4.82	4.1	6.1
RbCl(750°C)	1.5	2.1	2.9	3.18	4.86	4.80	3.5	6.9

Table III.1-1: Structural properties of molten alkali chlorides from neutron diffraction. From ref. (86).

first and second peak in $S_{++}(k)$ and $S_{--}(k)$ and the wave number k_2 that corresponds to the first peak in $S_{+-}(k)$. We must note the regularities $k_2 \simeq 1.4\ k_1 \simeq 1.1\ (2\pi/r_{+-})$ and $k_3 \simeq 1.9\ k_1$ that appear on the relative peak positions.

The next columns show the average positions r_{+-}, r_{++} and r_{--} of the first peak in the corresponding pair distribution functiions, i.e. the average distance of the three types of neighbouring pairs. In this case the regularities $r_{++} \simeq r_{--} \approx (1.4 \div 1.5)\ r_{+-}$ are also evident.

In the last two columns are reported the coordination numbers n_c and n_n for unlike ions. These two kinds of coordination number can be extracted from $r^2 g_{+-}(r)$ by integration (87). The

"close-contact" coordination number, n_c, is obtained from

$$n_c = 2\int_{r_o}^{r_{max}} 4\pi n r^2 g_{+-}(r)\, dr \qquad \text{(III.1-15)}$$

where r_o is the left-hand edge of the first peak in $g_{+-}(r)$ and r_{max} is the position of the first maximum in $r\, g_{+-}(r)$. Only data on short r-side are used. The "near-neighbour" coordination number, n_n, is defined through

$$n_n = \int_{r_o}^{r_{min}} 4\pi n r^2 g_{+-}(r)\, dr \qquad \text{(III.1-16)}$$

where r_{min} is the position of the first minimum in $r^2\, g_{+-}(r)$. We would like to stress the fact that the difference between these two sets of results is linked to the ambiguity of the definition of coordination number in a liquid. The reduction in coordination number from 6 (solid) to $\sim$ 4 (liquid) reflects the large increase in molar volume of the alkali halides on melting as can be checked from rel. (I.5-1).

(b. 2) Divalent-ion chlorides

Four molten divalent-ion chlorides have been extensively

studied by neutron diffraction experiments. They are $CaCl_2$ (83), $SrCl_2$ (85), $BaCl_2$ (84) and $ZnCl_2$ (45).

The pair distribution functions are compared in Figures (III.1-5), (III.1-6) and (III.1-7). The dependence of these functions on the ion sizes has been removed using for each salt the normalised distance $r/(r_+ + r_-)$ in which r_+ and r_- are the cation and anion radii. The main structural features of these four compounds are summed up in Table (III.1-2).

From Fig. (III.1-5) it is evident that the pair distribution functions $g_{++}(r)$ of $BaCl_2$ and $SrCl_2$ are similar. The first peaks of g_{CaCa} and g_{ZnZn} occur at a shorter distance than those

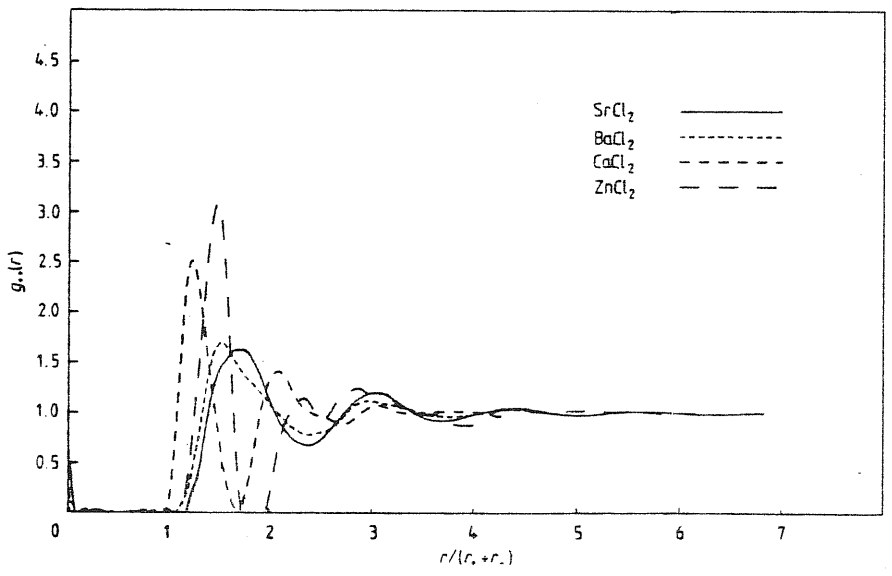

Fig. III.1-5: $g_{++}(r)$ for some molten 2-1 salts. From ref. (85).

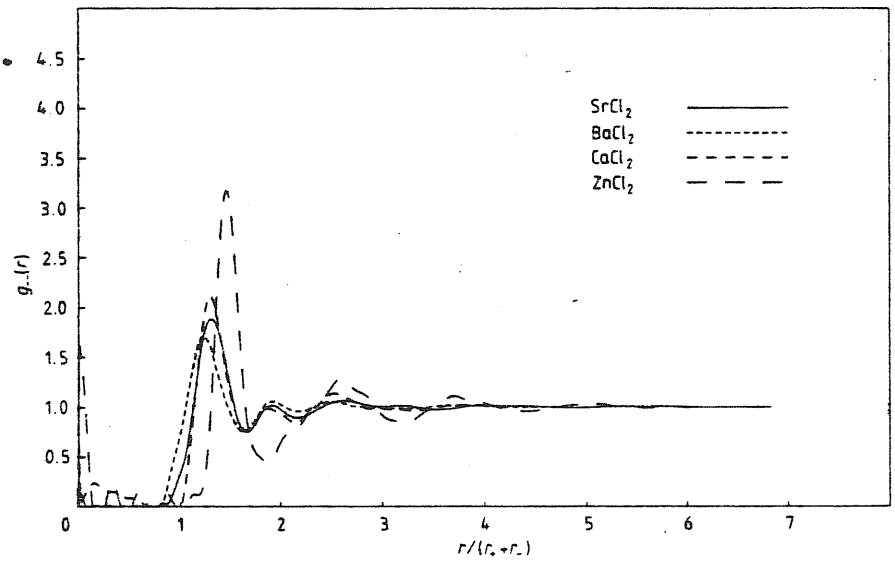

Fig. III.1-6: $g_{--}(r)$ for some molten 2-1 salts. From ref. (85).

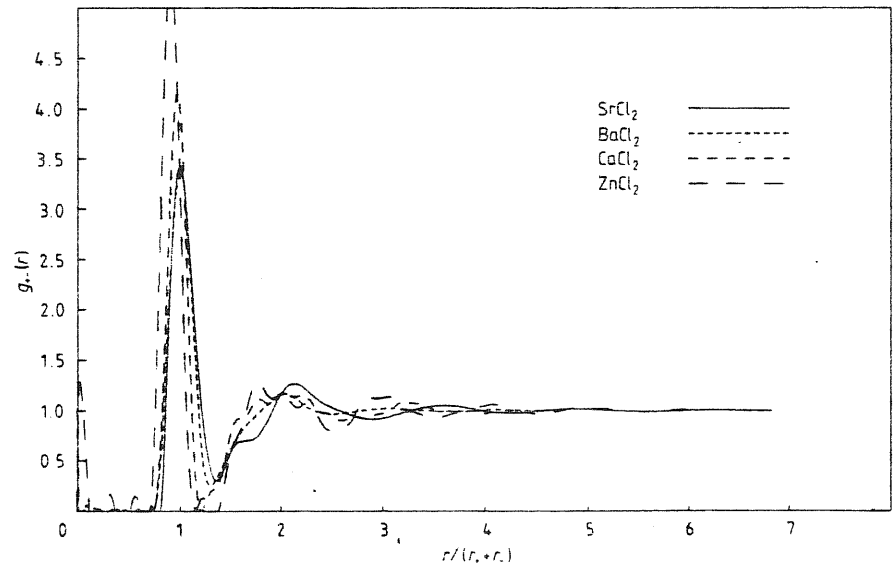

Fig. III.1-7: $g_{+-}(r)$ for some molten 2-1 salts. From ref. (85).

	Cation	Temp. (°C)	Distance of closest approach	Position of 1st peak	Height of 1st peak	Coordination number n_n	Coordination number n_c	Position of 1st minimum	Height of 1st minimum
$g_{++}(r)$	Zn	327	2.8	3.8	3.1	4.7		4.7	0.0
	Ca	820	2.7	3.6	2.5	4.2		4.8	0.1
	Sr	925	3.5	4.95	1.6	13.6		7.0	0.7
	Ba	1025	3.7	4.9	1.7	14.0		7.6	0.8
$g_{--}(r)$	Zn	327	3.0	3.71	3.1	8.6		4.7	0.4
	Ca	820	2.9	3.73	2.4	7.8		4.7	0.7
	Sr	925	2.4	3.80	1.9	9.3		4.8	0.7
	Ba	1025	2.5	3.86	1.7	7.0		5.1	0.7
$g_{-+}(r)$	Zn	327	1.9	2.29	5.2	4.3	4.3	3.0	0.0
	Ca	820	2.2	2.78	4.2	5.4	5.3	3.4	0.1
	Sr	925	2.4	2.9	2.9	6.9	5.1	4.0	0.3
	Ba	1025	2.4	3.1	3.4	7.7	6.4	4.2	0.3

Table III.1-2: Main features of the radial distributions of some molten alkaline-earth chlorides. From ref. (86).

of g_{BaBa} and g_{SrSr} and the first minima of the formers are very close to zero. Therefore the coordination number for g_{CaCa} and g_{ZnZn} are well defined while those for g_{SrSr} and g_{BaBa} are les well defined (for the values see Table (III.1-2)).

The pair distribution functions g_{ClCl} for this four compounds are shown in Fig. (III.1-6). In this case the g_{ClCl} for $BaCl_2$, $SrCl_2$ and $CaCl_2$ are similar while the first peak of $ZnCl_2$ is higher and occurs at higher distance.

The g_{+-} pair distribution functions (Fig. (III.1-7)) for $SrCl_2$ and $BaCl_2$ are also similar. The first peak of g_{ZnCl} is very high whereas the heigth of the g_{CaCl} peak is intermediate between the peaks of g_{ZnCl} and of g_{BaCl} and g_{SrCl}. The coordination numbers increase with cation size (see Table (III.1-2)).

The above observations on the pair distribution functions show that $SrCl_2$ and $BaCl_2$ on the one side, and $ZnCl_2$ on the other, have a rather different structure. The results for molten $CaCl_2$ indicate that this compound is intermediate between $BaCl_2$ and $ZnCl_2$.

The similarity of molten $SrCl_2$ and $BaCl_2$ is also reflected in the structure of these compounds in the high-temperature solid phase. At a temperature just below the melting point, $SrCl_2$ and $BaCl_2$ have the fluorite-type structure, and both show a superionic behaviour.

$SrCl_2$ shows a diffuse transition to the high-conductivity state over a range of temperature and without changes in crystal structure (88). The heat capacity has a peak which is used to define the transition temperature T_c (see Fig. (I.5-2)). Besides $BaCl_2$ shows a structural phase transition to the fluorite structure at T = 1193 °K and melts at T= 1233 °K. In the superionic state, the cation sublattice remains essentially unchanged while the anion sublattice is strongly disordered due to the appearance of a high dynamic concentration of Frenkel defects.

This behaviour is reflected in the liquid state where a good short-range ordering is shown by the partial structure factors of the cations and a poorer short range ordering is shown by the partial structure factors of anions. The freezing in the superionic phase can be regarded as driven by the marked cation ordering in the liquid in which the anions are subjected to a modulation of their singlet density by this cation sublattice order (19).

The structure of molten $ZnCl_2$ appears to be different to that of the other three chlorides. In Fig. (III.1-8) we see the partial structure factors corresponding to the pair correlation functions showed in the previous Figures. The very unusual feature is the presence of an additional extra peak,well resolved, in $S_{ZnZn}(k)$ at low values of k ($k \approx 1$ $\mathring{A}^{-1}$). The data listed in

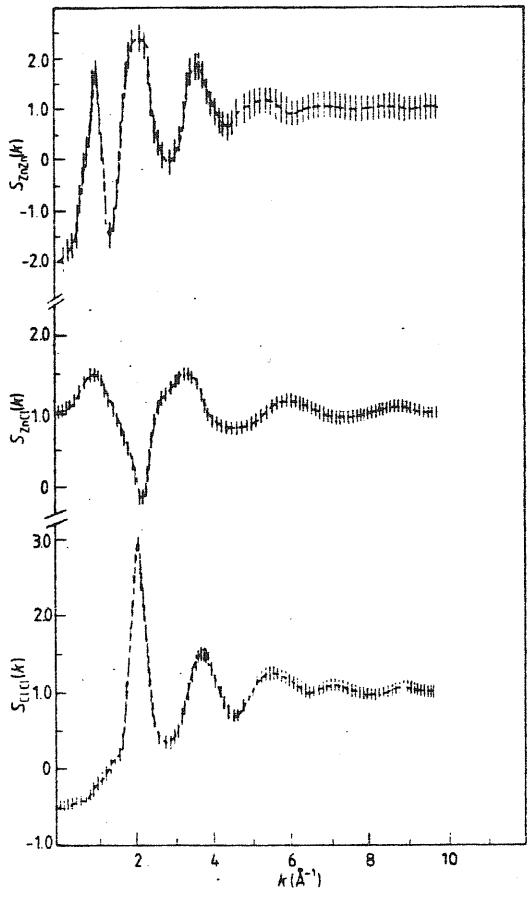

Fig. III.1-8: The partial structure factors for liquid $ZnCl_2$. From ref. (45).

Table (III.1-2) also show that the molten $ZnCl_2$ is characterised by a well defined local structure corresponding to a close-packed arrengement of Cl^- ions. The ratio $r_{ClCl} / r_{ZnCl} = 1.62 \pm 0.04$ is very close to the value $(8/3)^{1/2}$ for the perfect local tetrahedral coordination. As evident from Fig (III.1-9), the penetration of like ions into the first coordination shell does not occur because

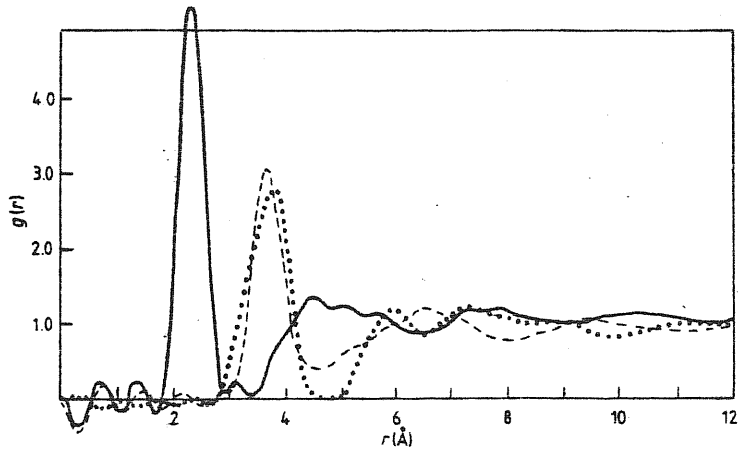

Fig. III.1-9: The pair distribution functions for liquid $ZnCl_2$; full curve, g_{ZnCl}; broken curve, g_{ClCl}; dotted curve, g_{ZnZn}. From ref. (45).

the small cations are shielded by the anions. These unusual properties of molten $ZnCl_2$ are due to the very high viscosity, the remarkably low electrical conductivity near freezing (T_m = 318 °C), and the supercooling possibility into a glassy state (45), with a glass transition temperature $T_g \simeq$ 115 °C.

III.2 Freezing of alkali halides

In this Section we shall discuss the freezing process of RbCl and NaCl using the microscopic theory given by March and Tosi (18). One of the major features in freezing of NaCl and RbCl is the large volume change across the liquid-solid transition $\Delta V/V \equiv \eta$, which is of the order of 15 - 20 %. They freeze into a f.c.c. lattice with a two-ion basis.

The basic equations have been recently developed by March and Tosi (18). These authors have also shown (20) that these equations, when applied to monatomic systems, are closely linked to the work of Ramakrishnan and Yussouff (17) (see also Chapter II Section 3). The basic set of equations relates the singlet densities ρ_1 and ρ_2 of the binary system to the partial direct correlation functions $\tilde{c}_{ij}(k)$. Therefore the basic input information required to develop the microscopic theory is the knowledge of the partial direct correlation functions $\tilde{c}_{ij}(k)$, or, more conveniently for present purposes, the charge-number (Q-N) counterparts. We shall see that in the freezing process for molten alkali halides, the two ionic components play essentially equal parts, and the most important structural parameters are $\tilde{c}_{NN}(k=0)$ (namely the compressibility) and $\tilde{c}_{QQ}(G_1)$ at the first set of reciprocal lattice vectors $\{\vec{G}_1\}$.

(a) Microscopic theory of freezing of NaCl and RbCl

The theory formulated in Chapter II can be generalised for binary systems with two single particle densities $\rho_1(\vec{r})$ and $\rho_2(\vec{r})$. A corresponding set of coupled equilibrium equations for these densities is obtained by expressing the thermodynamic potential as a functional of these densities and by requiring that Ω be a minimum. For coexistence between liquid (l) and solid (s) phases, the difference $\Delta\Omega = \Omega_s - \Omega_l$ must vanish.

The equilibrium equations for the single particle densities in the two-component ionic system, including the non-linear effects via three-body partial direct correlation functions are as follows

$$\ln\left(\frac{\rho_{is}(\vec{r}_1)}{\rho_{il}}\right) = \sum_j \int d\vec{r}_2\, c_{ij}(\vec{r}_1,\vec{r}_2)\,[\rho_{js}(\vec{r}_2) - \rho_{jl}]$$

$$+ \frac{1}{2}\sum_{j,k}\iint d\vec{r}_2\, d\vec{r}_3\, c^{(3)}_{ijk}(\vec{r}_1,\vec{r}_2,\vec{r}_3)\,[\rho_{js}(\vec{r}_2)-\rho_{jl}][\rho_{ks}(\vec{r}_3)-\rho_{kl}] \qquad \text{(III.2-1)}$$

for i = 1,2. The first term on the right-hand side contains the direct correlation functions $c_{ij}(\vec{r}_1,\vec{r}_2) = c_{ij}(|\vec{r}_1 - \vec{r}_2|)$ of the liquid and represents the first-order response to the change in densities. The three-body correlation functions $c^{(3)}_{ijk}(\vec{r}_1,\vec{r}_2,\vec{r}_3) = c^{(3)}_{ijk}(|\vec{r}_1 - \vec{r}_2|, |\vec{r}_1 - \vec{r}_3|)$ of the liquid which enter in the second

term are defined by the functional derivatives

$$c^{(3)}_{ijk}(\vec{r}_1,\vec{r}_2,\vec{r}_3) = \frac{\delta c_{ij}(\vec{r}_1,\vec{r}_2)}{\delta \rho_k(\vec{r}_3)} \quad . \tag{III.2-2}$$

The corresponding equation for the difference in thermodynamic potential is

$$\begin{aligned}\frac{\Delta\Omega}{k_BT} = & -\sum_i \int d\vec{r}_1 \left[\rho_{is}(\vec{r}_1)-\rho_{il}\right] \\ & + \frac{1}{2}\sum_{ij}\iint d\vec{r}_1\, d\vec{r}_2 \left[\rho_{is}(\vec{r}_1)+\rho_{il}\right] c_{ij}(\vec{r}_1,\vec{r}_2)\left[\rho_{js}(\vec{r}_2)-\rho_{jl}\right] \\ & + \frac{1}{6}\sum_{ij,k}\iiint d\vec{r}_1 d\vec{r}_2 d\vec{r}_3 \left[2\rho_{is}(\vec{r}_1)+\rho_{il}\right] c^{(3)}_{ijk}(\vec{r}_1,\vec{r}_2,\vec{r}_3)\left[\rho_{js}(\vec{r}_2)-\rho_{jl}\right] \\ & \times \left[\rho_{ks}(\vec{r}_3)-\rho_{kl}\right] \quad . \end{aligned} \tag{III.2-3}$$

We introduce now the Fourier expansions for the solid phase densities

$$\rho_{1s}(\vec{r}) = \frac{1}{2}\rho_l\left[1+\eta+\sum_{\vec{G}}{}' \rho_{\vec{G}}\, e^{i\vec{G}\cdot\vec{r}}\right] \tag{III.2-4}$$

and

$$\rho_{2s}(\vec{r}) = \frac{1}{2}\rho_l\left[1+\eta+\sum_{\vec{G}}{}' \rho_{\vec{G}}\, e^{i\vec{G}\cdot(\vec{r}+\vec{h})}\right] \tag{III.2-5}$$

where ρ_l is the density of the liquid and $\vec{h}$ is the vector joining the two ions in the unit cell of the crystal. We also Fourier analyse

the direct correlation functions by writing

$$c_{ij}(r) = \left(\frac{2}{N}\right) \sum_{\vec{k}} \tilde{c}_{ij}(k)\, e^{i\vec{k}\cdot\vec{r}} \qquad \text{(III.2-6)}$$

$$c^{(3)}_{ijk}(r) = \left(\frac{4}{N^2}\right) \sum_{\vec{k},\vec{k}'} \tilde{c}^{(3)}_{ijk}(\vec{k},\vec{k}')\, e^{(i\vec{k}\cdot\vec{r} + i\vec{k}'\cdot\vec{r}')} \quad . \qquad \text{(III.2-7)}$$

With the aid of equations (III.2-4)-(III.2-7) the freezing relations (III.2-1) and (III.2-3) can be rewritten in terms of Fourier transform. We assume that the only important contribution of the non-linear terms comes from the change of the compressibility in volume, which is expressed by the double Fourier transform of the quantity

$$c_{NNN}(\vec{r}_1,\vec{r}_2,\vec{r}_3) = \frac{1}{4} \sum_{i,j,k} \frac{\delta c_{ij}(\vec{r}_1,r_2)}{\delta \rho_k(\vec{r}_3)} \qquad \text{(III.2-8)}$$

in the limit of long wavelengths. If we denote this quantity by $\tilde{c}_{NNN}(0)$, the equilibrium equations for the Fourier components of the single particle density become

$$1+\eta = \frac{e^{[\eta \tilde{c}_{NN}(0) + \eta^2 \tilde{c}_{NNN}(0,0)]}}{V} \int d\vec{r}\; e^{[F_N(\vec{r}) + F_Q(\vec{r})]} \qquad \text{(III.2-9)}$$

and

$$2\rho_{\vec{G}} = \frac{e^{[\eta \tilde{c}_{NN}(0) + \eta^2 \tilde{c}_{NNN}(0,0)]}}{V} \int d\vec{r}\, e^{i\vec{G}\cdot\vec{r}}\, e^{[F_N(\vec{r}) + F_Q(\vec{r})]} \quad . \qquad \text{(III.2-10)}$$

Here

$$F_N(\vec{r}) = \sum_{\vec{G}}{}' \rho_{\vec{G}} \tilde{c}_{NN}(G)\, e^{i\vec{G}\cdot\vec{r}} \left[1 + e^{i\vec{G}\cdot\vec{h}}\right] \qquad \text{(III.2-11)}$$

and

$$F_Q(\vec{r}) = \sum_{\vec{G}}{}' \rho_{\vec{G}} \tilde{c}_{QQ}(G)\, e^{i\vec{G}\cdot\vec{r}} \left[1 - e^{i\vec{G}\cdot\vec{h}}\right] . \qquad \text{(III.2-12)}$$

Finally, the expression for the thermodynamic potential change on melting $\Delta\Omega$ is

$$\frac{\Delta\Omega}{NK_BT} = -\eta + \tilde{c}_{NN}(0)\left(\eta + \tfrac{1}{2}\eta^2\right) + 2\,\tilde{c}_{NNN}(0,0)\left(\tfrac{1}{2}\eta^2 + \tfrac{1}{3}\eta^3\right)$$

$$+ 2\sum_{\vec{G}}{}' \left[\tilde{c}_{NN}(G)\rho_{\vec{G}}^2 \cos^2\left(\tfrac{1}{2}\vec{G}\cdot\vec{h}\right) + \tilde{c}_{QQ}(G)\rho_{\vec{G}}^2 \sin^2\left(\tfrac{1}{2}\vec{G}\cdot\vec{h}\right)\right] , \qquad \text{(III.2-13)}$$

$\Delta\Omega$ being equal to zero at coexistence.

(b) Numerical prediction for NaCl and RbCl

The freezing equations of the previous Section have been written in a form which is most convenient for their numerical solution. We have assumed that the inclusion of the first two sets of lattice vectors only, $\{\vec{G}_1\}$ and $\{\vec{G}_2\}$, is sufficient. The set $\{\vec{G}_1\}$ are reciprocal vectors of the type (1,1,1) and correspond to the principal peak in the charge-charge structure factor $S_{QQ}(k)$ in the liquid. For the second set $\{\vec{G}_2\}$ we have choosen the vectors

of the type (2,2,0) corresponding to the principal peak in $S_{NN}(k)$.

We have solved the equations using as input $\tilde{c}_{QQ}(G_1)$ and $\tilde{c}_{NN}(k=0)$ in order to determine the volume change η, the value of $\tilde{c}_{NN}(G_2)$ and the Fourier components of the single particle densities at $\{\vec{G}_1\}$ and $\{\vec{G}_2\}$. In this calculation $\tilde{c}_{NNN}$ at long wavelengths has been treated like a free parameter. For ionic liquids, experimental information on the three-body correlation functions is laking and we cannot make comparison between experimental and theoretical values. However, the inclusion of the three-body correlation functions was suggested by the results of a previous work of Rovere, Tosi and March (89) on freezing of RbCl. In their analysis they found a value of $\tilde{c}_{NN}(G_2)$ in a reasonable good agreement with the measured value, but a value of $\tilde{c}_{NN}(k=0)$ appreciably more negative than the experimental value.

For RbCl and NaCl, the numerical results obtained are shown in Table (III.2-1). For RbCl the theory foresees $\tilde{c}_{NN}(G_2)$ to be in agreement with experiment. The value of $\tilde{c}_{NNN}(0,0)$ of - 105 is of the same order of magnitudes as that found for the corresponding three-body function for liquid argon by Ramakrishnan and Yussouff.

In the case of NaCl, the prediction of $\tilde{c}_{NN}(G_2)$ is only semiquantitative whereas the value of $\tilde{c}_{NNN}(0,0)$ is only about 1/3 of that for RbCl. One can see that, in both cases the Fourier

		$\tilde{c}_{NN}(0)$	$\tilde{c}_{QQ}(G_1)$	$\tilde{c}_{NN}(G_2)$	$\tilde{c}_{NNN}(0,0)$	η	$\rho_{\vec{G}_1}$	$\rho_{\vec{G}_2}$
RbCl	Th.	-7.33	0.75	0.29	-105	0.14	0.46	0.36
	Exp.	-7.33	0.75	0.29	----	0.142	----	----
NaCl	Th.	-6.3	0.72	0.28	-31	0.25	0.53	0.42
	Exp.	-6.3	0.72	0.15	----	0.25	----	----

Table III.2-1: Detailed numerical predictions on $\tilde{c}_{NN}(G_2)$, $\rho_{\vec{G}_1}$, $\rho_{\vec{G}_2}$ and $\tilde{c}_{NNN}(0,0)$.

components of the density are quite similar in magnitude and behaviour.

III.3 Freezing of $SrCl_2$ and $BaCl_2$

When compared to the alkali chlorides NaCl and RbCl, $SrCl_2$ and $BaCl_2$ show a completely different behaviour on freezing. In fact, $SrCl_2$ and $BaCl_2$ freeze into a superionic phase characterised by a fluorite-type structure in which the cation sublattice provides a periodic potential for still relatively moving anions while, as already seen, the molten alkali chlorides freeze into a normal f.c.c. phase. The volume change $\Delta V/V \equiv \eta$ on freezing for $SrCl_2$ and $BaCl_2$ is small and of the order of $\sim$ 2 - 4 %.

In a previous work on freezing into a superionic phase, March and Tosi (19) used a linear response theory to estimate the ratio of a particular Fourier component of the anion density to that of the corresponding component for the cation sublattice. Here we present a fully non-linear solution, which, as will be seen, validates their linear response assumption.

(a) Microscopic theory of freezing of $SrCl_2$ and $BaCl_2$ into a superionic phase

We Fourier analyse the singlet densities in the superionic

phase by writing

$$\rho_{is}(\vec{r}) = \rho_{is} + V^{-1}\sum_{\vec{G}}{}' \rho_{i\vec{G}}\, e^{i\vec{G}\cdot\vec{r}} \qquad \text{(III.3-1)}$$

for i = 1,2. If we also Fourier analyse the partial direct correlation functions by writing

$$c_{ij}(r) = (V\rho_L)^{-1}\sum_{\vec{k}} \tilde{c}_{ij}(k)\, e^{i\vec{k}\cdot\vec{r}} \qquad \text{(III.3-2)}$$

then, the component with $\vec{G} = 0$ of eq. (III.2-1) leads to

$$1+\eta = \frac{e^{\eta\sum_j \frac{\rho_{jL}}{\rho_L}\tilde{c}_{ij}(0)}}{V}\int d\vec{r}\, e^{\left[\sum_j\sum_{\vec{G}}{}' \frac{\tilde{c}_{ij}(G)\rho_{j\vec{G}}}{V\rho_L} e^{i\vec{G}\cdot\vec{r}}\right]} \qquad \text{(III.3-3)}$$

The quantity appearing in the first summation on the right-hand side of this equation can be related to N-Q direct correlation functions using

$$\sum_j \left(\frac{\rho_{jL}}{\rho_L}\right)\tilde{c}_{ij}(0) = \tilde{c}_{NN}(0) + \tilde{c}_{NQ}(0) \qquad \text{(III.3-4)}$$

The discussion of the behaviour at small k of the partial structure factors and the partial direct correlation functions for 2 : 1 liquids follows closely the one given by Rovere et al. (90) for

molten alkali halides, the main results we need below being

$$\tilde{c}_{NN}(0) = 1 - \frac{1}{S_{NN}(0)} = 1 - (\rho_L k_B T K_T)^{-1} \qquad \text{(III.3-5)}$$

and

$$\tilde{c}_{NQ}(0) = \frac{2\rho_{1L}(v_2 - v_1)}{\rho_L k_B T K_T} \qquad \text{(III.3-6)}$$

where K_T is the isothermal compressibility and v_1 and v_2 are the partial molar volumes of the two species, 1 now being the cation. The thermodynamic definition of v_i is

$$v_i = \left(\frac{\partial \mu_i}{\partial P}\right)_{T,N} . \qquad \text{(III.3-7)}$$

It is therefore clear that the difference in partial molar volumes of anion and cation enters the calculation of the volume change on freezing, via eq. (III.3-3).

The other equations entering the theory are the relations derived from (III.2-1) for the $\vec{G} \neq 0$ components

$$\frac{\rho_{i\vec{G}}}{V\rho_{iL}} = \frac{e^{\eta \sum_j \frac{\rho_{jL}}{\rho_L} \tilde{c}_{ij}(0)}}{V} \int dr\, e^{i\vec{G}\cdot\vec{r}} \left[\sum_j \sum_{\vec{G}}{}' \frac{\tilde{c}_{ij}(G)\rho_{j\vec{G}}}{V\rho_L} e^{i\vec{G}\cdot\vec{r}}\right] \qquad \text{(III.3-8)}$$

and the condition of coexistence of the two phases, which means equating to zero the difference $\Delta\Omega$ in their thermodynamic potentials.

This difference is given by

$$\frac{\Delta\Omega}{k_B T} = -(\rho_s - \rho_l)V + \frac{1}{2}V(\rho_s^2/\rho_l^2 - 1)\,\tilde{c}_{NN}(0)$$

$$+(2V\rho_l)^{-1}\sum_{i,j}\sum_{\vec{G}}{}' \tilde{c}_{ij}(G)\,\rho_{i\vec{G}}\,\rho_{j\vec{G}} \qquad \text{(III.3-9)}$$

in which the compressibility appears through $\tilde{c}_{NN}(0)$.

(b) Numerical predictions for $SrCl_2$ and $BaCl_2$

In the case of $SrCl_2$ and $BaCl_2$ the freezing equations are solved by including only the first set $\{\vec{G}_1\}$ of reciprocal lattice vectors. We have positioned this set just below the first peak in the cation-cation structure factor $S_{++}(k)$. The numerical solution is reached as follow: (i) we fix a value for $\tilde{c}_{NQ}(0)$ and we take $\tilde{c}_{++}(G_1)$ from experiment; (ii) we change the values of the volume change η and of the compressibility ($\tilde{c}_{NN}(0)$) until a solution is found; (iii) we repeat the same procedure, changing the value of $\tilde{c}_{NQ}(0)$ until a good agreement between the output $\tilde{c}_{+-}(G_1)$ and $\tilde{c}_{--}(G_1)$ and their experimental values is obtained. The results are listed in Table (III.3-1).

		$\tilde{c}_{NQ}(0)$	$S_{NN}(0)$	η	$\tilde{c}_{++}(G_1)$	$\tilde{c}_{+-}(G_1)$	$\tilde{c}_{--}(G)$	$P_1\vec{G}_1$	$P_2\vec{G}_1$
$BaCl_2$	Th.	-16	0.073	0.035	0.150	-3.1	-2.2	0.53	0.22
	Exp.	---	0.073	0.035	0.150	-2.3	-3.0	----	----
$SrCl_2$	Th.	-12	0.066	0.024	-0.46	-2.9	-1.2	0.42	0.24
	Exp.	---	0.066	0.024	-0.46	-2.5	-1.8	----	----

Table III.3-1: Numerical results of microscopic theory for $BaCl_2$ and $SrCl_2$.

The agreement with experiment of $\tilde{c}_{+-}(G_1)$ and of $\tilde{c}_{--}(G_1)$ is not quantitative but we must remember that only a set of reciprocal lattice vectors was used.

The negative values obtained for $\tilde{c}_{NQ}(0)$ for both salts imply, through eq. (III.3-6), that the molar volume of the cation is greater than that of the anion. The sign of $\tilde{c}_{NQ}(0)$ is in agreement with that found in the work of Abramo et al. (91) who have fitted to the measured structure factors the mean spherical approximation to a model of charged hard spheres. But the reverse situation is predicted from the ionic radii. However we believe that the negative sign can be caused by the large charge + 2 e on the cations, which tends to lead to a "classical Wigner lattice". The hole generated around a chosen cation is related to Coulomb repulsion rather than the ionic core radius.

The values listed in Table (III.3-1) have been derived solving the non-linear equations of the theory. We have also found that the values determined in this way agree with those obtained by linearising in $\rho_{-,\vec{G}}$, namely

$$\rho_{-,\vec{G}} = \frac{\tilde{c}_{+-}(G)\,\rho_{+,\vec{G}}}{(\rho_L/\rho_{-,s}) - \tilde{c}_{--}(G)} \qquad \text{(III.3-10)}$$

Of course, the extension of the present theory to a finite temperature

below the freezing point, at which the still moving chlorine ions experience the periodic lattice potential of the rigid cation sublattice, requires the knowledge of the anisotropic partial direct correlation function at the corresponding temperature.

III.4 Comparative discussion of freezing for different types of ionic materials

The freezing transition for the alkali chlorides NaCl and RbCl and for $SrCl_2$ and $BaCl_2$ has been determined by choosing the position of the stars of reciprocal lattice vectors $\{\vec{G}_1\}$, $\{\vec{G}_2\}$ in a suitable way, and consequently the experimental input partial direct correlation functions $c_{ij}(k)$. For the alkali chlorides NaCl and RbCl we have positioned the set $\{\vec{G}_1\}$ just under the principal peak in the charge-charge structure factor $S_{QQ}(k)$ of the liquid, whereas in the case of $SrCl_2$ and $BaCl_2$ we have positioned it under the principal peak in the cation-cation structure factor $S_{++}(k)$.

The molten alkali halides are characterised by a marked degree of ordering in the charge density and consequently by a strong first peak in $S_{QQ}(k)$. Therefore, we suggest that the freezing of alkali halides is driven by this charge ordering, and that the estimated value of about 5 for the charge-charge structure factor maximum at freezing (see Table (I.5-7)), can be viewed as the analogue for ionic liquids of the Hansen-Verlet rule of freezing for simple monatomic liquids with Lennard-Jones type interaction.

On the contrary, the molten $SrCl_2$ and $BaCl_2$ are characterized by a good short-range ordering of cations while the

structure factors S_{--} and S_{+-} have much less pronounced features. In this case we can think of the freezing into a superionic phase as driven by the cation ordering and this order provides a periodic potential that modulates the single anionic density.

The above considerations can be connected with defect properties. The principal peaks in S_{RbRb} and S_{ClCl} in liquid RbCl are of the same height, signalling a similar degree of order of cations and anions. This can be connected with the defective structure of the crystal in which an equal number of vacancies occurs on the two sublattices. The Schottky defects are the dominant type of defects. In contrast, the good ordering of cations in molten $SrCl_2$ and $BaCl_2$ can be connected with a crystal structure with anion Frenkel defects. Another evidence of the different part played by Schottky and Frenkel defects resides in the different volume change on freezing: large for NaCl and RbCl, small for $SrCl_2$ and $BaCl_2$. In fact, it is known that the volume of formation of Schottky defects is higher than that of Frenkel defects.

As last comment we note that the prediction on the difference of the partial molar volumes in $SrCl_2$ and $BaCl_2$, for which we have proposed the existence of a classical Coulomb hole due to the strong Coulomb repulsion between cations, could be verified by a small-angle scattering experiment.

CHAPTER IV

DEFECTS AND TRANSPORT IN HOT IONIC SOLIDS

CHAPTER IV

Defects and transport in hot ionic solids

In this Chapter we shall report a study of the defective structure of silver bromide from the melting point downward (92). The behaviour of AgBr in the high temperature region, where this material attains a rather high ionic conductivity before melting, will then be compared to and contrasted with that of fluorite-type superionic conductors.

As an introduction, we give in Section 1 an overview of the experimental information on the strusture of superionic materials. In the first part of this Section a systematic classification of the superionic materials is done and the specific trends of each group are illustrated. In the second part special emphasis is given to the defective structure of fluorites in the superionic phase, analysing recent neutron diffraction data. The experimental data are interpreted in terms of fluctuating clusters of anions. In the last part of this Section the superionic transition temperature T_c is correlated to the Frenkel pair formation energy E_F in crystals with fluorite structure (4). The transition is described using the Debye-Hückel theory. In order to explain the enhancement of defect concentration

at the transition point, the Coulomb interaction between defects is taken into account.

Section 2 presents the derivation of the intrinsic defect parameters of AgBr from experimental data. The bromine vacancy concentration is generally believed to be very low in solid AgBr and is often ignored in the charge neutrality equation. In this Section we show that the bromine vacancy concentration is by no means negligible at high temperaures but is of the order of the concentration of silver interstitials. Making use of N.M.R., diffusion and conductivity experimental data, a set of new Frenkel and Schottky defect parameters have been derived.

The new Frenkel and Schottky defect parameters have been used by Andreoni and Tosi (27), as reported in the second part of this Section, in a Debye-Hückel model, modified for saturation of screening at high defect concentrations. This work has led to the suggestion that the contemporaneous presence of Frenkel and Schottky disorder frustrates the superionic transition in AgBr. The model leads to melting accompanied by an anomalous ionic conductivity in the premelting region, as is observed in the conductivity experiments.

IV.1 Fluorite-type superionic conductors

(a) Superionic materials

Most ionic materials, generally referred to as superionics or fast-ion conductors, show in the high temperature solid phase, values of the ionic electrical conductivity quite comparable to those of simple ionic melts. The high ionic conductivity is a consequence of disorder in the sublattice of a component. Superionic conductors have the following characteristics: (i) the crystal bonding is ionic, (ii) the charge carriers are ions and (iii) the electronic conductivity is small.

The values of the electrical conductivity for a range of ionic and superionic materials are shown in Fig. (IV.1-1). Different behaviours are observed. For example, some superionic materials change gradually the electrical conductivity (as in β-alumina) whereas some others show an abrupt jump (as in AgI, Ag_3SI, etc.).

On the basis of this property and on the basis of the structures that allow fast-ion transport, and that can be "channelled", "layered" or generally disordered (93), the most important superionics can be classified under the following three main groups (21,94,95):

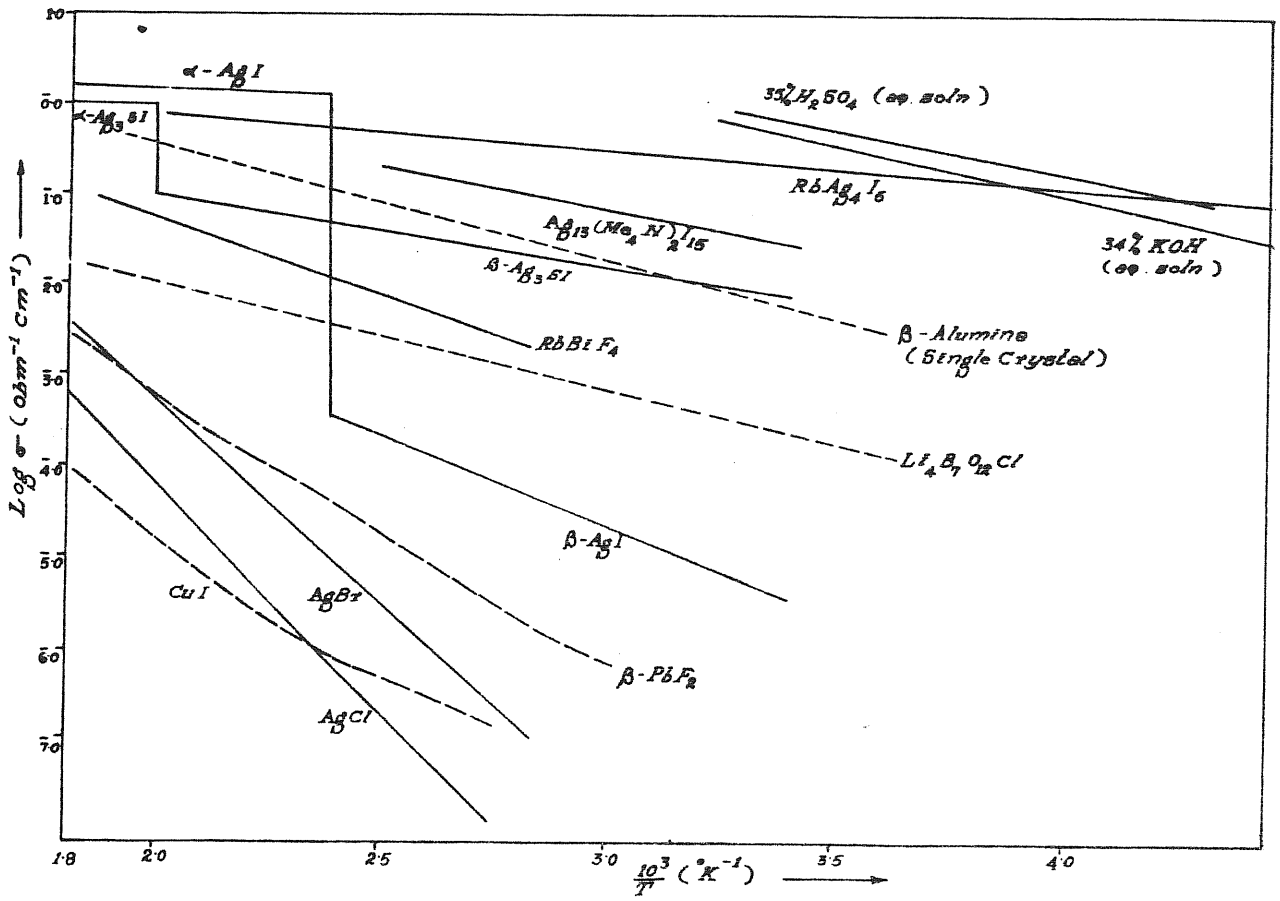

FIg. IV.1-1: Electrical conductivity versus temperature for some ionic and superionic solids. From ref. (21).

(i) The compound of this group which has been most extensively studied is the sodium β-alumina (see Fig. (IV.1-2) for the unit cell). Sodium β-alumina has hexagonal symmetry. The crystal consists of spinel bocks formed by four layers of oxigen and aluminium

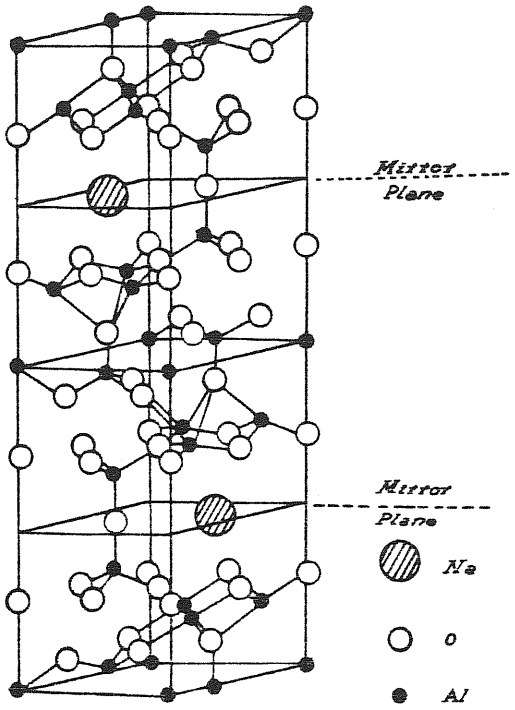

Fig. IV.1-2: Crystal structure of sodium β - alumina.

ions. The spinel bocks are separated by symmetry planes containing oxigen and sodium ions. The symmetry planes are perpendicular to the hexagonal symmetry axis and the sodium ions can move relatively freely in these planes. Sodium ions can occupy positions A and C (see Fig. (IV.1-3)). Their motion can be explained by an interstitialcy mechanism (97) in which a cation in an interstitial site jumps in an occupied adjacent site A, forming a new pair of interstitials and leaving behind an occupied site A. This mechanism requires an excess of Na^+ ions and therefore the ionic conductivity

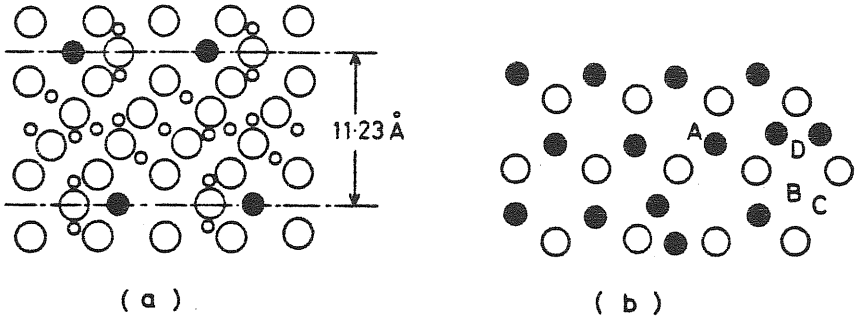

Fig. IV.1-3: (a) Cross section of sodium β -alumina containing the hexagonal axis; (b) Mirror plane perpendicular to the hexagonal axis. From ref. (94).

is a property of non-stoichiometric crystals. X-ray diffraction experiments carried on silver β -alumina (98) have shown a behaviour characteristic of a two-dimensional "liquid-like" lattice (see Fig. (IV.1-4)), for the cation sublattice at temperatures of the superionic phase.

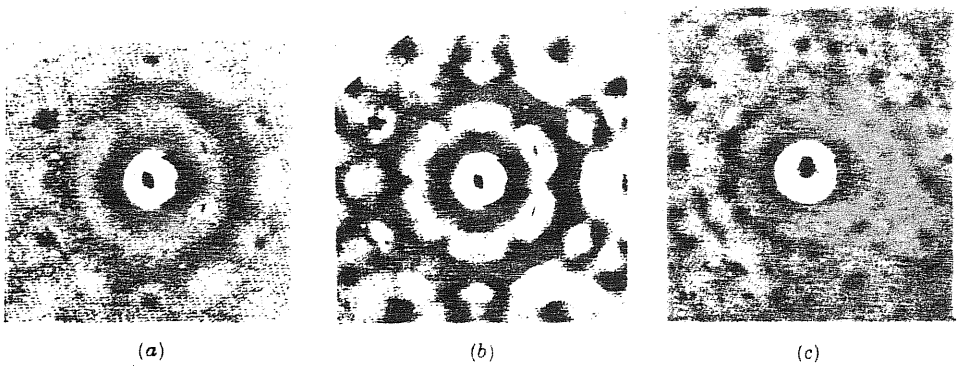

Fig. IV.1-4: X - ray diffuse scattering from silver β -alumina, with the hexagonal axis parallel to the incident beam at temperature (a) 700 °K, (b) 300 °K and (c) 77 °K. From ref. (98).

(ii) The prototype material of this group is the silver iodide, AgI. AgI has a first-order phase transition at T = 149 °C passing from the hexagonal wurzite structure with two unit formula per cell to a body cubic centred lattice with I^- ions at (0,0,0) and (1/2,1/2,1/2). Going through the transition, the ionic conductivity changes by several order of magnitude (see Fig. (IV.1-1)). In the high conductivity phase the Ag^+ ions are distributed on the tetrahedral interstices of the iodine sublattice. Because there are twelve such sites in the defective structure, the diffusion of Ag^+ ions occur from one tetrahedral site to an adjacent empty one (99). In Fig. (IV.1-5) the structure of the high conductivity phase of AgI is shown.

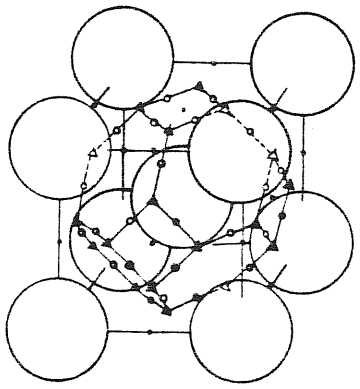

Fig. IV.1-5: Schematic structure of α-AgI. The iodine ions (circles) occupy a b.c.c. lattice and the silver ions sit preferentially at tetrahedral sites (triangles).

(iii) The fluorite structure is shown in Fig. (IV.1-6). The unit cell is a face cubic centred lattice with four unit formula. The structure can also be seen as a simple cubic lattice of anions whose centres are alternatively occupied by cations. Fluorite-type

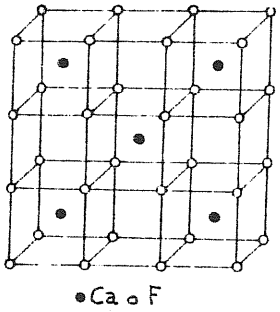

Fig. IV.1-6: Structure of CaF_2. Black circles are Ca, open circles are F. The Ca ions sit on a f.c.c. lattice.

materials show a diffuse transition to a high conductivity state few hundred degrees below the melting temperature (see Table (IV.1-1)), without change in structure. The ionic conductivity and the heat capacity are shown in Fig. (IV.1-7) for CaF_2 and $SrCl_2$.

At low temperatures the intrinsic defects present in fluorite are Frenkel pairs, i.e. fluorine vacancies and interstitials

Salt	T_m (°K)	T_c (°K)
CaF_2	1633	1430
SrF_2	1723	1400
BaF_2	1550	1230
$SrCl_2$	1146	1000
PbF_2	1158	705

Table IV.1-1: Melting temperatures T_m of fluorite crystals and transition temperatures to the superionic state, T_c.

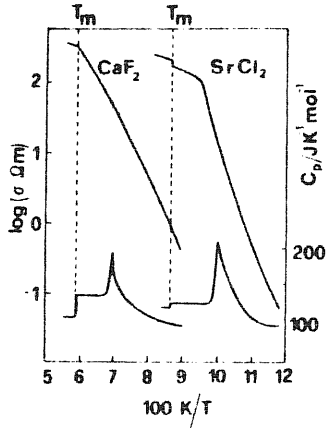

Fig.IV.1-7: Ionic conductivity σ (upper curves) and heat capacity c_p (lower curves) for CaF_2 and $SrCl_2$. From ref. (104).

(100). At high temperature the defective structure has been extensively studied by several neutron scattering techniques (101,102, 103) and the transition temperature, T_c, has been correlated to Frenkel pair formation energy E_F (4). The next two paragraphs will

will deal with these questions.

(b) Anion disorder in the superionic phase of fluorites

At low temperatures it is a well established fact that the predominant intrinsic defect in fluorite crystals is a Frenkel pair of an interstitial anion and an associated vacancy (100); the interstitial occupies the cube-centre site and the associated vacancy is at a greater distance then the next nearest-neighbour anion site (105).

Neutron scattering experiments (101,102,103) and molecular dynamic simulations on CaF_2 (106,107,108) and on $SrCl_2$ (107) indicate that at high temperature the disordered anions tend not to reside on the cube centre, suggesting that the cube-centre-interstitial model is unsatisfactory for the superionic phase. Alternative models have been formulated after analysis of the experimental data.

The neutron scattering spectrum from fluorites in the superionic state has revealed a coherent diffuse quasielastic component arising from the dynamically disordered anion sublattice (103). The energy spectrum is well described by a Lorentzian shape function $S(k,\omega)$ centred on zero energy transfer $\omega = 0$. The

integrated intensity $S(\vec{k}) = \int S(\vec{k},\omega)\,d\omega$ increases rapidly in the region of the transition temperature and it peaks prominently in the region $\vec{k} \cong \frac{2\pi}{a}(2.4,0,0)$. Simple defect models have been suggested to fit these data on S(k). Each model allows a fraction D of the anions to leave their regular sites and move to occupy different sites in the unit cell. There are two such different sites: (i) "R" sites at ($\pm(1/2-x), \pm(1/2-x), \pm(1/2-x)$) and (ii) "I" sites at ($\pm(1/4-y), \pm(1/4-y)$, 0), relative to the empty cube centre and in units of lattice parameter. By using a model in which equal number of displaced anions occupy the 12 "I" sites and the 8 "R" sites, a better agreement with experimental data is obtained.

This way, the anion defects are able to form simple fluctuating clusters , known as 2 : 2 : 2 clusters. The defect configuration cluster is reported in Fig. (IV.1-8): it consists of two anion interstitials placed near the mid-anion position and of two anion vacancies that do not held a critical position. The two neighbour anions nearest to the interstitials are relaxed from their regular lattice sites. The average clusters life-time is estimated to be $\approx 10^{-12}$ sec.

The cluster picture of defect allows us to make a distinction between the true interstitial anions of a Frenkel pair and the neighbouring anions relaxed from their regular sites. As a

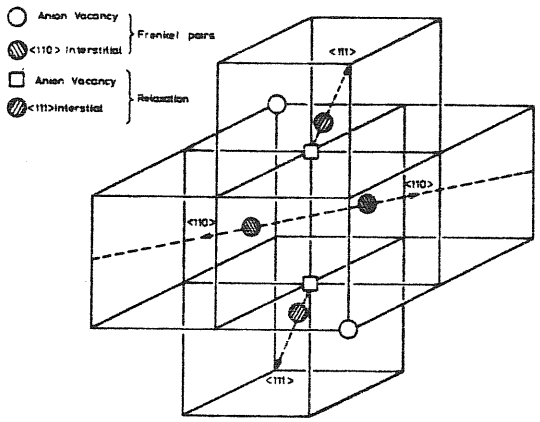

Fig. IV.1-8: Sketch of the arrengement of two interstitials, two vacancies and two relaxed anions giving agreement with neutron diffraction data from superionic PbF_2. From ref. (103).

cosequence, the Frenkel defects can increase ($\approx$ 24 % in PbF_2 above T_c) without any contradiction with the static energy calculations on the stable maximum numbers of Frenkel defects ($\approx 10 \div 20$ % as determined by Catlow (88)).

(c) Transition temperature and Frenkel defects in fluorite crystals

The values of defect concentration in the superionic

phase, expressed as a fraction of anions that leave their regular sites, D, are shown in Table (IV.1-2) for the four flourites PbF_2, $SrCl_2$, BaF_2 and CaF_2 (109). The temperatures of measurements, T_1, are also given. Below the transition temperature the defect

Salt	T_c (°K)	T_m (°K)	T_1 (°K)	D (%)
PbF_2	705	1158	973	49 ± 3
$SrCl_2$	1000	1146	1073	21 ± 6
BaF_2	1230	1550	1373	34 ± 6
CaF_2	1430	1633	1403	23 ± 3

Table IV.1-2: Values of T_c and T_m for four fluorites and values of D determined at T_1. Data from ref. (23).

concentration is much lower and, for example, in $SrCl_2$ the maximum value reached by the defect concentration is about 3 %. The transition has been described by March, Richardson and Tosi (4) using an extended Debye-Hückel theory. An instability of the Frenkel defect assembly was found while describing the rapid increase in Frenkel defects at the transition in terms of Coulomb interaction

between defects.

The concentration of non-interacting Frenkel defects in the state of equilibrium is given by

$$c_o = \exp\left(-G_F/(2k_BT)\right) \qquad \text{(IV.1-1)}$$

in which G_F is the Gibbs free energy of formation of a Frenkel defect. The interaction between defects leads to an enhancement factor $F(c)$ and the equilibrium condition without interaction (IV.1-1) is replaced by

$$c = c_o F(c) \quad . \qquad \text{(IV.1-2)}$$

According to the debye-Hückel theory, the enhancement factor $F(c)$ can be expressed through the relation

$$F(c) = \exp\left[e^2 k_D / [\varepsilon(1+k_D R)k_B T]\right] \qquad \text{(IV.1-3)}$$

where k_D is the usual inverse Debye length, ε the dielectric constant of the material and R the closest approach distance of a vacancy and an interstitial. At the transition temperature T_c the equilibrium equation (IV.1-2) becomes

$$\frac{E_F}{2k_BT_c} - \frac{S_F}{2k_B} + \ln c_c - \ln F(c_c) = 0 \qquad \text{(IV.1-4)}$$

where c_c is the defect concentration at T_c and E_F and S_F are respectively the formation energy and the formation entropy of the Frenkel defect. Kurosawa (3) has shown that when the concentration reaches a certain temperature dependence value the Coulomb interaction between defects induces an instability. The results for the defect concentration at the transition and for the critical temperature T_c of the instability are of the form (15)

$$c_c = f\left(\frac{k_BT_c}{e^2/\varepsilon R}\right) \qquad \text{(IV.1-5)}$$

and

$$k_BT_c = \frac{e^2 k_D(T_c)}{4\varepsilon[1 + k_D(T_c)R]^2} \; . \qquad \text{(IV.1-6)}$$

For the superionic materials for which $c_c \simeq 3\ \%$ and using the value $S_F = 5.6\ k_B$ for the Frenkel formation entropy (110), one can estimate that the Frenkel formation energy obeys the relation $E_F \geqslant 16\ k_BT_c$. This regularity can be verified by looking at the experimental data shown in Table (IV.1-3).

Salt	T_c (°K)	E_F (eV)	$10k_B T_c/E_F$
CaF_2	1430	2.71	0.45
SrF_2	1400	2.28	0.55
BaF_2	1230	1.91	0.56
PbF_2	705	1.0	0.61
$SrCl_2$	993	1.70	0.50

Table IV.1-3: Correlation of the superionic transition temperature and the Frenkel defect energy in fluorite-type crystals. From ref. (15).

IV.2 Silver bromide at high temperatures

Silver bromide, AgBr, is an ionic material with roksalt structure. At low temperatures the ionic intrinsic conductivity is of the order $10^{-4} \div 10^{-3}$, due to the presence of cationic Frenkel defects. At intermediate temperatures (about 100-150 °C below the melting point T_m = 701 °K), the ionic conductivity starts to rise, in an anomalous way, above the value extrapolated from low temperatures (26) (see Fig. (IV.2-1)). In the same interval of temperatures, the anionic diffusion coefficient becomes correspondingly large (24). At the melting point the conductivity rises to practically 1 $(\Omega\ \text{cm})^{-1}$.

Such behaviour can be contrasted with that of fluorites reported in the previous Section. At low temperatures the defects present in fluorites are of Frenkel-type. The fluorites present a diffuse phase transition to the highly conducting phase. This transition has been associated with an instability in an assembly of Frenkel defects interacting through Coulomb forces (4).

The behaviour of AgI is very different from that of AgBr. The low temperature structure of AgI is of wurtzite-type. It undergoes a structural phase transition to a b.c.c. lattice of iodine ions in which the silver ions are disordered over many sites,

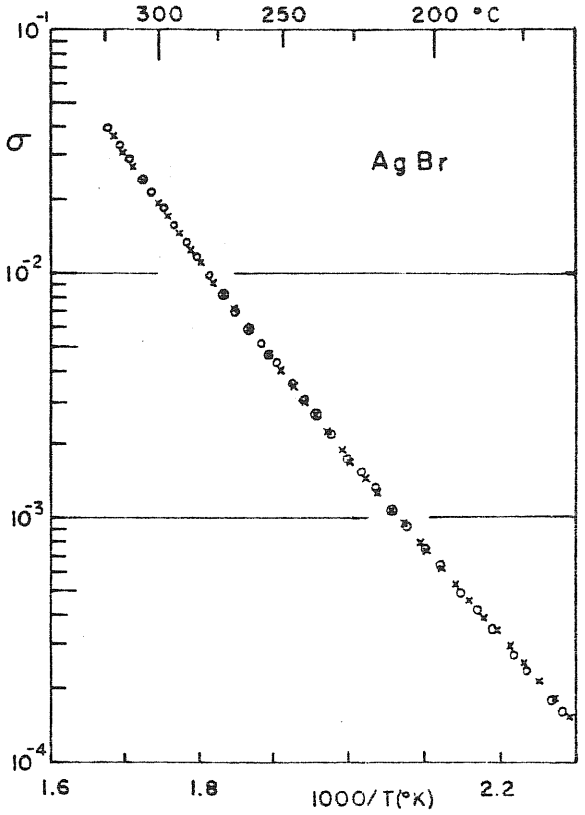

Fig. IV.2-1: Ionic conductivity σ of AgBr. Data from ref. (27).

at T_c = 420 °K. Correspondingly the ionic conductivity changes abruptly and AgI becomes superionic.

Now, let us present a detailed study of the defective structure of AgBr at high temperatures, in order to understand the lack of a superionic phase in this compound.

(a) Defective structure of AgBr

Although the literature titles are quite abundant as far as phisical properties of AgBr are concerned, the defect structure (specifically the Br^- defect structure) in AgBr has only been discussed in a limited number of papers. Electrical conductivity (26,111,112,113), Br nuclear magnetic resonance (22,23), Br^- self diffusion (24,25,114,115), thermodynamics of imperfections (116,117, 118) are the principal techniques by which information can be obtained on the concentration and the free energy of formation of defects in AgBr.

Many years ago some interest arose about whether the Schottky defect concentration would be high near the melting point. Kurnik (111) has given a value of the order of 10^{-2} for the atomic concentration of the free Br^- vacancies, $x_{v,Br}$. In recent literature (26,114) it is widely accepted that in AgBr the concentration of Schottky defects at high temperature is negligible compared to that of Frenkel defects. We do not share this point of view and present a determination of the intrinsic parameters of defects allowing explicitly for the presence of Schottky defects.

Aboagye and Friauf (26) and others judged that experimental evidence was against any appreciable concentration of Schottky

defects at any temperature in AgBr and therefore wrote the charge neutrality equation without the $x_{v,Br}$ term. Of course their set of derived AgBr thermodynamic parameters was somewhat affected by the omission. In fact, the set of intrinsic parameters for the Frenkel defects that they found fitting the low and intermediate temperature data on conductivity, did not allow them to reproduce the σ (T) anomaly, at temperatures above 550 °K. However, in the forthcoming discussion we shall make use of the experimental results of Aboagye and Friauf and Kao and Friauf (113) and of their formalism.

By conductivity measurements Kao and Friauf determined an excess Frenkel free energy $\Delta g_F^* = f(T)$ which, when subtracted from the Frenkel free energy $g_F^* = 1.134 - 6.55\ k_B T$ (eV) determined by Aboagye and Friauf, gives the product $x_{v,Ag}\ x_{i,Ag}$ according to the expression

$$x_{v,Ag}\ x_{i,Ag} = 2 \exp\left[- \frac{(g_F^* - \Delta g_F^*}{k_B T} \right] . \qquad \text{(IV.2-1)}$$

Here the factor 2 comes from the fact that the interstitial positions are twice the lattice sites.

The free energy $g_F^* = \varphi$ (T) and the excess free energy $\Delta g_F^* = f(T)$ are not perfectly correct when taken separately, as in their derivation, the concentration of bromine vacancies was not

taken into account in the charge neutrality equation. However as a first approximation, the difference $g_F^* - \Delta g_F^*$ is to be considered exact because it refers to the product $x_{v,Ag} x_{i,Ag}$, admittedly defined as x_o^2 in ref. (26). In eq. (IV.2-1) $x_{v,Ag}$ is the true silver-vacancy concentration and $x_{i,Ag}$ the true silver-interstitial concentration. At not too low temperatures, the charge neutrality equation can be written as follows

$$x_{v,Ag} - x_{i,Ag} = x_{v,Br} \quad . \qquad \text{(IV.2-2)}$$

If the value of $x_{v,Br}$ is known, the true values of $x_{v,Ag}$ and $x_{i,Ag}$ can be determined from equations (IV.2-1) and (IV.2-2).

Assuming that the diffusion of Br^- ions in AgBr is essentially based on a free-vacancy mechanism (92), $x_{v,Br}$, as a function of temperature, can be determined from the relation

$$x_{v,Br} = \frac{12\, D_L}{f'\, \nu_{v,Br}(T)\, a^2} \qquad \text{(IV.2-3)}$$

where $f' = 0.782$ is the tracer correlation factor, a is the lattice parameter of the unit cell of AgBr, $\nu_{v,Br}$ is the Br^- vacancy jump frequency and D_L is the diffusion coefficient in the lattice. The vacancy jump frequency, $\nu_{v,Br}$, can be determined by using the

X-ray diffraction data of Berry and Skillman (119) and the N.M.R. data (22,23). For $\nu_{v,Br}$ we get the following expression

$$\nu_{v,Br} = 9.9^{+4.1}_{-4.6} \times 10^{13} \exp\left[-(0.74 \pm 0.01)/k_B T\right] s^{-1} \quad \text{(IV.2-3)}$$

At low temperature, the diffusion coefficient D_L is given by (92)

$$D_L = 6.7 \times 10^{3} \exp(-1.86/k_B T) \quad cm^2 s^{-1} \quad \text{(IV.2-4)}$$

while the high temperature values of D_L are taken from the experimental data of Tannhauser (24).

The true Frenkel and Schottky free energies g_F and g_S are defined by the relations

$$x_{v,Ag}\, x_{i,Ag} = 2 \exp\left[-(g_F - \Delta g_{extra,F} - \Delta g_{DHL})/k_B T\right] \quad \text{(IV.2-5)}$$

$$x_{v,Ag}\, x_{v,Br} = \exp\left[-(g_S - \Delta g_{extra,S} - \Delta g_{DHL})/k_B T\right] . \quad \text{(IV.2-6)}$$

$\Delta g_{extra,F}$ and $\Delta g_{extra,S}$ are contributions to nonlinearities and Δg_{DHL} is the Lidiard contribution (120,26). The temperature dependence of mole fractions $x_{i,Ag}$ and $x_{v,Br}$ is reported in Fig. (IV.2-2); the free energies $g'_F = g_F - \Delta g_{extra,F}$ and $g'_S = g_S - \Delta g_{extra,S}$, which can be determined by iteration from

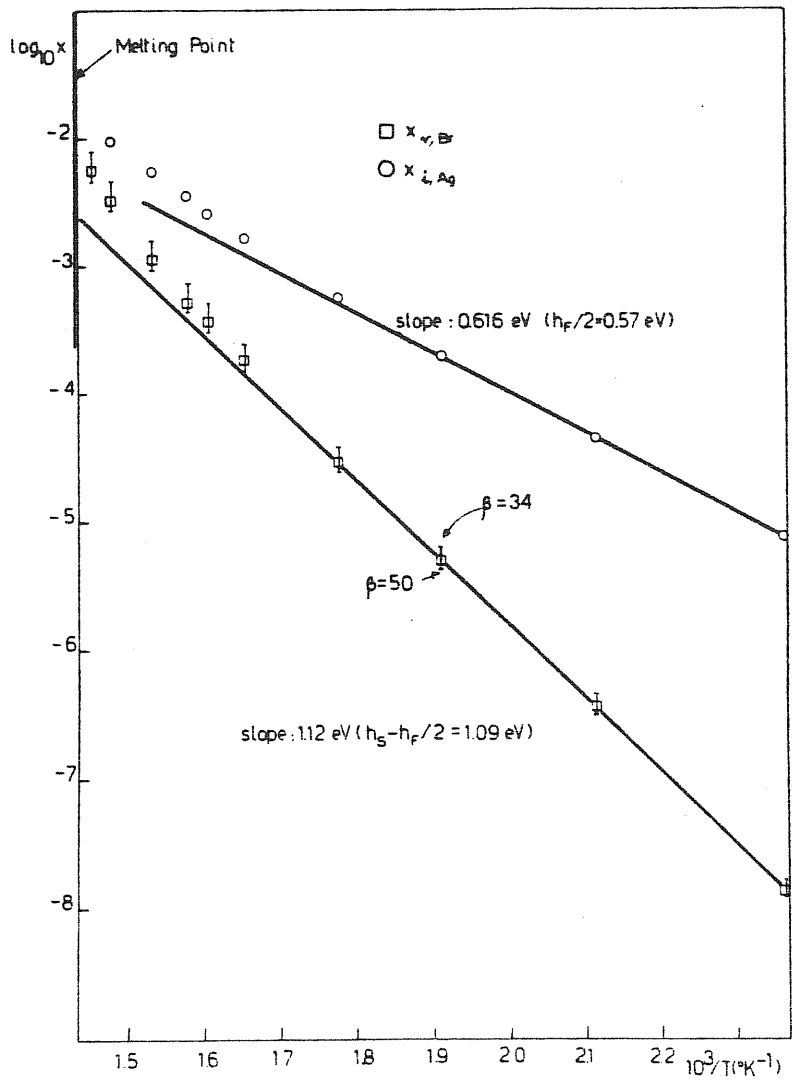

Fig. IV.2-2: Temperature variation of mole fractions of defects in AgBr. From ref. (92).

equations (IV.2-5) and (IV.2-6) are plotted against T in Fig. (IV.2-3). All the intrinsic defect parameters determined are listed in Table (IV.2-1).

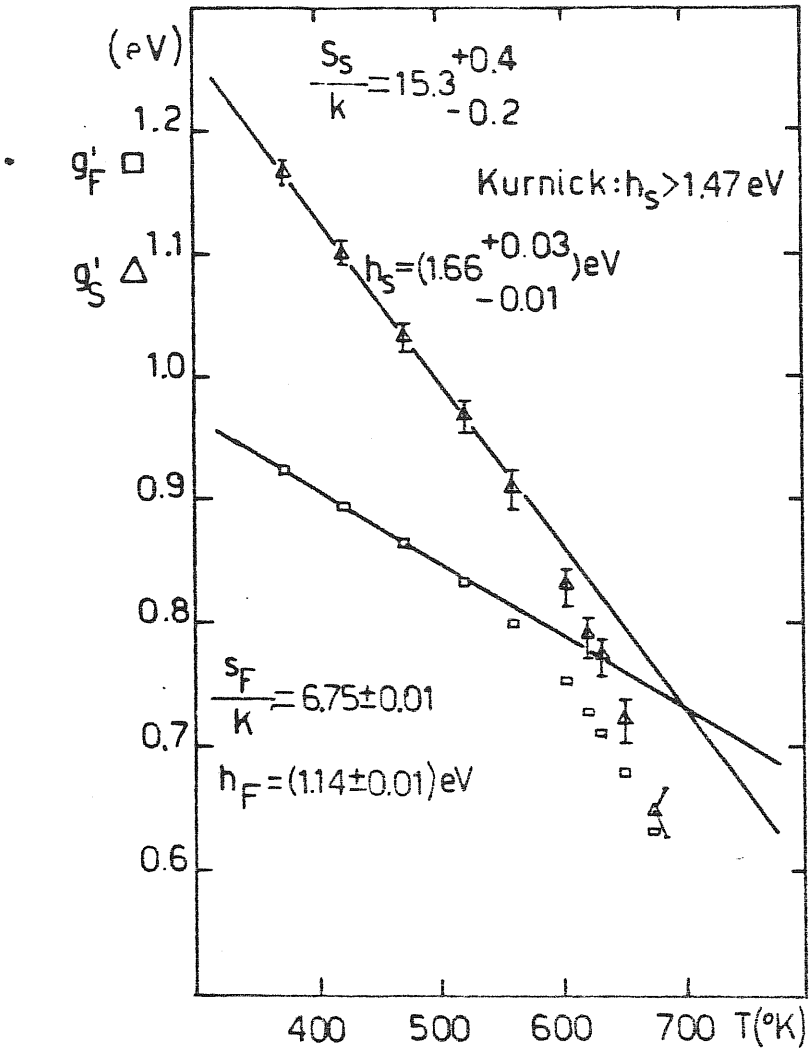

Fig. IV.2-3: Free energy of formation of Schottky and Frenkel defects in AgBr. From ref. (92).

E_F(eV)	E_S(eV)	S_F/k	S_S/k
1.14	1.66	6.75	15.3

Table IV.2-1: Intrinsic defective parameters in AgBr.From ref. (92).

From the results obtained we can reach the conclusion that:

(i) The formation energy E_F of a Frenkel defect is lower than the formation energy E_S of a Schottky defect and this is in agreement with the low temperature behaviuor of AgBr as a Frenkel conductor. The large value of the formation entropy, S_S, indicates the correctness of this model based on both Frenkel and Schottky defects.

(ii) The high concentration of Schottky defects in the high temperature region improves, although slightly, the agreement with the experimental conductivity data.

(b) Instability and melting in AgBr

The intrinsic defective parameters that we have obtained have recently been used by Andreoni and Tosi (27). They constructed a model for a conductor with a mixed assembly of Frenkel and Schottky defects, treating the interactions between defects in the framework of the Debye-Hückel theory modified for saturation of screening at high defect concentration. This way, they showed possible interpretations for the lacking of a high temperature superionic

phase in AgBr. We shortly report their analysis.

The equilibrium concentration of interstitials x_i in an interacting assembly of mixed Frenkel and Schottky defects is given by

$$x_i (1+\rho)^{1/2} = \sqrt{2}\ \exp\left[-g_F/2k_BT\right] \qquad \text{(IV.2-7)}$$

or equivalently

$$\frac{E_F}{2k_BT} - \frac{e^2 k}{2\varepsilon k_BT} = \frac{S_F}{2k_B} - \ln x_i + \frac{1}{2}\ln\left(\frac{2}{1+\rho}\right) \qquad \text{(IV.2-8)}$$

Here

$$k = \left[\frac{8\pi e^2 (1+\rho)}{\varepsilon v k_BT}\right]^{1/2} x_i^{1/2} \qquad \text{(IV.2-9)}$$

is the Debye-Hückel inverse screening length, where $\rho = \frac{x_{v,A}}{x_i}$ is the ratio between the concentration of the anion vacancies and that of the interstitials, which only depends on the intrinsic formation free energies. The quantity v is the volume per ion pair in the crystal. E_F and E_F have the usual meaning.

The equation (IV.2-8) is of the same type as the corresponding equation deduced some years ago by Kurosawa (3). This equation shows an instability at a certain temperature T_c. If $\rho \ll 1$ for temperatures below T_c, which means disorder of Frenkel type, we call the instability at T_c a "Frenkel instability". If $\rho \gg 1$ for temperatures below Tc, which means disorder of Schottky type, we

call the instability a "Schottky instability".

Following March, Richardson and Tosi (4) the Frenkel instability is associated to a transition in a superionic phase, in which a sublattice is disordered. This is the case of superionic fluorites. Following Kurosawa (3) the Schottky instability reflects the tendency for the whole crystal to melt. This seems to be the case of the alkali halides.

The solution for x_i and $x_{v,A}$ in AgBr as function of T obtained by Andreoni and Tosi (27) using the data of the previous Section are shown in Fig. (IV.2-4) (full lines). The value obtained for is about 1/3 and this, together with the data obtained for "isolated" assemblies of Frenkel and Schottky defects, means that the instability is still of the Frenkel type, though the presence of the Schottky defects cannot be neglected.

This simple Debye-Hückel model does not have a solution for $T > T_c$. Andreoni and Tosi have overcome this deficiency by introducing the saturation of the screening length in the simple Debye-Hückel theory, as the concentration of defects increase. The results for x_i and $x_{v,A}$ at temperatures above T_c are shown in Fig. (IV.2-4) (dashed lines). The saturation of the screening length has been switched on abruptly at T_c and for the inverse screening length the value k_c obtained at $T = T_c$ has been used.

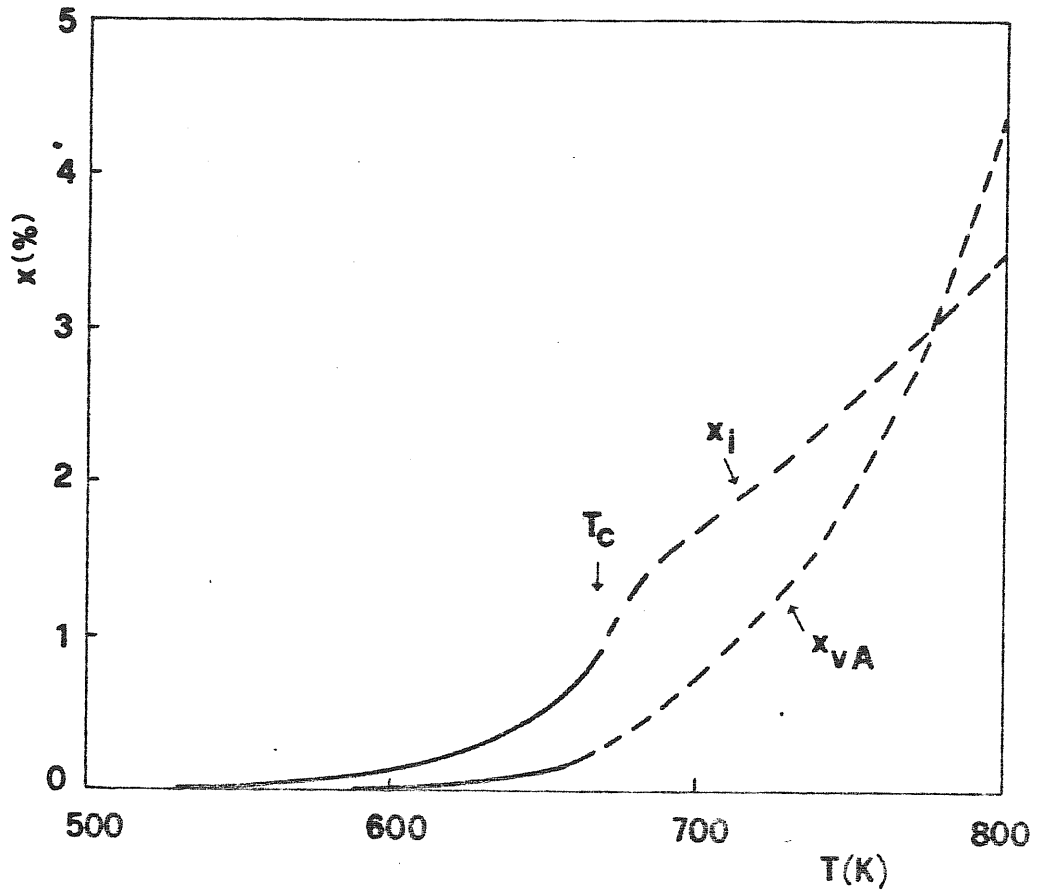

Fig. IV.2-4: Concentrations of interstitials, x_i, and anion vacancies x_{vA} in AgBr as function of temperature. Full lines up to T_c are obtained by the Debye-Hückel theory; dashed lines at high temperatures are obtained by including saturation of screening. From ref. (27).

The principal effect of the saturation of the screening length is a rapid increase of defect concentrations and, at $T \simeq 780$ °K, a crossing point $x_{v,A} = x_i$ is found.

The results are not quantitative but qualitatively this model explains the anomaly in the ionic conductivity and the absence

of a superionic phase in AgBr which is frustrated by the rapid increase of the anion Schottky defect concentration. The temperature of the crossing point, though too high, can be taken as indicative of the melting transition.

SUMMARY

The main original results of this Thesis are as follows.

(i) Numerical predictions for the freezing of the alkali halides RbCl and NaCl into a "normal" solid phase. In particular, the structural predictions for RbCl are in excellent agreement with liquid structure data, while the numerical estimates of the Fourier components of the particle densities at the first two reciprocal lattice vectors (simply related to Debye-Waller factors in the hot solid), still wait for experimental check. For NaCl, the agreement with the data is less good, but still semiquantitative. In both cases the behaviour of the Fourier components of the particle densities are quite similar in magnitude.

(ii) Numerical predictions for the freezing of the alkaline-earth halides $SrCl_2$ and $BaCl_2$ into a fast-ion conducting phase. Semiquantitative agreement with liquid structure data is again obtained. Most importantly, our results have stessed differences in the freezing process between "normal" and superionic materials, which appear through the different behaviour of the volume of freezing and through a behaviour of the anion-lattice structure in

the hot solid which may be assimilated to that of a modulated "lattice liquid". A role played by the difference in the partial molar volumes in the freezing of the alkaline-earth halides has been demostrated and interpreted.

(iii) A determination of the intrinsic parameters of defects in the hot AgBr solid from experimental data. The main result is that, in the high temperature region immediately below the melting point, the orders of magnitute of the Frenkel and Schottky defect concentrations are comparable.

Further results are a simple analysis of the freezing parameters of many metals into various structures by means of the theory of freezing, and an analysis of the calculation of the entropy of freezing for the hard sphere liquid within the same theory.

In conclusion, I may mention some interesting directions of further development of this work:

(i) calculations of the structure of the liquid solid interface for ionic materials, generalising studies for monatomic systems already given by Haymet and Oxtoby (16) and Harrowell and Oxtoby (121), the main new point of interest being the role played by the interfacial dipole layer;

(ii) extensions of the theory to the freezing of a modulated liquid, in particular in connection with the superionic transition in the fluorite materials and with simulation work on the two-dimensional classical plasma in an external periodic potential (122).

BIBLIOGRAPHY

1. R.M. Cotterill, E.J. Jensen and W.D. Kristensen,in "Anharmonic Lattice, Structural Transitions and Melting", edited by T. Riste (Noord-hoff, 1974).

2. A.B. Ubbelode, "The Molten State of Matter",(John Wiley & Sons, 1978).

3. T. Kurosawa, J. Phys. Soc. Jap., 12, 338(1957).

4. N.H. March, D.D. Richardson and M.P. Tosi, Sol. State Comm., 35, 903(1980).

5. S.F. Edwards and M. Warner, Phil. Mag., A40, 257(1979).

6. See, for example, J.A. Reissland, "The Physics of Phonons", (Wiley, 1973).

7. J.P. Hansen and L. Verlet,Phys. Rev., 184, 151(1969).

8. S.M. Stishov, Sov. Phys. Usp., 17, 625(1975).

9. S.M. Stishov, Sov. Phys. Usp., 11, 816(1969).

10. D. Frenkel, and J.P. Mc Tague, A. Rev. Phys. Chem., 31, 491(1980).

11. W.G. Hoover and M. Ross, Contemp. Phys., 12, 339(1971).

12. J.P. Hansen and I.R. Mc Donald, The Theory of Simple Liquids, (Academic Press, 1976) Chap. 10.

13. D. Chandler, Acc. Chem. Res., 7, 246(1974).

14. L. Verlet, in "Statistical Mechanics", edited by K. Freed and J.C. Light, (University of Chicago, 1974).

15. N.H. March and M.P. Tosi, "Coulomb Liquids", (Academic Press, 1984).

16. A.D.J. Haymet and D.W. Oxtoby, J. Chem. Phys., 74, 2559(1981).

17. T.V. Ramakrishnan and M. Yussouff, Phys. Rev., B19, 2775(1979).

18. N.H. March and M.P.Tosi, Phys. Chem. Liq., 11, 79(1981).

19. N.H. March and M.P. Tosi, Phys. Chem. Liq., 11, 89(1981).

20. N.H. March and M.P. Tosi, Phys. Chem. Liq., 11, 129(1981).

21. S. Chandra, "Superionic Solids", (North-Holland,1981).

22. F. Reif, Phys. Rev., 100, 1597(1955).

23. K.D. Becker and H. Richtering, Ber. Bunsenges. Phys. Chem., 78, 461(1974).

24. D.S. Tannhauser, J. Phys. Chem. Solids., 5, 224(1958).

25. S.R. Williams and L.W. Barr, J. Physique, Colloq. 34, C9-173 (1973).

26. J.K. Aboagye and R.J. Friauf, Phys. Rev., B11, 1654(1975).

27. W. Andreoni and M.P. Tosi, Solid State Ionics, 11, 49(1983).

28. W.G. Hoover, S.G. Gray and K.W. Johnson, J. Chem. Phys., 55, 1128(1971).

29. L.D. Landau and E.M. Lifshitz, "Statistical Physics", (Pergamon Press, Oxford, 1969).

30. T.H. Berlin and E.W. Montroll, J. Chem. Phys., 20, 75(1952).

31. A.J.C. Ladd and L.V. Woodcock, Chem.Phys. Lett., 51, 155(1977).

32. A.J.C. Ladd and L.V. Woodcock, Mol. Phys., 36, 611(1978).

33. W.B. Streett, H.J. Raveche and R.D. Mountain, J. Chem. Phys., 61, 1960(1974).

34. J.P. Hansen, Phys. Rev., A2, 221(1970).

35. J.P. Hansen, Phys. Rev., A8, 3096(1973).

36. E.L. Pollock and J.P. Hansen, Phys. Rev., A8, 3110(1973).

37. W.L. Slattery, G.D. Doolen and H.E. De Witt, Phys. Rev., A21, 2087(1980).

38. W.L. Slattery, G.D. Doolen and H.E. De Witt, Phys. Rev., A26, 2255(1982).

39. W.G. Hoover and F.H. Ree, J. Chem. Phys., 49, 3609(1968).

40. M. Lasocka, Phys. Letters, 51A, 137(1975).

41. F.A. Lindemann, Z. Physik, 11, 609(1910).

42. M. Ross, Phys. Rev., 184, 233(1969).

43. S. Toxvaerd, J. Chem. Phys., 69,4750(1978).

44. J.P. Hansen and D. Schiff, Mol. Phys., 25, 1281(1973).

45. S. Biggin and J.E. Enderby, J. Phys., C14, 3129(1981).

46. H. Ohmo and K. Furukawa, J. Chem. Soc. Faraday Trans., I77, 1981 (1981).

47. C.E. Derrington, A. Lindner and M. O'Keefe, J. Solid State Chem., 15, 171(1975).

48. T. Forland in B.R. Sundheim, "Fused Salts" (Mc Graw-Hill, 1964).

49. J.L. Tallon and W.H. Robinson, Phys. Lett., 87A, 365(1982).

50. J.L. Tallon, Phys. Lett., 76A, 139(1980).

51. J.L. Tallon, Solid State Comm., 42, 243(1982).

52. J.L. Tallon, Phys. Lett., 87A, 361(1982).

53. L. Pietronero, Phys. rev., B17, 3946(1978).

54. N.H. March and M.P. Tosi, Phys. Chem. Liq., 10, 185(1980).

55. H. Reiss, S.W. Mayer and J.L. Katz, J. Chem. Phys., 35, 820 (1961).

56. J.G. Kirkwood and E. Monroe, J. Chem. Phys., 9, 514(1941).

57. S.V. Tyablikov, J. exp. theor. Phys., 17, 386(1947).

58. A.A. Vlasov, J. exp. theor. Phys., 8, 291(1938).

59. H.J. Raveché and C.A. Stuart, J. Chem. Phys., 63, 1099(1975).

60. H.J. Raveché and R.F. Kayser, J. Chem. Phys., 68, 3632(1978).

61. J.D. Weeks, S.A. Rice and J.J. Kozak, J. Chem. Phys., 52, 2416(1970).

62. B. Jancovici, Physica, 31, 1017(1965).

63. R. Lovett, J. Chem. Phys., 66, 1225(1977).

64. R. Lovett and F.P. Buff, J. Chem. Phys., 72, 2425(1980).

65. V.N. Ryzhov and E.E. Tareeva, Theor. Math. Phys., 48, 835 (1981).

66. B. Bagchi, C. Cerjan and S.A. Rice, J. Chem. Phys.,79,5595(1983).

67. R. Evans, Adv., Phys., 28, 143(1979).

68. A.D.J. Haymet, J. Chem. Phys., 78, 4641(1983).

69. N.D. Mermin, Phys. Rev., 137,A1441(1965).

70. P. Hoenberg and W. Kohn, Phys. Rev. 136, B864(1964).

71. R. Balescu, "Equilibrium and Nonequilibrium Statistical Mechanics" (Wiley, 1975).

72. M. Yussouff, Phys. Rev. B23, 5871(1981).

73. E. Thiele, J. Chem. Phys., 39, 474(1963).

74. M.S. Wertheim, Phys. Rev. Lett., 10, 321(1963). J.Math. Phys. (NY) 5, 643(1964).

75. J.K. Percus and G.J. Yevick, Phys. Rev., 110, 1(1958).

76. M. Rovere and M.P. Tosi, to be published.

77. B. D'Aguanno, M. Rovere, N.H. March and M.P. Tosi, Phys. Chem. Liq., 13, 113(1983).

78. A.B. Bhatia and D.E. Thornton, Phys. Rev., B2, 3004(1970).

79. E.W.J. Mitchell, P.F.J. Poncet and R.J. Stewart, Phil. Mag., 34, 721(1976).

80. F.G. Edwards, et al. J. Phys., C8, 3483(1975).

81. S. Biggin and J.E. Enderby, J. Phys., C15, L305(1982).

82. J.Y. Derrien and J. Dupuy, J. Physique, 36, 191(1975).

83. S. Biggin and J.E. Enderby, J.Phys., C14, 3577(1981).

84. F.G. Edwards et al., J. Phys., C11, 1053(1978).

85. R.L. McGreevy and E.W.J. Mitchell, J. Phys., C15, 5537(1982).

86. P.V. Giaquinta and M.P.Tosi, unpublished work.

87. Y. Waseda, "The Structure of Non-Crystalline Materials" (McGrew-Hill, 1980).

88. C.R.A. Catlow, Comm. Solid State Phys., 9, 157(1980).

89. M. Rovere, M.P. Tosi and N.H. March, Phys. Chem. Liquids, 12, 177(1982).

90. M. Rovere et al., Phil. Mag., B39, 167(1979).

91. M.C. Abramo, M. Parrinello and M.P. Tosi, J. Nonmet., 2, 67(1974).

92. L.G. Conti, B. D'Aguanno and O.A.P. Tavares, unpublished work.

93. H. Wiedersich and S. Geller, in "The Chemistry of Extended Defects in Non-metallic Solids", ed. L. Eyring and M. O'Keeffe (North Holland, 1971).

94. W. Hayes, Contemp.Phys., 19, 469(1978).

95. A. Hooper, Contemp. Phys., 19, 147(1978).

96. C.R. Peters et al., Acta Cryst., B37, 1826(1971).

97. M.S. Whittingham and R. Huggings, J. Chem. Phys., 54, 414(1971).

98. J.P. Boilot et al., in "Superionic Conductors", ed. by G.D. Mahan and W.L. Roth (Plenum Press, 1976).

99. R.J. Cava, F. Reidinger and B.J. Wuensch, Sol. St. Comm., 24, 411(1977).

100. A.B. Lidiard, "Cr stals with the Fluorite Structure",ed. by W. Hayes (Clarendon, 1974).

101. M.H. Dickens et al., Sol. State Phys., 11, L583(1978).

102. M.H. Dickens et al., in "Fast Ion Transport in Solids", ed. by P. Vashishta, J.N. Mundy and G.K. Shenoy, (North-Holland, 1979).

103. K. Clausen et al., Sol. State Ionics, 5, 589(1981).

104. M. O'Keeffe and B.G. Hyde, Phil. Mag., 33, 219(1976).

105. M.J. Gillan and D.D. Richardson, J. Phys., C12, L61(1979).

106. A. Rahman, J. Chem. Phys., 65, 4845(1976).

107. M. Dixon and M.J. Gillan,J. Phys., C11, L65(1978).

108. G. Jacucci and A. Rahman, J. Chem. Phys., 69, 4117(1978).

109. M.T. Hutchings, Argonne Symposium on Neutron Scattering, A.I.P. Conf. Proc.(1982).

110. P.W.M. Jacobs and S. H. Ong, Cryst. Lattice Defects, 8, 177(1980).

111. S.W. Kurnick, J. Chem. Phys., 20, 218(1952).

112. R.J. Friauf, J. Phys. Chem., 66, 2380(1962).

113. R.J. Friauf, J. Physique, 38, 1077(1977).

114. A.P. Batra and L.M. Slifkin, J. Phys., C9, 947(1976).

115. A.P. Batra and L.M. Slifkin, J. Phys., C11, L317(1978).

116. A.W. Lawson, J. Appl. Phys., 33, 466(1962).

117. F.A. Kröger, J. Phys. Chem. Solids, 26, 901(1965).

118. P. Muller, Phys. Stat. Sol., 21, 693(1967).

119. C.R. Berry and D.C. Skilman, J. Crystal Growth, 2, 141(1968).

120. A.B. Lidiard, "Handbuch der Physik", edited by S. Flügge, (Springer-Verlag, 1957), vol.XX, p.246.

121. P. Harrowell and D.W. Oxtoby,J. Chem. Phys., 80 ,1639(1984).

122. P. Vashishta, private comunication.